Sedimentology, stratigraphy, and U-Pb detrital-zircon geochronology of the Meall Dearg Formation, Stoer Group, Torridonian succession, north-western Scotland

by

Lorraine Elizabeth Lebeau

A thesis submitted in partial fulfillment
of the requirements for the degree of
Master of Science (MSc) in Geology

The Faculty of Graduate Studies
Laurentian University
Sudbury, Ontario, Canada

THESIS DEFENCE COMMITTEE/COMITÉ DE SOUTENANCE DE THÈSE
Laurentian Université/Université Laurentienne
Faculty of Graduate Studies/Faculté des études supérieures

Title of Thesis Titre de la thèse	Sedimentology, stratigraphy, and U-Pb detrital-zircon geochronology of the Meall Dearg Formation, Stoer Group, Torridonian succession, north-western Scotland
Name of Candidate Nom du candidat	Lebeau, Lorraine
Degree Diplôme	Master of Science
Department/Program Département/Programme	Geology
Date of Defence Date de la soutenance	September 14, 2018

APPROVED/APPROUVÉ

Thesis Examiners/Examinateurs de thèse:

Dr, Alessandro Ielpi
(Co-Supervisor/Co-directeur de thèse)

Dr. Maarten Krabbendam
(Co-Supervisor/Co-directeur de thèse)

Dr. William J. Davis
(Committee member/Membre du comité)

Dr. Katherine Hahn
(External Examiner/Examinateur externe)

Approved for the Faculty of Graduate Studies
Approuvé pour la Faculté des études supérieures
Dr. David Lesbarrères
Monsieur David Lesbarrères
Dean, Faculty of Graduate Studies
Doyen, Faculté des études supérieures

ACCESSIBILITY CLAUSE AND PERMISSION TO USE

Abstract

The Meall Dearg Formation is a c.1.2 billion year old sandstone, and represents the uppermost unit of the Stoer Group (Torridonian succession, north-western Scotland). Originally described as purely fluvial, the Meall Dearg Formation is here reappraised to represent coeval fluvial-channelised, floodbasin, and aeolian erg environments by facies analysis and petrographic methods. Evidence from palaeoclimate indicators points to humid conditions at time of deposition — inferred from clastic rather than evaporitic floodbasin strata. U-Pb detrital-zircon geochronology resolved provenance from the underlying Lewisian Gneiss Complex (comprising several juxtaposed terranes). Erosion from the Assynt, Gruinard, and Gairloch terranes provided most sediment supply. A statistical comparison of ages from the fluvial and aeolian deposits revealed that both underwent sediment transfer and/or were supplied from comparable terranes. The Meall Dearg Formation, a post-rift fill, is largely comparable to the coeval, pre-Rodinian Gardar-Rift sequence of Greenland.

Keywords

Mesoproterozoic, Stoer Group, Torridonian, rift basin, palaeoclimate, U-Pb detrital-zircon geochronology, Lewisian Gneiss Complex, fluvial-aeolian

Co-Authorship Statement

Several collaborators, listed as co-authors, contributed to the work presented herein. The co-authors provided scientific guidance, supervision, and help with laboratory analyses and sample collection in the field. Dr. Alessandro Ielpi directed the project.

Chapter 2 is co-authored with Dr. Alessandro Ielpi (Laurentian University). Fieldwork and sample selection was completed by the candidate under the supervision of Dr. Ielpi. Sample preparation was completed by the candidate. The first draft and initial interpretations were completed by the candidate with guidance from Dr. Ielpi. Dr. Ielpi edited subsequent drafts of the manuscript and provided scientific input for the candidate to investigate and follow up on. Dr. Ielpi drafted many figures for the manuscript.

Chapter 3 is co-authored by Dr. Alessandro Ielpi (Laurentian University), Dr. Maarten Krabbendam (British Geological Survey), and Dr. William Davis (Geological Survey of Canada). Field work and sample collection was completed by the candidate supervised by Dr. Ielpi and Dr. Krabbendam. Sample preparation (crushing, milling, separation of heavy material by Wilfley table) was completed by the candidate. Analytical techniques (heavy mineral separation, Franz magnetic separator, and sensitive high-resolution ion-microprobe analysis) were executed in Dr. Davis's laboratory, with assistance of the candidate and Dr. Ielpi. Dr. Davis also wrote a subsection of the "methods". Dr. Krabbendam drafted a table and provided figures and ArcGIS files that were later modified for the manuscript. The first draft was written by the candidate with scientific guidance from all three co-authors. All three co-authors edited subsequent drafts of the manuscript and provided scientific input.

Acknowledgements

Dr. Ielpi is acknowledged for providing a fantastic research project. Dr. Ielpi has been an outstanding supervisor, professor, and friend throughout this entire project. With his aid I have drastically improved my skills as a researcher, field geologist, and writer, and for such I am highly appreciative. Co-author Dr. Maarten Krabbendam from the British Geological Survey is also greatly acknowledged for insightful scientific discussion, for sample collection, and editing. Dr. Bill Davis from the Geological Survey of Canada is also acknowledged for offering his geochronological expertise, guidance and editing. Both Laurentian University, and a Discovering Grant from the Natural Sciences and Engineering Research Council of Canada provided financial support. Willard Desjardins and Phillipe Trudel are thanked for offering their time and effort for sample preparation. Tom Pestaj and Nicole Rayner from the Geological Survey of Canada are recognized for their assistance during analytical work. Colleagues Cedric Mayer and Natasha Cyples are thanked for their scientific input and support.

Table of Contents

List of Tables

List of Figures

List of Appendices

Chapter 1

1. Introduction to thesis

1.1 Statement of the problem

This thesis investigates the sedimentology, palaeoflow patterns, petrography, and detrital-zircon geochronology of the c.1.2 Ga Meall Dearg Formation (Torridonian succession, north-western Scotland). The Meall Dearg Formation is exposed along shallowly dipping beds of cross-bedded arkose approximately 300 m thick along the seaboard of Stoer Peninsula and Enard Bay, both located near the hamlet of Lochinver, in the district of Assynt. Classically described as purely fluvial in origin (Stewart, 2002), the Meall Dearg Formation is here reappraised to be associated with coeval fluvial channel-belt, floodbasin, and aeolian erg depositional environments. Palaeoclimate indicators from clastic facies associations are typically considered unreliable, usually interpreted from a single depositional environment. In addition, delineating original catchment basin shape and size, or basin topography of Precambrian continental sandstone successions also remains questionable. The Meall Dearg Formation provides the opportunity for a more reliable palaeoclimate interpretation with three coeval depositional environments, rather than one.

A previous provenance study of the Meall Dearg Formation pointed out that some detrital-zircons had enigmatic young ages (i.e., ages that did not conform with typical Archean ages in the Lewisian Gneiss Complex), and that it needs further study (Rainbird et al., 2001). With the newly found knowledge of a partly aeolian origin, detrital-zircon

geochronology was necessary to investigate the origin of these enigmatic grains with a new perspective of depositional setting and a more robust (statistically significant) number of zircons. In addition, detrital-zircon analysis allows the opportunity to test if age distributions from the fluvial and aeolian deposits can provide semi-quantitative insight into their interrelationship regarding sediment transfer. At a greater scale, the Meall Dearg Formation represents the final stages of sediment fill in a pre-Rodinian rift basin. The general configuration of Supercontinent Rodinia is contentious in detail, and the geographic relationships among pre-Rodinian continental blocks are even less understood. This study sets out to draw correlations with other pre-Rodinian sedimentary sequences to contribute to this knowledge gap. Specific research questions pertaining to the problems delineated above are outlined below.

1.2 Goals and research questions

- To advance the general understanding of Mesoproterozoic terrestrial sedimentary environments, with outcrop and analytical evidence from the Torridonian succession of Scotland.

The Torridonian sucession, encompassing the Meall Dearg Formation, is a thick sandstone package just over 10 km thick and covers an area of approximately 200 by 40 km (Stewart, 2002). It is among the best-preserved Precambrian sedimentary rock records worldwide, and stands as a record of Mesoproterozoic continental landscapes from c. 1.2 to 1.0 Ga. The Torridonian succession has been the subject of study for almost 200 years to date, yet a detailed study of the Meall Dearg Formation is still lacking. Facies analysis combined with palaeoflow measurements and petrography allows for the delineation of

depositional environments of Mesoproterozoic continental landscapes (including fluvial-channel deposits, floodbasin deposits, and aeolian ergs).

- To investigate the interaction between fluvial channel-belt, floodbasin, and aeolian depositional systems in a pre-vegetation landscape.

Examples of coexisting fluvial, floodbasin and aeolian environments are rare in the geologic record, especially in the Precambrian (Aspler and Chiarenzelli, 1997; Hadlari et al., 2006; Almeida et al., 2009; Simpson et al., 2012). Evidence of their interaction is fundamental to understand the dynamics of pre-vegetation landscapes.

- To discuss the Meall Dearg Formation's rock record in terms of palaeoclimate indicators.

Inferences on climate from clastic records are often fraught with uncertainty, and require comparison with independent proxies. Especially when depositional environments are analysed individually, climate inferences become highly uncertain due to non-unique solutions, lack of independent testing, or overprinting of environmental signals (e.g., an ephemeral style river can either be caused by a quickly discharged and small catchment basin rather than an arid local climate (Frakes et al., 2005; Jerolmack and Paola, 2010). In the case of the Meall Dearg Formation, the analysis of multiple co-existing depositional environments (e.g., fluvial, floodbasin, and aeolian) allows to disentangle climate indicators in a more reliable fashion.

- Can a robust dataset of detrital-zircon ages resolve the provenance of the Stoer Group, and be used to rigorously test a rift-basin model for the first depositional phase of the Torridonian succession?

Previous work on the Meall Dearg Formation investigated provenance studies by analysing only 18 detrital-zircon grains (Rainbird et al., 2001). These grains pointed to local source rock from the Lewisian Gneiss Complex (the basement rock presently exposed in contact with the Stoer Group), pointing to a locally derived – probably rift – basin setting; however, a few enigmatic younger grains were also identified. Here, 309 zircon grains were analysed from the Meall Dearg Formation — a statistically significant and robust dataset (Vermeesch, 2004) — in order to gain insight on these enigmatic grains and test whether they are consistent with a locally derived rift basin framework.

- Can detrital-zircon age distributions from coeval fluvial and aeolian deposits provide insight on fluvial-aeolian interaction in a pre-vegetation landscape?

The interaction of fluvial and aeolian depositional environments is highly topical in clastic sedimentology, although this aspect has seldom been investigated in the Precambrian rock record. Again, the occurrence of coeval and depositionally-linked fluvial and aeolian deposits in the Meall Dearg Formation makes it an ideal natural laboratory to investigate interactions between these two depositional environments in a Mesoproterozoic landscape.

- Is the Stoer Group stratigraphically related to other pre-Rodinian sedimentary sequences?

Rodinia is a postulated Meso- to Neoproterozoic supercontinent that included most of the known Precambrian cratonic blocks, and its assembly has been related to some of the largest orogenic events in the Earth's record (Torsvik, 2003, Cawood 2007). Most pre-Rodinian Mesoproterozoic sedimentary sequences have been interpreted to be deposited in active continental margin settings that are prone syn-depositional magmatism (Cawood et al., 2007), and many of them underwent significant deformation and metamorphism during later phases of continental collision. This is notably not the case for the Stoer Group and few other preserved successions such as the Gardar Rift located in present-day southern Greenland. Stratigraphic similarities between these two Mesoproterozoic rift-basin fills are also discussed in this thesis.

1.3 Structure of thesis

This dissertation is presented in three chapters, chapter 2 and 3 are written as manuscripts for publication in refereed scientific journals. Each of the manuscripts will be published as independent articles, so there is repetition in the introduction and geological setting of each chapter. Chapter 2 is a published paper entitled " **Fluvial channel-belts, floodbasins, and aeolian ergs in the Precambrian Meall Dearg Formation (Torridonian of Scotland): Inferring climate regimes from pre-vegetation clastic rock records**" (published in 2017 in the Elsevier journal *Sedimentary Geology, vol. 357, pp. 53-71*). This paper presents a facies analysis of the Meall Dearg Formation, with the final goal of delineating its record of depositional environments. Chapter 3 is written as a manuscript entitled "**Detrital-zircon provenance of a Torridonian fluvial-aeolian sandstone: The 1.2 Ga Meall Dearg Formation, Stoer Group (Scotland)**" (to be submitted to the Elsevier journal *Precambrian Research*). This paper presents a detrital-

zircon geochronology provenance study of the Meall Dearg Formation to characterise sedimentary source areas, and hence catchment basin size, fluvial and aeolian interactions, and basin setting.

1.4 Statement of responsibilities

Field work and sample collection was completed by the candidate with the assistance and supervision of Dr. Alessandro Ielpi and Dr. Maarten Krabbendam. Field work was completed in May 2016. Dr. Krabbendam was invited as a co-author and secondary supervisor for his full-rounded expertise on the geology of Scotland. Dr. Krabbendam (Geologist at the British Geological Survey of Edinburgh, Scotland) accompanied the candidate and Dr. Ielpi (Assistant Professor of Sedimentology at Laurentian University) to help with sampling for detrital-zircon analysis. For the results described in chapter 1, Mr. Willard Desjardins at Laurentian University cut samples and prepared thin sections. For the results described in chapter 2, samples were cut, crushed, milled, and passed through Wilfley Table by the candidate with help of fellow graduate student Phillipe Trudel. The heavy sediment was sent to Dr. Davis (head of the Geochronology Laboratory at the Geological Survey of Canada, Ottawa) for detrital-zircon geochronological analysis. Here, Dr. Davis and associated laboratory personnel (*e.g.* Ms. Nicole Rayner) further handled the samples by passing them through methylene iodide and a magnetic separator, and by casting the zircons in an epoxy puck. The zircons were then imaged by cathodoluminescence and backscatter. Analysis by sensitive-high resolution ion-microprobe (SHRIMP) was undertaken by Dr. Davis and lab technologist Tom Pestaj with the assistance of the candidate and Dr. Ielpi. Dr. Davis performed raw data corrections and is co-authoring chapter 2. Chapter 2 was written by the candidate

with editing by Dr. Ielpi. Chapter 3 was written by the candidate with edits by Dr. Ielpi, Dr. Krabbendam, and Dr. Davis.

1.5 Statement of original contributions

The following points outline the original contributions made by this study:

- Reappraises the Meall Dearg Formation. Previously thought to represent solely a fluvial system, here it is interpreted to represent the product of fluvial, floodbasin, and aeolian depositional systems.

- Documents stratigraphy, palaeoflow measurements, petrography from all three facies types mentioned above.

- Provides for the first time a statistically significant number of zircon for detrital-zircon geochronology studies on the rock unit. Previously only 18 grains were analysed, here are 309 grains are analysed.

- Provides a new interpretation of sedimentary provenance at the local terrane scale (*e.g.*, derivation from the Assynt terrane of the Lewisian Gneiss Complex, rather than generally stating “from the local Lewisian Gneiss Complex”).

- Provides evidence of fluvial and aeolian interaction in the Mesoproterozoic, tested by the comparison of detrital-zircon age distributions.

- Provides estimates of catchment basin surface at the time of Meall Dearg Formation deposition.

- Confirmation of the Stoer Group to represent a local rift basin.

1.6 References

Almeida, R.P., Janikian, L., Fragoso-Cesar, A.R.S., Marconato, A., 2009. Evolution of a rift basin dominated by subaerial deposits: the Guaritas Rift, Early Cambrian, Southern Brazil. Sedimentary Geology 217, 30–51.

Aspler, L.B., Chiarenzelli, J.R., 1997. Initiation of ~2.45–2.1 Ga intracratonic basin sedimentation of the Hurwitz Group, Keewatin Hinterland, Northwest Territories, Canada. Precambrian Research 81, 265–297.

Cawood, P.A., Nemchin, A.A., Strachan, R., Prave, T., Krabbendam, M., 2007. Sedimentary basin and detrital-zircon record along East Laurentia and Baltica during assembly and breakup pf Rodinia. Journal of the Geological Society of London 164, 257-275.

Hadlari, T., Rainbird, R.H., Donaldson, J.A., 2006. Alluvial, eolian and lacustrine sedimentology of a Paleoproterozoic half-graben, Baker Lake Basin, Nunavut, Canada. Sedimentary Geology 190, 47–70.

Rainbird, R.H., Hamilton, M.A., Young, G.M., 2001. Detrital-zircon geochronology and provenance of the Torridonian, NW Scotland. Journal of the Geological Society of London 158, 15-27.

Simpson, E.L., Eriksson, K.A., Mueller, W.U., 2012. 3.2 Ga eolian deposits from the Moodies Group, Barberton Greenstone Belt, South Africa: implications for the origin of first- cycle quartz sandstones. Precambrian Research 214–215, 185–191.

Stewart, A.D., 2002. The later Proterozoic Torridonian rocks of Scotland: Their sedimentology,

geochemistry, and origin. Geological Society, London, Memoir vol. 24, 136 p.

Torsvik, T.H., 2003. The Rodinia Jigsaw Puzzle. Science 300, 1379-1381.

Vermeesch, P., 2004. How many grains are needed for a provenance study? Earth and Planetary Sciences Letters 224, 441-451.

Chapter 2

2. Fluvial channel-belts, floodbasins, and aeolian ergs in the Precambrian Meall Dearg Formation (Torridonian of Scotland): Inferring climate regimes from pre-vegetation clastic rock records

Lorraine E. Lebeau*, Alessandro Ielpi

Harquail School of Earth Sciences, Laurentian University, Sudbury, Ontario P3E 2C6, Canada

* Corresponding author at: Harquail School of Earth Sciences, Laurentian University, 935 Ramsey Lake Road, Sudbury, ON, Canada P3E 2C6. Tel./fax: +1 705 675 1151.

E-mail address: llebeau@laurentian.ca (L. Lebeau)

2.1 Abstract

The interpretation of climate regimes from facies analysis of Precambrian clastic rocks has been challenging thus far, hindering full reconstructions of landscape dynamics in pre-vegetation environments. Yet, comparisons between different and co-active sedimentary realms, including fluvial-channelised, floodplain, and aeolian hold the potential to shed further light on this thematic. This research discusses a fluvial-aeolian record from the 1.2 Ga Meall Dearg Formation, part of the classic Torridonian succession of Scotland. Tentatively considered to date as a braided-fluvial deposit, this unit is here reappraised as the record of fluvial channel-belts, floodbasins, and aeolian ergs. Fluvial deposits with abundant transitional- to upper-flow regime structures (mostly cross-beds

with tangential sets and plane/antidunal beds) and simple, low-relief sediment bars indicate a low-sinuosity, ephemeral style. Floodbasin deposits consist of plane and cross-beds ubiquitously bounded by symmetrical ripples, and rare sediment bars related to the progradation of splay complexes in temporary flooded depressions. Aeolian deposits occur nearby basement topography, and are dominated by large-scale, pin-stripe laminated cross-beds, indicative of intermountain ergs. Neither ephemeral-fluvial nor intermountain aeolian systems can be considered as reliable indicators of local climate, since their sedimentary style is respectively controlled by catchment size and shape, and basin topography relative to groundwater tables. In contrast, the occurrence of purely clastic – rather than carbonate or evaporitic – floodplain strata can be more confidently related to humid regimes. In brief, this study provides new insight into an overlooked portion of the Torridonian succession of Scotland, and discusses climate inferences for Precambrian clastic terrestrial rocks.

2.2 Introduction

Precambrian terrestrial environments have attracted consistent scientific interest in the past few decades (Long, 1978, 2011; Eriksson et al., 1998, 2001, 2004; Bose et al., 2012), and similarities have been postulated to both modern unvegetated landscapes on Earth and extra-terrestrial realms (Wood, 2006; Burr et al., 2013; Ielpi, 2016; Santos et al., 2016). Many modern unvegetated landscapes are found in arid environments, where hydrologic systems are controlled by excess evaporation, flash-flooding subject to rapid infiltration, low groundwater tables, and limited vegetation cover (Carroll and Bohacs, 1999; Bullard and McTanish, 2003; Mountney, 2006; Miall, 2016). As a result, modern desert drainages are dominantly ephemeral (Bullard and McTanish, 2003) unless

recharged by a large, continent-scale drainage (Syvitski et al., 2000, 2003); likewise, modern arid-climate shallow lakes and floodbasins (defined as a depressed portion of a floodplain prone to repeated flooding; cf. Jorgensen and Fielding, 1996) are for the most part evaporitic (sensu Carroll and Bohacs, 1999), i.e. characterised by negative water budgets. This is in contrast with what is observed in the Precambrian terrestrial rock record, where a variety of hydrologic regimes (i.e. not limited to evaporitic) have been documented for systems with interacting fluvial and aeolian deposition (Ross, 1983; Aspler et al., 1994; Hadlari et al., 2006; Long, 2011; Bállico et al., 2017). In other words, modern unvegetated landscapes are limited to arid climate zones, whereas Precambrian counterparts were barren irrespective of palaeoclimate; therefore, the lack of modern unvegetated analogues for certain terrestrial Precambrian climate settings is a major limitation to date. To overcome this limitation, the comparison between the sedimentary style of different pre-vegetation terrestrial environments – including fluvial channel-belts, floodplains, lakes, and aeolian ergs – holds great potential. Such approach has been however seldom proposed in the past (Tirsgaard and Øxnevad, 1998; Hadlari et al., 2006; Almeida et al., 2009; Fralick and Zaniewski, 2012; Marconato et al., 2014), and refined depositional models are still warranted to disentangle climate signals from pre-vegetation continental clastic rock records (Tirsgaard and Øxnevad, 1998; Marconato et al., 2014). The characterisation of Precambrian floodplain strata in particular has been challenging thus far, due to their sand-rich character and architectural similarity to the products of other continental sedimentary systems (Marconato et al., 2014).

To contribute to this topic, new outcrop evidence is presented from the Torridonian succession of Scotland, which is renowned as one of the most compelling sedimentary

records of Precambrian terrestrial environments (Fig. 1A). The Torridonian succession has received continuing attention in the last century (Stewart, 2002 and references therein), although some portions of it still lack a proper sedimentologic framework. One striking example is the Mesoproterozoic Meall Dearg Formation, the youngest unit of the 1.2 Ga Stoer Group, which was previously considered as the product of a sandy braided fluvial system (Stewart, 2002). A description of fluvial-channel, floodbasin, and aeolian deposits is for the first time presented for this rock unit. The relationships between these depositional realms are discussed in terms of climate inferences that can be extrapolated from Precambrian clastic records. The goals of this research are: (1) to advance the general understanding of Mesoproterozoic terrestrial environments, with outcrop evidence from the Torridonian succession of Scotland; (2) to investigate the interaction between fluvial-channel, floodbasin, and aeolian systems in a pre-vegetation landscape; and 3) to discuss the Meall Dearg's rock record in terms of palaeoclimate indicators.

2.3 Geological setting

The Torridonian succession spans from c. 1.2 to 1.0 Ga and represents one of the major stratigraphic components of the United Kingdom, as well as one the best-preserved Precambrian sedimentary rock records worldwide. The earliest descriptions of Torridonian rocks date back to 1819 by Dr. John MacCulloch (MacCulloch, 1819). In recent years, the Torridonian succession has attracted attention due to its outstanding record of Precambrian sedimentary environments, early life, palaeoclimate, and tectonic settings (among others: Williams, 1966, 2001; Gracie and Stewart, 1967; Nicholson, 1993; McManus and Bajabaa, 1998; Young, 1999a, 1999b; Rainbird et al., 2001; Prave, 2002; Williams and Foden, 2012; Santos and Owen, 2016; Ielpi et al., 2016; Brasier et

al., 2016). Detailed review of the entire succession was first undertaken by Peach et al. (1907), and more recently by Stewart (2002). The Torridonian succession is almost exclusively composed of siliciclastic sedimentary rocks, most of which are thick sandstone packages exposed along the north-western Highlands of Scotland. Its full stratigraphic development is just over 10 km in thickness, and covers an area of approximately 200 by 40 km (Stewart, 2002; Fig. 1A).

The Torridonian succession nonconformably overlies the Archean to Paleoproterozoic Lewisian Gneiss Complex, and is unconformably covered by Cambrian nearshore-marine sedimentary rocks. Aside from local faulting, the Torridonian succession underwent limited deformation, and records negligible metamorphism. The stratigraphy of the succession is sub-divided, from the oldest to the youngest, into the Stoer, Sleat, and Torridon groups (Stewart, 2002) (Fig. 1A). The c. 1.2 Ga Stoer Group has a maximum thickness of 2 km and includes a full record of proximal to distal terrestrial environments, from scree slopes, fluvial (both channelised and overbank), lacustrine, and aeolian (Ielpi et al., 2016). Past palaeogeographic and tectonic reconstructions point to deposition in a rift basin near the margin of Laurentia (Stewart, 1982; Rainbird et al., 2001; Ielpi et al., 2016). Its current geographic extent is limited by the nonconformable contact with the Lewisian Gneiss complex and the regional post-depositional Coigach fault zone (Fig. 1B).

The internal stratigraphy of the Stoer Group is sub-divided, base upwards, into the Clachtoll, Bay of Stoer, and Meall Dearg formations (Stewart, 2002). The Clachtoll and lower Bay of Stoer formations are composed of basal breccias overlain by fluvial channelised and overbank deposits (Ielpi et al., 2016). Overbank deposits consist of

sandy splay complexes prograding into mud-dominated floodbasins. Wet-aeolian tracts and minor shallow-lacustrine deposits have also been documented (Ielpi et al., 2016) in the Clachtoll and lowermost Bay of Stoer formations. The upper Bay of Stoer Formation is represented by the impact-related Stac Fada Member (Amor et al., 2007; Parnell et al., 2011), and the mud-dominated, shallow-lacustrine Poll a'Mhuilt Member (Stewart, 2002). The Poll a'Mhuilt Member displays a shallowing upward trend (Stewart, 2002) and is overlain by the Meall Dearg Formation. The contact between the mud-dominated Poll a'Mhuilt Member and the locally coarse-grained base of the Meall Dearg Formation is irregular and erosive (Stewart, 2002).

The Meall Dearg Formation, the focus of this study, is a sandstone so far tentatively considered as entirely fluvial in origin (Stewart, 2002). The formation is best exposed at type sections along the seaboard of Stoer Peninsula and Enard Bay (Figs. 1B–D, 2). These two sections are roughly 250 m and 300 m thick respectively, and both consist of beds dipping westward at 20° to 30°. A minor exposure, not considered in this study but described in Stewart (2002), is located some 30 km to the southwest of Enard Bay, at Rubha Réidh.

2.4 Methods

This study is based on field examinations complemented by classic petrography. Fieldwork on coastal outcrops exposed on the north-western Scottish seaboard was undertaken in May 2016. Data collection consisted of targeted rock sampling for petrographic analysis, analysis of sedimentary facies and relative associations, systematic collection of palaeocurrent indicators, stratigraphic bed-by-bed logging, and line-drawing of panels for architectural reconstructions along cliff exposures.

Sixteen sandstone hand samples were thin sectioned for petrographic assessment, using rigorous counting procedures (Chayes, 1956). Grain size, rounding, sorting, and lithology (i.e. quartz, feldspar, and rock fragments) were recorded on 75 point counts per sample, totaling 1200 point counts, and were reported on a QFR diagram using the Folk's (1968) classification. This preliminary and qualitative (cf. Coutand et al., 2006) assessment has since been improved by petrographic analysis of detrital- zircons in the Stoer Group described in Chapter 3.

Five stratigraphic sections, 6 to 85 m thick, were measured: three at Stoer Peninsula (i.e. Stoer 1, 2, 3) and two at Enard Bay (i.e. Enard Bay 1 and 2). Stratigraphic logging and facies analysis was performed in a bed- by-bed fashion following the guidelines of Collinson et al. (2006) and Mountney (2006). Line-drawing and architectural elements analysis was accompanied by palaeocurrent measurements and followed the guidelines of Brookfield (1977), Miall (1994), Miall and Jones (2003), and Eastwood et al. (2012). Palaeocurrent indicators, totaling 435 measurements, were collected along every bedding surface going up section and corrected for tectonic dip directly in the field. Palaeocurrent vectors and directions were based on: fluvial foreset-dip direction of cross-beds (planar and trough) and of ripple cross-laminae (McKee and Weir, 1953; High and Picard, 1974;); aeolian cross-laminae and their relations to bounding surfaces (cf. Brookfield (1977); and trends of symmetrical ripple crests recording wave passages in planview (Clifton, 2006). Styles of macroform outbuilding were inferred based on the angle between the dip of accretionary surfaces and local palaeoflow (cf. Miall, 1994; Long, 2006, 2011; Ielpi and Rainbird, 2015), as follows: <60°, down-flow accretion; 60–120°, mixed down-flow/lateral accretion; and 120–180°, up-flow accretion.

2.5 Facies associations

Three facies associations (totalling seventeen facies) were identified and logged (Figs. 3 and 4), and later related to three different depositional settings. Sedimentary facies related to waterflows and airflows are summarised in Tables 1 and 2, respectively, with some facies occurring in multiple associations. The erosional stratigraphic base of the Meall Dearg Formation is exposed at both Stoer Peninsula and Enard Bay, whereas the stratigraphic top has been removed by erosion.

2.5.1 Erosively bounded, cross-stratified-dominated arkose and lithic arkose

This facies association composes the entire sections of Stoer 1 and 2 (Fig. 3), and also occurs at the top of section Enard Bay 2. Deposits are composed of ~95% sandstone with subordinate gravel and mudstone, with their features summarised in Table 1. Thin sectioned samples reveal that the sandstone consists of arkose and lithic arkose with moderate to good sorting (Fig. 5). One sample representative of the lowermost, gravel-rich Meall Dearg Formation consists of a poorly sorted feldspathic litharenite that is rich in gneiss and quartz granules. Grains are dominantly sub-angular to sub-rounded, with low to medium sphericity (Fig. 6A–B). Interstitial material consists of iron-oxide cement and, less commonly, quartz cement or voids.

Approximately 50% of the exposed sections consist of planar cross-stratified deposits (Fpx), 0.1–0.8 m thick, often with asymptotic bases concordant with the lower bounding surfaces. Another 30% is represented by plane beds (Fpb) that exhibit primary current lineation in planview (Fig. 6D). Also common are bedforms with undulatory plane-parallel stratification and asymmetric crests (Fab), the latter point to upstream migration with respect to adjacent cross-beds. These undulatory bedforms are 0.4 m in amplitude

and ~1.2 m in wavelength, and are in places soft-sediment deformed (dewatering structures and contorted, disrupted strata) at their core (Fig. 6E). Trough cross-stratified deposits are subordinate, and occur in both solitary sets (Ftx) and within compound cross-stratified beds ~1.5 m thick (Fcx) (Figs. 7–8). Small undulatory plane-parallel stratified bedforms (~0.1 m thick) are seldom preserved within compound cross-stratified beds (Fig. 6C). Less common but still significant are: soft-sediment deformed beds (Fsd; Fig. 7), consisting of contorted, disrupted strata; sand dykes and syn-depositional faults offsetting ~0.2 m are also observed (Fig. 6F); cross-laminated sets, 0.1–0.5 m thick, with unidirectional ripples (Frl; Fig. 6G); and symmetrically rippled beds, ~0.05 m thick (Fwr). Massive, structureless sandstone in beds ~0.05 m thick (Fms) and weathered mudstone in beds ~0.1 m thick (Fwm) are limited to a few occurrences.

The architecture of this facies association is denoted by stacked tabular beds that are 0.5 to 2 m thick (Figs. 7–8), and organised in bedsets 5–10 m thick bounded by sharp non-erosional surfaces (sensu Allen, 1963); these sharp non-erosional surfaces exhibit desiccation cracks (Fig. 6H), and preserve wave ripples in planview. Individual beds are bounded by either flat gradational surfaces or, more often, by sub-planar, irregular erosional boundaries, the latter with ~0.6 m of erosional relief over 5 m along strike. Compound cross-stratified beds contain inclined surfaces that can be both accretionary and erosional; in both cases, these surfaces dip down-flow with respect to the cross-bed laminae (Fig. 8).

2.5.2 Interpretation: fluvial channel-belts

The abundance of arkose with sub-angular to sub-rounded grains, low to medium sphericity, and moderate to good sorting is indicative of a proximal sediment source, i.e.

limited duration of sediment transport, reworking, and chemical weathering (Allen, 1982). This is consistent with the local concentration of gneissic gravel likely derived from the nearby Archean basement rocks. The wide spectrum of represented grain sizes and sedimentary facies points to waterflows with variable strengths and regimes. Specifically, supercritical flows are recorded by planar-stratified deposits with primary current lineation and by undulatory plane-parallel stratified bedforms interpreted to represent antidunes (Fielding, 2006). Transitional, sub-critical to critical flows are responsible for the deposition of planar cross-beds with curved foresets and tangential bases (Røe and Hermanssen, 2006). The tabular geometry and lateral continuity of the facies points to limited flow confinement, i.e. deposition in mobile belts of shallow and wide channels (Skelly et al., 2003). Local concentrations of pebbles in these deposits indicate flow strength sufficient to entrain gravel, likely with processes of rolling or passive transport during substrate shift (Stear, 1983). More confined flow (likely contained in deeper/narrower channel-belts) are instead recorded by trough cross-stratified and compound cross- stratified beds (Harms et al., 1975; Rainbird, 1992). Inclined accretionary and erosional surfaces in compound cross-stratified beds are interpreted to represent, respectively, outgrowth and reworking of in-channel bars (Haszeldine, 1983). The absence of scoop-shaped scours suggests that drainage focusing along stable conduits did not occur. The relationships between local palaeoflow and accretionary surface attitude indicate downstream-bar migration (Fig. 8). While these confined flows were for the most part sub-critical, small-scale undulatory bedforms (i.e. antidunes) within compound cross-stratified beds suggest discharge fluctuations sharp enough to record episodic super-critical regimes (Fielding et al., 2009). Ripple-cross

laminated deposits are consistent with both late-stage filling of channelised depressions (Ielpi et al., 2014), or with rapidly waning and expanding flows at channel terminations (Tunbridge, 1984).

Accessory facies such as soft-sediment deformed beds indicate the fluidisation and sudden dewatering of cohesion-less sediment (based on the abundance of dewatering structures; Owen et al., 2011; Owen and Santos, 2014), while massive beds indicate depositional immobilisation of dense, bedload-dominated sand flows (Reading and Collinson, 1996). Finally, thin wave-ripple cross-laminated beds and weathered mudstone relate to transitory breaks in sedimentation, when wave agitation in wind-swept ponds (Clifton, 2006), or sub-aerial exposure of the sediment surface (Kraus and Gwinn, 1997), took place respectively.

2.5.3 Wave-ripple bounded, cross-stratified-dominated arkose

This facies association is entirely represented by sandstone, ranging from fine- to coarse-grained (Table 1). It encompasses the entire section of Stoer 3 (Fig. 3). Thin-sectioned samples reveal that the sandstone consists entirely of arkose with moderate sorting and slightly higher mineralogical maturity than the fluvial channel-belt facies association, i.e. very rare to absent lithics (Fig. 5). The arkose exhibits a rhythmic alternation between finer-grained, well-sorted (Fig. 9A), and coarser-grained, poorly-sorted (Fig. 9B) laminae. Overall, grains range from sub-angular to rounded, with variable degrees of sphericity, locally high. Interstitial material consists of iron oxide, quartz-feldspar, and less commonly calcite cement.

Symmetrically ripple-cross laminated sandstone (Fwr) is ubiquitous, and composes

roughly 25% of the exposed sections (Fig. 3). Symmetrically rippled sandstone is observed in discrete beds ~0.7 m thick (Fig. 9C), or along most stratal boundaries (Fig. 9D). Planar-cross bedded sandstone (Fpx) and compound cross-bedded sandstone (Fcp) each comprise ~15% of the facies association, and occur in beds 0.1– 2.3 m thick. Individual cross-beds are seldom soft-sediment deformed (Fig. 9E), and exhibit low-angle foresets in places. Compound cross-beds also contain rare undulatory, plane-parallel stratified bedforms (Fig. 9F). Also common (~11% of the facies association) is planar- bedded sandstone (Fpb), in beds 0.1–1.4 m thick (Fig. 9G). Rare but still significant are: trough cross-bedded sandstone (Ftx), in beds ~1.2 m thick and with minor soft-sediment deformation; sets ~0.6 m thick of three-dimensional and low-relief, symmetrically rippled sandstone (Fcr) (Fig. 9H); beds ~0.4 m thick of massive sandstone (Fms); and beds ~0.7 m thick of asymmetrically rippled sandstone (Frl).

Deposits of this facies association are composed of stacked tabular beds typically ~2 m thick (Fig. 10). Single beds are in most cases bounded by flat, non-erosional surfaces with symmetrical ripples preserved. Truncation surfaces are similarly sub-horizontal, and display a scalloped erosional topography with up to 1 m of relief over 5 m along strike. The inclined surfaces contained within compound cross-beds are uniformly dipping in a direction consistent with local palaeoflow, indicating downstream accretion (Fig. 10).

2.5.4 Interpretation: floodbasins

While some of the facies recognised at section Stoer 3 also typify the fluvial channel-belt facies association, the establishment of an altogether separate facies association is warranted based on: distinct petrographic aspects, ubiquitous structures related to oscillatory flows, and distinct stratal architecture. Moderately sorted arkose with sub-

angular to sub-rounded grains is overall indicative of transport by waterflows, although the scarcity of lithics and locally high sphericity is indicative of enhanced reworking (Allen, 1982). The well-defined alternation of laminae with different grade and sorting suggests rhythmic fluctuations in transport energy, possibly due to agitation in standing waterbodies. Also, the widespread occurrence of symmetrical ripples in discrete beds or along stratal boundaries related to oscillatory flows generated by wave agitation in shallow waters (Clifton, 2006). These elements are in principle consistent with either a shallow lacustrine settings within the wave base (Basilici, 1997) or with a fluvial extra-channel environment subject to temporary flooding, such as a floodbasin fed by distributary channels (Tunbridge, 1984; Ielpi, 2012; Assine et al., 2015). While a proper distinction between shallow lakes and floodbasins is to some extent semantic, the second option – floodbasin – is preferred since the facies association lacks any mud, which is instead a major component of lacustrine strata preserved elsewhere in the Stoer Group (Stewart, 2002; Ielpi et al., 2016).

Wave reworking is recorded along most stratal boundaries, indicating recurrent bed agitation in between sedimentation episodes. Elsewhere, stacks of symmetrically rippled sandstone indicate more thorough reworking by waves during sediment delivery. In places, three-dimensional symmetrical ripples indicate the combination of oscillatory and unidirectional flows (Perillo et al., 2014). Fluvial-dominated sedimentation episodes are recorded by the deposition of compound cross-bedded, planar cross-bedded, and trough cross-bedded sandstone, all indicative of unidirectional, lower-regime waterflows (MacNaughton et al., 1997; Hadlari et al., 2006; Ahmed et al., 2014). Specifically, trough cross-beds relate to the accretion of 3D dunes in somewhat confined settings, such as

distributary channels (MacNaughton et al., 1997; Hadlari et al., 2006; Cain and Mountney, 2009). Planar cross-beds indicate less confined waterflows, and may be related to the accretion of 2D dunes within wide distributary channels or to the progradation of splay complexes (Mjøs et al., 1993; Fisher et al., 2008; van Toorenenburg et al., 2016). Transitional to upper-flow regimes are recorded by low-angle cross-beds and antidunes within compound cross-beds, respectively (Fielding, 2006). Also consistent with episodic high-energy conditions are plane-parallel laminated beds and soft-sediment deformed cross-beds, the latter related to a combination of fast dewatering after sediment-load drop or to flow-induced shearing (Jackson, 1975; Røe and Hermanssen, 2006; Owen and Santos, 2014). Other facies such as massive and asymmetrically rippled sandstone indicate depositional freezing of bedload-dominated events and traction/fallout during lower regime flows, respectively; both of these facies can be interpreted as either part of distributary-channel fills, or as the product of bedload-dominated flows feeding splay complexes.

2.5.5 Large-scale, tangential cross-stratified-dominated arkose

This facies association consists of six sedimentary facies and is entirely represented by sandstone, ranging from fine- to coarse-grained (Fig. 11; Table 2). This association composes the entire section of Enard Bay 1, and the lower section at Enard Bay 2 (Figs. 4 and 12A–B, E). Thin-sectioned samples reveal that the sandstone consists exclusively of arkose (Fig. 5) with good sorting, closed packing, and rare quartz cement (Figs. 11A–C and 12E). Grains are dominantly sub-rounded and less commonly either sub-angular or very well rounded (Fig. 11A–B). Grains exhibit variable degrees of sphericity (both low and high). Interstitial material consists of equally common oxide and quartz-feldspar

cement.

Approximately 95% of the exposed sections at Enard Bay consist of large-scale (~5 m thick) planar cross-beds (Alx; Fig. 11D) displaying persistent and monotonous lamination defined by a sharp grain size segregation, identified directly in the field as pin-stripe lamination (Figs. 11E and 12D). Laminated foresets dip at either high angles (~30°) or low angles (~5°), and tangential toesets are common in both cases (Fig. 11F). Subordinate plane-parallel laminated sandstone beds (Apb), ~ 1.1 m thick, compose roughly 4% of the facies association, and likewise exhibit pin-stripe lamination. Soft-sediment deformation is observed preferentially as small-scale (~0.1 m thick) contorted stratification (Fig. 11G) within the Alx facies; small-scale syn-depositional faulting (Fig. 12F) is also pervasive nearby the erosional contact with fluvial deposits. Large-scale soft-sediment deformation (i.e. ~1 m thick) has instead been observed in rare instances (Fig. 4). Found along stratal boundaries, although less common, are ~10 mm-thick wave-rippled sandstone (Awr) and sandstone with adhesion warts (Aaw), the latter associated with soft-sediment deformation. Adhesion-rippled sandstone (Aar) is limited to a single occurrence within a thick Alx bed (Fig. 4) floored by poorly defined desiccation structures (Fig. 11H).

The architecture of this facies association is denoted by large-scale cross-beds bounded by a hierarchy of erosional surfaces (Figs. 13 and 14), as follows: (i) inclined boundaries separating foresets with a slightly different dip direction; (ii) inclined boundaries, extending for as much as 30 m along strike and featuring a curved attitude, and truncating individual cross-beds; the attitude of these bounding surfaces defines angles of 60°–150° with the dip direction of cross-beds (Figs. 13 and 14); (iii) large-scale sub-planar

boundaries, observed for as much as 150 m along strike, displaying up to 0.5 m of erosional relief over 20 m along strike, and truncating all other bounding surfaces.

2.5.6 Interpretation: aeolian ergs

The dominance of arkose with good sorting, sub-rounded grains, and local high sphericity is indicative of prolonged sediment reworking and selective mechanisms of transport (Allen, 1982). Strong compaction likely removed any evidence of original open framework. These features are typically associated with wave-swept coastal environments, very distal fluvial settings, or aeolian settings; the latter hypothesis is preferred based on the distinctive occurrence of pin-stripe lamination (Fryberger and Schenk, 1988), large-scale cross-bedding, and adhesion structures. The observed spectrum of facies points to a range of wind regimes: low wind strengths are recorded by the high-angle Alx cross-beds, which point to a combination of grain-flow, grain-fall, and wind-ripple migration along high-relief dunes. By comparison, transitional to high wind strengths are recorded by the low-angle Alx cross-beds, which can be related to dominant grain-fall processes during migration of low-relief aeolian bedforms (Chakraborty, 1991). In both cases, tangential toesets are indicative of smoothing of the lower dune face by sustained winds. Sand sheets recorded by facies Apb, although subordinate, indicate that even higher-strength winds were associated with sediment bypass or build-up of planar wind-ripple beds (Kocurek and Fielder, 1982; Dal' Bó and Basilici, 2015). Based on their attitude and hierarchy relative to accepted classifications (Brookfield, 1977; Fryberger, 1993; Mountney, 2006), bounding surfaces separating foresets (i) are related to dune re-activation; bounding surfaces separating cross-beds (ii) are related to dune superimposition; and higher-order bounding surfaces (iii) can be related to either

processes of interdune migration or erg deflation. At the current scale of exposure, little can be said regarding the prevalent dune geometry, even though clustered dip directions of cross- beds might indicate transverse morphology (Mountney and Jagger, 2004; Collinson et al., 2006).

A number of features indicate that the sediment substrate was at times cohesive due to dampness. Aar (ripples) and Aaw (warts) record the adhesion of dry sand onto humid surfaces during consistent and changing winds, respectively (Kocurek and Fielder, 1982; Mountney, 2006). Soft-sediment deformation requires a moderate degree of cohesion during episodes of localised dune lee-side slope failure (at small scales; Cain and Mountney, 2009) or, at larger scales, in response to dune overriding along a saturated surface (Doe and Dott, 1980) or possibly even seismic shaking (Bryant and Miall, 2010). Temporary damp conditions and sand cohesion may have been favoured by a number of factors, including increased atmospheric humidity, episodic rainfall, or a groundwater table shallow enough to allow for evapotranspiration (Doe and Dott, 1980; Mountney, 2006). In any event, the presence of a groundwater table, seldom emerging along interdune areas, is recorded by desiccation structures and wave ripples (Mountney and Thompson, 2002).

2.6 Palaeogeography

Inferences on the palaeogeography of the Stoer Group rift basin at times of Meall Dearg deposition can be extrapolated from regional facies distribution and from the comparison of sediment dispersal patterns (Fig. 15). Exposures of the Stoer Group are roughly aligned along a north-south transect (Fig. 2), which represents a section near-normal to regional sediment dispersal (Fig. 15). The nonconformity flooring the Stoer Group

defines two main depressions (at Stoer Peninsula and Poolewe, respectively), separated by a basement high at Enard Bay (Fig. 2). Field relationships (Figs. 1D and 2; see also Stewart, 2002) suggest that such basement high likely acted as a significant topographic confinement during times of deposition of the lower Stoer Group (i.e. Clachtoll and Bay of Stoer formations), and was progressively buried during the deposition of the Meall Dearg Formation. As a consequence, the basement relief observed between Enard Bay and Stoer Peninsula is not the result of post-depositional deformation, suggesting that fluvial and aeolian systems might have co-existed and shared lateral relationships during basin filling. Evidence of coeval fluvial and aeolian deposition is validated by the direct juxtaposition of the Meall Dearg Formation atop the Poll a' Mhuilt Member (a key red bed) observed at Stoer Peninsula (fluvial associated) and Enard Bay (aeolian associated). Exposures of direct fluvial-aeolian interaction is present in the uppermost section at Enard Bay (Fig. 12).

At Stoer Peninsula (Fig. 15), fluvial palaeoflows from planar cross-bedding (Fpx), trough cross-bedding (Ftx), and asymmetrically ripple cross-laminated beds (Frl) together yield a focused, unimodal distribution towards the WSW (Stoer 1) and W (Stoer 2). Floodbasin palaeoflows collected at Stoer 3 yield a more dispersed, unimodal distribution to the NW. At the same section, wave-ripples are indicative of surface-wave agitation along the NNW-SSE. Unidirectional palaeoflow indicators at Stoer Peninsula reveal a gradual northward increase of palaeoflow dispersion (Fig. 15).

At Enard Bay, aeolian palaeoflows from cross-laminated beds yield a consistently western, focused palaeowind direction (Enard Bar 1 and 2; Fig. 15). Superimposition surfaces in between aeolian cross-beds reveal focused, yet polymodal attitudes, with a

prevalent dip towards the north-northeast. In other words, superimposition surfaces dip in most cases in a direction near-perpendicular to that of aeolian transport (Fig. 15). A small dataset of fluvial palaeoflows at Enard Bay indicates mildly dispersed WSW-ward transport. By comparison, palaeoflow indicators collected on cross-beds at Rubha Reidh by Stewart (2002) indicates SE-ward transport (his fig. 17; Fig. 15). Wave-ripple crests at the same section trend along a NW-SE direction, a direction that is at high angles to the measurements at section Stoer 3.

2.7 Discussion

Fluvial channel-belts, floodplains, and aeolian ergs have been rarely documented together within individual pre-vegetation rock units (Aspler and Chiarenzelli, 1997; Hadlari et al., 2006; Almeida et al., 2009; Simpson et al., 2012), and evidence of their interaction is fundamental for shedding light on the dynamics of pre-vegetation landscapes. In this context, the facies associations and palaeogeography of the Meall Dearg Formation are discussed here in terms of depositional style and significance for inferring climate regimes from clastic records.

2.7.1 Depositional style

Current understanding is that the Stoer Group deposited within a rift basin, possibly a half graben, the flanks of which were likely located along the current traces of the Moine thrust and Minch fault (Stewart, 2002). Despite some degree of tectonism inferred during the deposition of the Stoer Group – based on palaeocurrent reversals, regional downwarping of strata (Stewart, 2002), and evidence of syn-depositional faulting (Beacom et al., 1999) – the Meall Dearg Formation likely represents a late stage of rift filling, something classically related to tectonic near-quiescence and reduced palaeo-

slope (Leeder and Gawthorpe, 1987; Prosser, 1993; Pascucci et al., 1999). That being said, prominent local basement topography – and thus steeper palaeo-slopes – existed locally at Enard Bay but became progressively burried (Figs. 1 and 2).

The headwaters of the fluvial channel-belts were located in the eastern flank of the Stoer Group basin, and drained in a direction perpendicular to the basin axis, as expected in lateral systems feeding into an axial drainage (Fig. 16). Above the contrasting mudstone of the Poll a' Mhuilt Member, the overlying Meall Dearg Formation begins with an erosional base and sharp grain size change fining upwards. This is consistent with a sudden equilibration of fluvial gradient following a minor – likely transient – episode of landscape degradation (Attal et al., 2008; Williams and Foden, 2011). By comparison, the remainder of the Meall Dearg Formation exhibits homogenous sediment grade, pointing to a state of dynamic equilibrium between subsidence, aggradation, and sediment supply. These grain size trends can again be related to near-tectonic quiescence that characterises late rifting stages (Martins-Neto, 2000).

The palaeoflow rotation observed up-section at Stoer Peninsula (Fig. 15) may relate to lateral migration along a fluvial system with distributive planform (Chakraborty et al., 2010; Hartley et al., 2010; Weissmann et al., 2010), or to the individuation of a weak across-plain gradient during basin filling (Todd and Went, 1991; Ielpi and Rainbird, 2016). Overall focused fluvial palaeoflow measurements point to limited sinuosity (Fig. 15), in accordance with the sub-parallel relationships between the dip of accretionary surfaces and local palaeoflow in fluvial channel-belts (Fig. 8). The lack of exposures at the km scale hampers a full geometric characterisation of the Meall Dearg channels and, as such, the studied alluvium cannot be confidently framed into any planform stream

classification (e.g., sheet-braided vs. channel-braided). Notwithstanding, the abundance of planar over trough cross-beds indicates that most flows had a poor degree of confinement, as expected in terminal fluvial systems with gentle palaeo-slopes and little constriction (Tunbridge, 1984). This inference is corroborated by the depositional architecture of fluvial deposits, which points to the dominance of tabular sandbodies floored by shallowly erosional surfaces and a lack of high-relief sediment bars (Figs. 7 and 8). Such architectural features have been often documented in pre-vegetation fluvial settings (Davies et al., 2011), although in this specific case they can simply be ascribed to fluvial distality (Fisher et al., 2008; Cain and Mountney, 2009; Fig. 16). This depositional style strikingly differs from that of fluvial channel-belt deposits preserved beneath in the Clachtoll and Bay of Stoer formations and (unconformably) above the Meall Dearg Formation in the Torridon Group (Owen and Santos, 2014; Ielpi and Ghinassi, 2015; Ielpi et al., 2016), again corroborating the distal nature and low regional palaeo-slopes in the later stages of the Stoer Group deposition.

The onset of clastic rather than evaporitic floodbasin conditions in the Stoer Group basin indicates there was a positive hydrologic balance relative to accommodation and sediment supply and allowed for the emergence of a groundwater table in basin depocentral areas (Abels et al., 2009; Fig. 16). While this is clearly recorded at Stoer Peninsula, the abundance of wave-rippled facies at Rubha Réidh (Stewart, 2002) suggests that floodbasin conditions may have established at several locations and times throughout the basin. A population of wave- ripple crests in alluvial settings relates to local winds agitating the surface of temporary waterbodies, as well as to the direction of their shore-lines (Collinson et al., 2006). Wave-ripple crests trend in discordant directions at Stoer

and Rubha Réidh (Fig. 15), and their strike defines oblique to sub-normal angles with the assumed north-south axis of the Stoer Group basin (Stewart, 2002), suggesting that temporary waterbodies in the floodbasins were not topographically constrained (as expected in low-relief settings).

Notably, floodbasin and shallow-lacustrine strata rich in mud fraction are abundant elsewhere in the lower Stoer Group (Ielpi et al., 2016). As such, the sand-dominated character of the floodbasin deposits in the Meall Dearg Formation remains not fully understood, although it can be at least in part explained either with a decline in mud production in the basin due to change in weathering style (e.g., from chemical to physical), or due to the entrainment and bypass of fines by aeolian processes (Dott et al., 1986). The abundance of aeolian facies itself in the Meall Dearg Formation may favour the second hypothesis. Whether the floodbasins recorded in the Meall Dearg Formation represent hydrologically open or closed systems is currently unknown, given the limited amount of available exposure. The lack of evaporite or carbonate deposits, i.e. the clastic dominated nature of the floodbasin facies, suggests an overall positive water budget (Carroll and Bohacs, 1999). Also, the repetitive sedimentary motif defined by cross-beds bounded by wave rippled sets throughout the entire section at Stoer 3 essentially indicates a state of equilibrium between hydrologic recharge, infiltration, and evaporation (Carroll and Bohacs, 1999).

Aeolian deposits at Enard Bay display a motif characterised by: (1) accretion, migration, and reactivation of dunes, with predominantly westward growth; (2) dune superimposition, with the creation of surfaces dipping preferentially towards ENE; (3) deposition of subordinate sand sheets or – rarely – wave-swept interdune strata; and (4)

occasional reworking of aeolian deposits by fluvial systems. This motif can be explained in terms of wind direction, sediment availability, and groundwater table level (Kocurek and Lancaster, 1999). Westward winds overpassing the eastern flank of the Stoer Group basin (Fig. 16) accelerated and gained sufficient strength to entrain sand-grained detritus (Hunt et al., 1988), eventually becoming sediment-saturated. The source area of aeolian sand could have been a blanket of proximal sediment and/or a bedrock exposed to intense abrasion (Mountney and Russell, 2004). It is not excluded that sediment previously reworked by fluvial processes constituted a significant source for aeolian processes, based on the similar petrographic features of fluvial and aeolian sand (Fig. 5). In any event, these westward winds likely expanded and decelerated upon entering the Stoer Group basin (Kocurek and Havholm, 1993), losing strength and thus creating favourable conditions for growth and migration of aeolian bedforms. Superimposition surfaces record the overpassing and stacking of aeolian bedforms (Mountney, 2006), with associated wind perturbations generating some degree of dune erosion. The predominant attitude of superimposition surfaces mimics that of the regional palaeo-slope defined by the basement high at Enard Bay. In any event, high wind-strength and sediment-starved phases are recorded by flat truncation surfaces, which relate to deflation and temporary planation of the aeolian field (Brookfield, 1977). Aeolian sand eroded from the Enard Bay area might have constituted a component of the sediment budget for the fluvial depositional systems located to the north (i.e., Stoer Peninsula).

The majority of observed aeolian facies points to dry processes (Table 2). This was possibly favoured by the proximity to the palaeo-topographic high of Enard Bay (Fig. 2), i.e. a topographic setting elevated above the basin groundwater table for significant

timespans (Mountney, 2006). Minor amounts of facies pointing to damp/wet conditions such as adhesion structures and wave ripples within interdune ponds are however consistent with episodic shallowing or emergence of said groundwater table, possibly during periods of limited aeolian bedform build-up (Crabaugh and Kocurek, 1993), or during wetter seasons. The truncation of aeolian deposits operated by fluvial processes in the upper Meall Dearg Formation at Enard Bay further indicates that the local groundwater table was likely in hydrologic connection with a nearby fluvial system (Fig. 16), capable at times of migrating laterally and reworking aeolian sand (Langford, 1989)

2.7.2 Inferences on climate regimes from clastic Precambrian systems

Inferences on climate from clastic records are often fraught with uncertainty, and require comparison with independent proxies especially when looking into deeper geological time (Frakes et al., 2005). A number of studies have inferred Precambrian climate regimes from either individual (Sønderholm and Tirsgaard, 1998; Bállico et al., 2017) or two interacting clastic depositional systems (Eriksson and Simpson, 1993; Tirsgaard and Øxnevad, 1998). When depositional environments are analysed individually, inferences on climate have uncertainty owing to the overprint of environmental signals by sedimentary transport (Jerolmack and Paola, 2010). In contrast, the analysis of depositional style of multiple depositional environments – in this case fluvial channel-belts, floodbasins, and aeolian ergs – allows to disentangle climate indicators in a more reliable fashion.

Fluvial deposits at Stoer Peninsula and Enard Bay contain abundant transitional- to upper-flow regime structures attributed to high-flow strength and sharp discharge fluctuations, elements typical of ephemeral fluvial systems (Eriksson and Simpson,

1993). In the absence of vegetation, Precambrian hydrologic regimes would have been more sensitive to precipitation events. Some authors proposed that pre-vegetation rivers, lacking any buffer on surface runoff, had ephemeral discharge regimes irrespective of climate (Eriksson et al., 1998; Bose et al., 2012). If correct, the Precambrian fluvial rock record should preserve a major fraction of upper-flow regime structures, which record fast discharge fluctuations. While the Meall Dearg Formation could in principle fit with such model, other studies prompted caution based on the preservation of thick successions pointing to perennial discharge (Rainbird, 1992; Eriksson and Simpson, 1993; Nicholson, 1993; Ielpi and Rainbird, 2016), or even the preservation of deposits pointing to co-eval perennial and ephemeral discharge within the same rock unit (Long, 2006; Marconato et al., 2014), including examples from the lower Stoer Group (Ielpi et al., 2016). The role of catchment area is often neglected despite its relative importance (Syvitski and Milliman, 2007), possibly because ancient catchment areas are difficult to estimate. Basins fed by large catchments with well integrated recharge networks are more likely characterised by perennial baseline discharge, while basins fed by small catchments are more prone to sharp discharge fluctuations (Syvitski et al., 2000, 2014; Dai and Trenberth, 2002). The upward transition throughout the Stoer Group towards progressively more distal and ephemeral fluvial systems may simply indicate catchment-basin shrinkage. This hypothesis would be consistent with the distal depositional settings recorded in the fluvial Meall Dearg facies, and could be related in turn to upland degradation and reduction in catchment area (Cain and Mountney, 2009). That being said, an underlying climate control on fluvial activity might be recorded in the 5–10 m thick rhythms bounded by either wave-ripples or desiccation structures (Fig. 3), elements

tentatively related to fluctuations in groundwater table and hence hydrologic recharge (Abels et al., 2009).

Aeolian deposits at Enard Bay indicate mostly dry conditions at time of deposition (consistent with the scarcity of quartz cement, indicating limited evapotranspiration), with only sporadic evidence of a shallow or emerging groundwater table (Figs. 4 and 11). Decametre-scale rhythms bounded by adhesion structures, soft-sediment deformed deposits, or wave ripples similarly indicate periodic groundwater shallowing or emergence (cf. Bállico et al., 2017; Fig. 4). It is uncertain, however, whether this motif is an effect of climate or, simply, deposition at elevated topography near the Enard Bay basement high (Figs. 2 and 16; Mountney and Howell, 2000). In other words, aeolian deposition in topographically elevated settings above the basin depocentre is expected to be less influenced by the groundwater table, irrespective of actual climate regimes. Finally, the floodbasin deposits at Stoer Peninsula indicate a permanently positive water budget and repeated emergence of the groundwater table, based on widespread structures related to oscillatory flows and lack of desiccation structures (Figs. 3 and 10). Relatively humid climate regimes at times of floodbasin deposition are corroborated by the lack of carbonate or chemical deposits, elements more characteristic of overfilled basins (sensu Carroll and Bohacs, 1999). The hypothesis of humid conditions is also corroborated by geochemical evidence (quartz/[quartz+feldspar] and plagioclase/total feldspar) suggesting temperate settings throughout the Stoer Group deposition (van de Kamp and Leake, 1997). In addition, palaeomagnetic studies place the Stoer Group 10^{o} – 20^{o}N, consistent with today's semi-arid climate zone, marginal to lower tropical-humid climates along the equator (Stewart & Irving, 1974; Stewart, 1991). However, this palaeomagnetic data may

be unreliable because of Mesozoic magnetic overprinting (Stewart, 2002). In synthesis, Precambrian fluvial-channelised and aeolian systems cannot be ultimately considered per se reliable indicators of climate – at least at the local scale – unless the recognition and analysis of coeval floodplain strata is used to corroborate interferences on hydrologic budgets, and thus actual climate regime.

2.8 Conclusions

This research presents an integrated depositional model for the interaction between fluvial channel-belts, floodbasins, and aeolian ergs in a pre-vegetation setting, and discusses these aspects in terms of climate regime. The Meall Dearg Formation, the youngest unit of the ~1.2 Ga Stoer Group, was deposited in a rift basin near the margin of Laurentia (Rainbird et al., 2001). Refined analyses of sedimentology, stratigraphy, and depositional architecture were performed at Stoer Peninsula and Enard Bay, two key locations on the north-western seaboard of the Scottish Highlands. These analyses reveal the record of a range of co-existing terrestrial environments. The deposits of fluvial channel-belts are composed of stacks of tabular, shallowly erosive beds showing features consistent with an ephemeral fluvial system, such as: abundance of transitional- to upper-regime flows, including widespread planar-cross stratification with curved-asymptotic sets, planar-laminated beds, and preserved antidunes; and compound cross-stratified sets indicating accretion and migration of small fluvial bars in shallow, low-sinuosity channels. Floodbasin deposits are characterised by tabular beds preserving wave ripples along their boundaries. These beds are for the most part planar-cross stratified, planar-laminated, or wave-ripple laminated, features indicative of splay complexes prograding into repeatedly flooded ponds. Finally, aeolian deposits consist of pin-stripe laminated

sandstone organised in large-scale planar cross-beds. Aeolian bedforms are bounded by superimposition surfaces and, rarely, by flat deflation surfaces. Scattered preservation of adhesion structures and wet-interdune deposits are reflective of intermountain ergs sporadically subject to damp conditions. Analysis of sediment dispersal indicates dominant westward fluvial transport, likely from uplands bordering the eastern flank of the Stoer Group basin. Similarly, palaeowind directions indicate prevalent west- ward aeolian transport.

Fluctuations in groundwater table might have been recorded by metre- to decametre-scale rhythms in both fluvial and aeolian deposits. However, the integrated analysis of three individual but coeval sedimentary systems reveals that neither ephemeral-fluvial nor dry-aeolian systems are necessarily indicative of any specific climate regime, while the occurrence of clastic floodplain strata containing widespread oscillatory flow structures can be more reliably related to positive hydrologic budgets and thus humid conditions. This inference is in accordance with independent geochemical proxies that portray an overall temperate climate regime for the Stoer Group (van de Kamp and Leake, 1997; Stewart, 2002). This research integrates sedimentological analyses on three coeval and interacting depositional systems, shedding additional light on Mesoproterozoic landscape dynamics.

2.9 Acknowledgements

This work is part of the M. Sc. project of the lead author, and was supported by a Discovery Grant to AI from the Natural Sciences and Engineering Research Council of Canada. Reviewers Philip Fralick (Lakehead University), André Marconato (Universidade Federal de Ouro Preto), and Editor Brian Jones are thanked for stimulating

comments and editorial guidance. Maurício Santos (UFABC) is also acknowledged for commenting on an early draft. Dr. Maarten Krabbendam (British Geological Survey) visited the outcrops with the authors and is thanked for stimulating discussions.

2.10 References

Abels, H.A., Aziz, H.A., Ventra, D., Hilgen, F.J., 2009. Orbital climate forcing in mudflat to marginal lacustrine deposits in the Miocene Teruel Basin (Northeast Spain). Journal of Sedimentary Research 79, 831–847.

Ahmed, S., Bhattacharya, J.P., Garza, D.E., Li, Y., 2014. Facies architecture and stratigraphic evolution of a river-dominated delta front, Turonian Ferron Sandstone, Utah, U.S.A. Journal of Sedimentary Research 84, 97–121.

Allen, J.R.L., 1963. The classification of cross-stratified units with notes on their origin. Sedimentology 2, 93–114.

Allen, J.R.L., 1982. Sedimentary Structures, Their Character and Physical Basis. Elsevier, Amsterdam (Netherlands) (593 pp.).

Almeida, R.P., Janikian, L., Fragoso-Cesar, A.R.S., Marconato, A., 2009. Evolution of a rift basin dominated by subaerial deposits: the Guaritas Rift, Early Cambrian, Southern Brazil. Sedimentary Geology 217, 30–51.

Amor, K., Hesselbo, S.P., Porcelli, D., Thrackrey, S., Parnell, J., 2007. A Precambrian proximal ejecta blanket from Scotland. Geology 36, 303–306.

Aspler, L.B., Chiarenzelli, J.R., 1997. Initiation of ~2.45–2.1 Ga intracratonic basin sedimentation of the Hurwitz Group, Keewatin Hinterland, Northwest Territories, Canada. Precambrian Research 81, 265–297.

Aspler, L.B., Chiarenzelli, J.R., Bursey, T.L., 1994. Ripple marks in quartz arenites of the Hurwitz Group, Northwest Territories, Canada: evidence for sedimentation in a vast, early Proterozoic, shallow, fresh-water lake. Journal of Sedimentary Research A64, 282–298.

Assine, M.L., Merino, E.R., Pupim, F.M., Macedo, H.A., Santos, M.G.M., 2015. The Quaternary alluvial systems tract of the Pantanal Basin, Brazil. Brazilian Journal of Geology 45, 475–489.

Attal, M., Tucker, G.E., Whittaker, A.C., Cowie, P.A., Roberts, G.P., 2008. Modeling fluvial incision and transient landscape evolution: influence of dynamics channel adjustment. Journal of Geophysical Research, Earth Surface 113, JF000893.

Bállico, M.B., Scherer, C.M.S., Mountney, N.P., Souza, E.G., Reis, A.D., Raja Gabaglia, G.P., Magalhães, A.J.C., 2017. Sedimentary cycles in a Mesoproterozoic aeolian erg-margin succession: Mangabeira Formation, Espinhaço Supergroup, Brazil. Sedimentary Geology 349, 1–14.

Basilici, G., 1997. Sedimentary facies in an extensional and deep-lacustrine deposi- tional system: the Pliocene Tiberino Basin, Central Italy. Sedimentary Geology 109, 73–94.

Beacom, L.E., Anderson, T.B., Holdswroth, R.E., 1999. Using basement-hosted clastic dykes as syn-rifting palaeostress indicators: an examples from the basal Stoer Group, northwest Scotland. Geological Magazine 136, 301-310.

Bose, P.K., Eriksson, P.G., Sarkar, S., Wright, D.T., Samanta, P., Mukhopadhyay, S.,

Mandal, S., Banerjee, S., Altermann, W., 2012. Sedimentation patterns during the Precambrian: a unique record? Marine and Petroleum Geology 33, 34–68.

Brasier, A.T., Culwick, T., Battison, L., Callow, R.H.T., Brasier, M.D., 2016. Evaluating evidence from the Torridonian Supergroup (Scotland, UK) for eukaryotic life on land in the Proterozoic. In: Brasier, A.T., McIlroy, D., McLoughlin, N. (Eds.), Earth Systems Evolution and Early Life: A Celebration of the Work of Martin

Brasier. Geological Society, London, Special Publication vol. 448 (doi: 10.1144:SP448.13).

Brookfield, M.E., 1977. The origin of bounding surfaces in ancient aeolian sandstones. Sedimentology 24, 303–332.

Bryant, G., Miall, A., 2010. Diverse products of near-surface sediment mobilization in an ancient eolianite: outcrop features of the early Jurassic Navajo Sandstone. Basin Research 22, 578–590.

Bullard, J.E., McTanish, G.H., 2003. Aeolian-fluvial interactions in dryland environments: examples, concepts and Australia case study. Progress in Physical Geography 27, 471–501.

Burr, D.M., Perron, J.T., Lamb, M.P., Irwin, R.P., Collins, G.C., Howard, A.D., Sklar, L.S., Moore, J.M., Ádámkovics, M., Baker, V.R., Drummond, S.A., Black, B.A., 2013. Fluvial features on Titan: insights from morphology and modeling. Geological Society of America Bulletin 125, 299–321.

Cain, S.A., Mountney, N.P., 2009. Spatial and temporal evolution of a terminal fluvial fan system: the Permian Organ Rock Formation, South-east Utah, USA. Sedimentology 56, 1774–1800.

Carroll, A.R., Bohacs, K.M., 1999. Stratigraphic classification of ancient lakes: balancing tectonic and climate controls. Geology 27, 99–102.

Chakraborty, T., 1991. Sedimentology of a Proterozoic erg: the Venkatpur Sandstone, Pranhita-Godvari Valley, south India. Sedimentology 38, 301–322.

Chakraborty, T., Kar, R., Ghosh, P., Basu, S., 2010. Kosi megafan: historical records, geomorphology and the recent avulsion of the Kosi River. Quaternary International 227, 143–160.

Chayes, F., 1956. Petrographic Modal Analysis. Jon Wiley & Sons Inc., New York (USA) (139 pp.).

Clifton, H.E., 2006. A re-examination of facies models for clastic shorelines. In: Posamentier, H.W., Walker, R.G. (Eds.), Facies Models Revisited. SEPM Special Publication vol. 84, pp. 293–337.

Collinson, J.D., Mountney, N.P., Thompson, D.B., 2006. Sedimentary Structures. Terra Publishing, Enfield (UK) (292 pp.).

Coutand, I., Carrapa, B., Deeken, A., Schitt, A.K., Sobel, E., Strecker, M.R., 2006. Propagation of orographic barriers along an active range front: insights from sandstone petrography and detrital apatite fission-track thermochronology in the

intramontane Angastaco basin, NW Argentina. Basin Research 18, 1–12.

Crabaugh, M., Kocurek, G., 1993. Entrada sandstone: an example of a wet aeolian system. In: Pye, K. (Ed.), The Dynamics and Environmental Context of Aeolian Sedimentary Systems. Geological Society, London, Special Publication vol. 72, pp. 103–126.

Dai, A., Trenberth, K.E., 2002. Estimates of freshwater discharge from continents: latitudinal and seasonal variations. Journal of Hydrometeorology 3, 660–687.

Dal' Bó, P.F.F., Basilici, G., 2015. Intermontane eolian sand sheet development, Upper Tulum Valley, central-western Argentina. Brazilian Journal of Geology 45, 97–115.

Davies, N.S., Gibling, M.R., Rygel, M.C., 2011. Alluvial facies evolution during the Palaeozoic greening of the continents: case studies, conceptual models and modern analogues. Sedimentology 58, 220–258.

Doe, T.W., Dott, R.H., 1980. Genetic significance of deformed cross bedding—with examples from the Navajo and Weber Sandstones of Utah. Journal of Sedimentary Petrology 50, 793–811.

Dott Jr., R.H., Byers, C.W., Fielder, G.W., Stenzel, S.R., Winfree, K.E., 1986. Aeolian to marine transition in Cambro-Ordovician cratonic sheet sandstones of the northern Mississippi Valley, U.S.A. Sedimentology 33, 345–367.

Eastwood, E.N., Kocurek, G., Mohrig, D., Swanson, T., 2012. Methodology for

reconstructing wind direction, wind speed and duration of wind events from aeolian cross-strata. Journal of Geophysical Research - Earth Surface 117. http://dx.doi.org/ 10.1029/2012JF002368.

Eriksson, K.A., Simpson, E.L., 1993. Siliciclastic braided-fluvial sediments intercalated within continental flood basalts in the Early to Middle Proterozoic Mount Isa Inlier, Australia. In: Marzo, M., Puigdefábregas, C. (Eds.), Alluvial Sedimentation. Special Publications of the International Association of Sedimentologists vol. 17, pp. 473–488.

Eriksson, P.G., Condie, K.C., Tirsgaard, H., Mueller, W.U., Altermann, W., Miall, A.D., Aspler, L.B., Catuneanu, O., Chiarenzelli, J.R., 1998. Precambrian clastic sedimentation systems. Sedimentary Geology 120, 5–53.

Eriksson, P.G., Martins-Neto, M.A., Nelson, D.R., Aspler, L.B., Chiarenzelli, J.R., Catuneanu, O., Sarkar, S., Altermann, W., Rautenbach, C.J. de W., 2001. An introduction to Precam- brian basins: their characteristics and genesis. Sedimentary Geology 141–142, 1–35.

Eriksson, P.G., Bumby, A.J., Popa, M., 2004. Sedimentation through time. In: Eriksson, P.G., Altermann, W., Nelson, D.R., Mueller, W.U., Catuneanu, O. (Eds.), The Precambrian Earth: Tempos and Events. Developments in Precambrian Geology vol. 12, pp. 593–680.

Fielding, C.R., 2006. Upper flow regime sheets, lenses and scour fills: extending the range of architectural elements for fluvial sediment bodies. Sedimentary Geology

190, 227–240.

Fielding, C.R., Allen, J.P., Alexander, J., Gibling, M.R., 2009. Facies model for fluvial systems in the seasonal tropics and subtropics. Geology 37, 623–626.

Fisher, J.A., Krapf, C.B.E., Lang, S.C., Nichols, G.J., Payemberg, T.H.D., 2008. Sedimentology and architecture of the Douglas Creek terminal splay, Lake Eyre, central Australia. Sedimentology 55, 1915–1930.

Folk, R.L., 1968. Petrology of Sedimentary Rocks. Hemphill Publishing Co., Austin (USA) (182 pp.).

Frakes, L.A., Francis, J.E., Syktus, J.I., 2005. Climate Modes of the Phanerozoic. Cambridge University Press, Cambridge (UK) (275 pp.).

Fralick, P., Zaniewski, K., 2012. Sedimentology of a wet, pre-vegetation floodplain assemblage. Sedimentology 59, 1030–1049.

Fryberger, S.G., 1993. A review of aeolian bounding surfaces, with examples from the Permian Minnelusa Formation, USA. In: North, C.P., Prosser, D.J. (Eds.), Characterization of Fluvial and Aeolian Reservoirs. Geological Society, London, Special Publication vol. 73, pp. 167–197.

Fryberger, S.G., Schenk, C.J., 1988. Pin stripe lamination: a distinctive feature of modern and ancient eolian sediments. Sedimentary Geology 55, 1–15.

Gracie, A.J., Stewart, A.D., 1967. Torridonian sediments at Enard Bay, Ross-shire. Scottish Journal of Geology 3, 181–194.

Hadlari, T., Rainbird, R.H., Donaldson, J.A., 2006. Alluvial, eolian and lacustrine sedimentology of a Paleoproterozoic half-graben, Baker Lake Basin, Nunavut, Canada. Sedimentary Geology 190, 47–70.

Harms, J.C., Southard, J.B., Walker, R.G., 1975. Depositional environments as interpreted from sedimentary structures and stratification sequences. SEPM Short Course 9 (249 pp.).

Hartley, A.J., Weissmann, G.S., Nichols, G.J., Warwick, G.L., 2010. Large distributive fluvial systems: characteristics, distribution, and controls on development. Journal of Sedimentary Research 80, 167–183.

Haszeldine, R.S., 1983. Fluvial bars reconstructed from a deep, straight channel, upper Carboniferous coalfield of northeast England. Journal of Sedimentary Petrology 53, 1233–1247.

High Jr., L.R., Picard, M.D., 1974. Reliability of cross-stratification types as paleocurrent indicators in fluvial rocks. Journal of Sedimentary Research 44, 158–168.

Horowitz, D.H., 1982. Geometry and origin of large-scale deformation structures in some ancient wind-blown sand deposits. Sedimentology 29, 155–180.

Hunt, J.C.R., Leibovich, S., Richards, K.J., 1988. Turbulent shear flows over low hills. Quarterly Journal of the Royal Meteorological Society 114, 1435–1470.

Ielpi, A., 2012. Anatomy of major coal successions: facies analysis and sequence stratigraphy of a brown coal-bearing valley fill to lacustrine tract (Upper Valdarno

Basin, Northern Apennines, Italy). Sedimentary Geology 265–266, 163–181.

Ielpi, A., 2016. Lateral accretion of modern unvegetated rivers: remotely sensed fluvial-aeolian morphodynamics and perspectives on the Precambrian rock record. Geological Magazine http://dx.doi.org/10.1017/S001675681600025X.

Ielpi, A., Ghinassi, M., 2015. Planview style and palaeodrainage of Torridonian channel belts: Applecross Formation, Stoer Peninsula, Scotland. Sedimentary Geology 325, 1–16.

Ielpi, A., Rainbird, R.H., 2015. Architecture and morphodynamics of a 1.6 Ga fluvial sandstone: Ellice Formation of Elu Basin, Arctic Canada. Sedimentology 62, 1950–1977.

Ielpi, A., Rainbird, R.H., 2016. Highly variable Precambrian fluvial style recorded in the Nelson Head Formation of Brock Inlier (Northwest Territories, Canada). Journal of Sedimentary Research 86, 199–216.

Ielpi, A., Gibling, M.R., Bashforth, A.R., Lally, C., Rygel, M.C., Al-Silwadi, S., 2014. Role of vegetation in shaping Early Pennsylvanian braided rivers: architecture of the Boss Point Formation, Atlantic Canada. Sedimentology 61, 1659–1700.

Ielpi, A., Ventra, D., Ghinassi, M., 2016. Deeply channelled Precambrian rivers: remote sensing and outcrop evidence from the 1.2 Ga Stoer Group of NW Scotland. Precambrian Research 281, 291–311.

Jackson II, R.G., 1975. Hierarchical attributes and a unifying model of bed forms

composed of cohesionless material and produced by shearing flow. Geological Society of America Bulletin 86, 1523–1533.

Jerolmack, D.J., Paola, C., 2010. Shredding of environmental signals by sediment transport.Geophysical Research Letters 37, L19401.

Jopling, A.V., Walker, R.G., 1968. Morphology and origin of ripple-drift cross-lamination, with examples from the Pleistocene of Massachusetts. Journal of Sedimentary Petrology 38, 971–984.

Jorgensen, P.J., Fielding, C.R., 1996. Facies architecture of alluvial floodbasin deposits: three-dimensional data from the Upper Triassic Callide Coal Measures of east-central Queensland, Australia. Sedimentology 43, 479–495.

van de Kamp, P.C., Leake, B.E., 1997. Mineralogy, geochemistry, provenance, and sodium metasomatism of Torridonian rift basin clastic rocks, NW Scotland. Scottish Journal of Geology 33, 105–124.

Kocurek, G., Fielder, G., 1982. Adhesion structures. Journal of Sedimentary Petrology 52, 1229–1241.

Kocurek, G., Havholm, K.G., 1993. Eolian sequence stratigraphy—a conceptual framework. In: Weimer, P., Posamentier, H.W. (Eds.), Siliciclastic Sequence Stratigraphy. American Association of Petroleum Geologists, Memoir vol. 58, pp. 393–409.

Kocurek, G., Lancaster, N., 1999. Aeolian system sediment state: theory and Mojave

Desert Kelso dune field example. Sedimentology 46, 505–515.

Kraus, M.J., Gwinn, B., 1997. Facies and facies architecture of Paleogene floodplain deposits, Wollwood Formation, Bighorn Basin, Wyoming, USA. Sedimentary Geology 114, 33–54.

Langford, R.P., 1989. Fluvial-aeolian interactions: part I, modern systems. Sedimentology 36, 1023–1035.

Leeder, M.R., Gawthorpe, R.L., 1987. Sedimentary models for extensional tilt-block/half- graben basins. In: Coward, M.P., Dewey, J.F., Hancock, P.L. (Eds.), Continental Exten- sional Tectonics. Geological Society, London, Special Publication vol. 28, pp. 139–152.

Leslie, A.G., Smith, M., Soper, N.J., 2008. Laurentian margin evolution and the Caledonian orogeny—a template for Scotland and East Greenland. Geological Society of America Memoirs 202, 307–343.

Long, D.F.G., 1978. Proterozoic stream deposits: some problems of recognition and inter- pretation of ancient fluvial systems. In: Miall, A.D. (Ed.), Fluvial Sedimentology. Cana- dian Society of Petroleum Geology Memoir vol. 5, pp. 313–342.

Long, D.F.G., 2006. Architecture of pre-vegetation sandy-braided perennial and ephemeral river deposits in the Paleoproterozoic Athabasca Group, northern Saskatchewan, Canada as indicators of Precambrian fluvial style. Sedimentary Geology 190, 71–95.

Long, D.G.F., 2011. Architecture and depositional style of fluvial systems before land plants: a comparison of Precambrian, Early Paleozoic and modern river deposits. In: Davidson, S.K., Leleu, S., North, C. (Eds.), From River to Rock Record: The Preservation of Fluvial Sediments and Their Subsequent Interpretation. SEPM Special Publication vol. 97, pp. 37–61.

MacCulloch, J., 1819. A Description of the Western Islands of Scotland, Including the Isle of Man Comprising an Account of their Geological Structure; With Remarks on Their Agriculture, Scenery, and Antiquities. Hurst, Robinson, and Co., London (UK) (585 pp.).

MacNaughton, R.B., Dalrymple, R.W., Norbonne, G.M., 1997. Early Cambrian braid-delta deposits, MacKenzie Mountains, north-western Canada. Sedimentology 44, 587–609. Marconato, A., Almeida, R.P., Turra, B.B., Fragoso-Cesar, A.R.S., 2014. Pre-vegetation flood- plains and channel-belts in the late Neoproterozoic-Cambrian Santa Bárbara group (Southern Brazil). Sedimentary Geology 300, 49–61.

Martins-Neto, M.A., 2000. Tectonics and sedimentation in a Paleo/Mesoproterozoic rift-sag basin (Espinhaço basin, southeastern Brazil). Precambrian Research 103, 147–173.

McKee, E.D., Weir, G.W., 1953. Terminology for stratification and cross-stratification in sedimentary rocks. Geological Society of America Bulletin 64, 381–390.

McManus, J., Bajabaa, S., 1998. The importance of air escape processes in the formation

of dish- and-pillar and tepee structures within modern and Precambrian fluvial deposits. Sedimentary Geology 120, 337–343.

Miall, A.D., 1994. Reconstructing fluvial macroform architecture from two-dimensional outcrops: examples from the Castlegate Sandstone, Book Cliffs, Utah. Journal of Sedimentary Research B64, 146–158.

Miall, A.D., 2016. Facies models. In: Miall, A.D. (Ed.), Stratigraphy: A Modern Synthesis. Springer International Publishing, pp. 161–214.

Miall, A.D., Jones, B.G., 2003. Fluvial architecture of the Hawkesbury Sandstone (Triassic), near Sydney, Australia. Journal of Sedimentary Research 73, 531–545.

Mjøs, R., Walderhaug, O., Prestholm, E., 1993. Crevasse splay sandstone geometris in the Middle Jurassic Ravenscar Group of Yorkshire, UK. In: Marzo, M., Puigdefábregas, C. (Eds.), Alluvial Sedimentation. Special Publications of the International Association of Sedimentologists vol. 17, pp. 167–184.

Mountney, N.P., 2006. Eolian Facies Models. In: Posamentier, H.W., Walker, R.G. (Eds.), Facies Models Revisited. SEPM Special Publication vol. 84, pp. 19–83.

Mountney, N.P., Howell, J., 2000. Aeolian architecture, bedform climbing and preservation space in the Cretaceous Etjo Formation, NW Namibia. Sedimentology 47, 825–849.

Mountney, N.P., Jagger, A., 2004. Stratigraphic evolution of an aeolian erg margin system: the Permian Cedar Mesa Sandstone, SE Utah, USA. Sedimentology 51,

713–743.

Mountney, N.P., Russell, A.J., 2004. Sedimentology of cold-climate aeolian sandsheet deposits in the Askja region of northeast Iceland. Sedimentary Geology 166, 223–244.

Mountney, N.P., Thompson, D.B., 2002. Stratigraphic evolution and preservation of aeolian dune and damp/wet interdune strata: an example from the Triassic Helsby Sandstone Formation, Chesshire Basin, UK. Sedimentology 49, 805–833.

Nicholson, P.G., 1993. A basin reappraisal of the Proterozoic Torridon Group, northwest Scotland. In: Frostick, L., Steel, R.J. (Eds.), Tectonic Controls and Signatures in Sedimentary Successions. Special Publications of the International Association of Sedimentologists vol. 20, pp. 183–202.

Owen, G., Santos, M.G.M., 2014. Soft-sediment deformation in a pre-vegetation river system: the Neoproterozoic Torridonian of NW Scotland. Proceedings of the Geologists' Association 125, 511–523.

Owen, G., Moretti, M., Alfaro, P., 2011. Recognising triggers for soft-sediment deformation: current understanding and future directions. Sedimentary Geology 235, 133–140.

Parnell, J., Mark, D., Fallick, A.E., Boyce, A., Thackery, S., 2011. The age of the Mesoproterozoic Stoer Group sedimentary and impact deposits, NW Scotland. Journal of the Geological Society, London 168, 349–358.

Pascucci, V., Merlini, S., Martini, I.P., 1999. Seismic stratigraphy of the Miocene-Pleistocene sedimentary basins of the Northern Tyrrhenian Sea and western Tuscany (Italy). Basin Research 11, 337–356.

Peach, B.N., Horne, J., Gunn, W., Clough, C.T., Hinxman, L.W., Teal, J.J.H., 1907. The geological structure of the north-west Highlands of Scotland. Memoirs of the Geological Survey of Great Britain. Hedderrick & sons, ltd., Glasgow (UK) (825 p.).

Perillo, M.M., Best, J.L., Garcia, M.H., 2014. A new phase diagram for combined-flow bedforms. Journal of Sedimentary Research 84, 301–313.

Prave, A.R., 2002. Life on land in the Proterozoic: evidence from the Torridonian rocks of northwest Scotland. Geology 30, 811–814.

Prosser, S., 1993. Rift-related linked depositional systems and their seismic expression. In: Williams, G.D., Dobb, A. (Eds.), Tectonics and Seismic Sequence Stratigraphy. Geolog- ical Society, London, Special Publication vol. 71, pp. 35–66.

Rainbird, R.H., 1992. Anatomy of a large-scale braid-plain quartzarenite from the Neoproterozoic Shaler Group, Victoria Island, Northwest Territories, Canada. Canadian Journal of Earth Sciences 29, 2537–2550.

Rainbird, R.H., Hamilton, M.A., Young, G.M., 2001. Detrital-zircon geochronology and provenance of the Torridonian, NW Scotland. Journal of the Geological Society of London 158, 15–27.

Reading, H.G., Collinson, J.D., 1996. Clastic coasts. In: Reading, H.G. (Ed.), Sedimentary Environments: Processes, Facies and Stratigraphy. Blackwell Science, Oxford (UK), pp. 154–231.

Røe, S.L., Hermanssen, M., 2006. New aspects of deformed cross-strata in fluvial sand-stones: examples from Neoproterozoic formations in northern Norway. Sedimentary Geology 186, 283–293.

Ross, G.M., 1983. Proterozoic aeolian quartz arenites from the Hornby Bay Group, Northwest Territories, Canada: Implications for Precambrian aeolian processes. Precambrian Research 20, 149–160.

Santos, M.G.M., Owen, G., 2016. Heterolithic meandering-channel deposits from the Neoproterozoic of NW Scotland: Implications for palaeogeographic reconstructions of Precambrian sedimentary environments. Precambrian Research 272, 226–243.

Santos, M.G.M., Mountney, N.P., Peakall, J., 2016. Tectonic and environmental controls on Palaeozoic fluvial environments: reassessing the impacts of early land plants on sedimentation. Journal of the Geological Society of London. http://dx.doi.org/10. 1144/jgs2016-063.

Simpson, E.L., Eriksson, K.A., Mueller, W.U., 2012. 3.2 Ga eolian deposits from the Moodies Group, Barberton Greenstone Belt, South Africa: implications for the origin of first- cycle quartz sandstones. Precambrian Research 214–215, 185–191.

Skelly, R.L., Bristow, C.S., Ethridge, F.G., 2003. Architecture of channel-belt deposits in

an aggrading shallow sandbed braided river: the lower Niobrara River, northeast Nebraska. Sedimentary Geology 158, 249–270.

Sønderholm, M., Tirsgaard, H., 1998. Proterozoic fluvial style: response to changes in accommodation space (Rivieradal sandstones, eastern North Greenland). Sedimentary Geology 120, 257–274.

Stear, W.M., 1983. Morphological characteristics of ephemeral stream channel and overbank splay sandstone bodies in the Permian Lower Beaufort Group, Karoo Basin, South Africa. In: Collinson, J.D., Lewin, J. (Eds.), Modern and Ancient Fluvial Systems. International Association of Sedimentologists vol. 6, pp. 405–420.

Stewart, A.D., Irving, E., 1974. Palaeomagnetism of Precambrian sedimentary rocks from NW Scotland and apparent polar wandering path of Laurentia. Geophysical Journal of the Royal Astronomical Society 37, 51-72.

Stewart, A.D., 1991. Geochemistry, provenance and climate of the Upper Proterozoic Stoer Group in Scoatland. Scottish Journal of Geology 26, 89-97.

Stewart, A.D., 2002. The later Proterozoic Torridonian rocks of Scotland: their sedimentology, geochemistry, and origin. Geological Society, London, Memoirs 24 (136 pp.). Syvitski, J.P., Milliman, J.T., 2007. Geography, and humans battle for dominance over the delivery of fluvial sediment to coastal ocean. The Journal of Geology 115, 1–19.

Syvitski, J.P., Morehead, M.D., Bahr, D.B., Mulder, T., 2000. Estimating fluvial

sediment transport: the rating parameters. Water Resources Research 36, 2747–2760.

Syvitski, J.P., Peckham, S.D., Hilberman, R., Mudler, T., 2003. Predicting the terrestrial flux of sediment to the global ocean: a planetary perspective. Sedimentary Geology 162, 5-24.

Syvitski, J.P., Cohen, S., Kettner, A.J., Brakenridge, C.R., 2014. How important and different are tropical rivers? – an overview. Geomorphology 227, 5–17.

Tirsgaard, H., Øxnevad, I.E.I., 1998. Preservation of pre-vegetational mixed fluvio–aeolian deposits in a humid climatic setting: an example from the Middle Proterozoic Eriksfjord Formation, Southwest Greenland. Sedimentary Geology 120, 295–317.

Todd, S.P., Went, D.J., 1991. Lateral accretion of sand-bed rivers: examples from the Devonian Glashabeg Formation, SW Ireland and the Cambrian Alderney Sandstone Formation, Channel Islands. Sedimentology 38, 997–1020.

van Toorenenburg, K.A., Donselaar, M.E., Noordijk, N.A., Weltje, G.J., 2016. On the origin of crevasse-splay amalgamation in the Huesca fluvial fan (Ebro Basin, Spain): implica- tions for connectivity in low net-to-gross fluvial deposits. Sedimentary Geology 343, 156–164.

Tunbridge, I.P., 1984. Facies model for a sandy ephemeral stream and clay playa complex; the Middle Devonian Trentishoe Formation of North Devon, U.K. Sedimentology 31, 697–715.

Tye, R.S., Coleman, J.M., 1989. Evolution of Atchafalaya lacustrine deltas, south-central Louisiana. Sedimentary Geology 65, 95–112.

Tye, R. S., Coleman, J. M., 1989. Evolution of Atchafalaya lacustrine deltas, south-central Louisiana. Sedimentary Geology 65, 95–112.

Weissmann, G.S., Hartley, A.J., Nichols, G.J., Scuderi, L.A., Olson, M., Buehler, H., Banteah, R., 2010. Fluvial form in modern continental sedimentary basins: distributive fluvial systems. Geology 38, 39–42.

Williams, G.E., 1966. Planar cross-stratification formed by the lateral migration of shallow streams. Journal of Sedimentary Petrology 36, 742–746.

Williams, G.E., 2001. Neoproterozoic (Torridonian) alluvial fan succession, northwest Scotland, and its tectonic setting and provenance. Geological Magazine 138, 161–184.

Williams, G.E., Foden, J., 2011. A unifying model for the Torridon Group (early Neoproterozoic), NW Scotland: product of post Grenvillian extensional collapse. Earth-Science Reviews 108, 34–49.

Williams, G.E., Foden, J., 2012. Reply: a unifying model for the Torridon Group (early Neoproterozoic), NW Scotland: product of post Grenvillian extensional collapse. Earth-Science Reviews 111, 86–89.

Wood, L.J., 2006. Quantitative geomorphology of the Mars Eberswalde delta. Geological Society of America 118, 557–566. Young, G.M., 1999a. A geochemical

investigation of palaeosols developed on Lewisian rocks beneath the Torridonian Applecross Formation, NW Scotland. Scottish Journal of Geology 35, 107–118.

Young, G.M., 1999b. Some aspects of the geochemistry, provenance and palaeoclimatology of the Torridonian, NW Scotland. Journal of the Geological Society, London 156, 1097–1111.

2.11 Figures

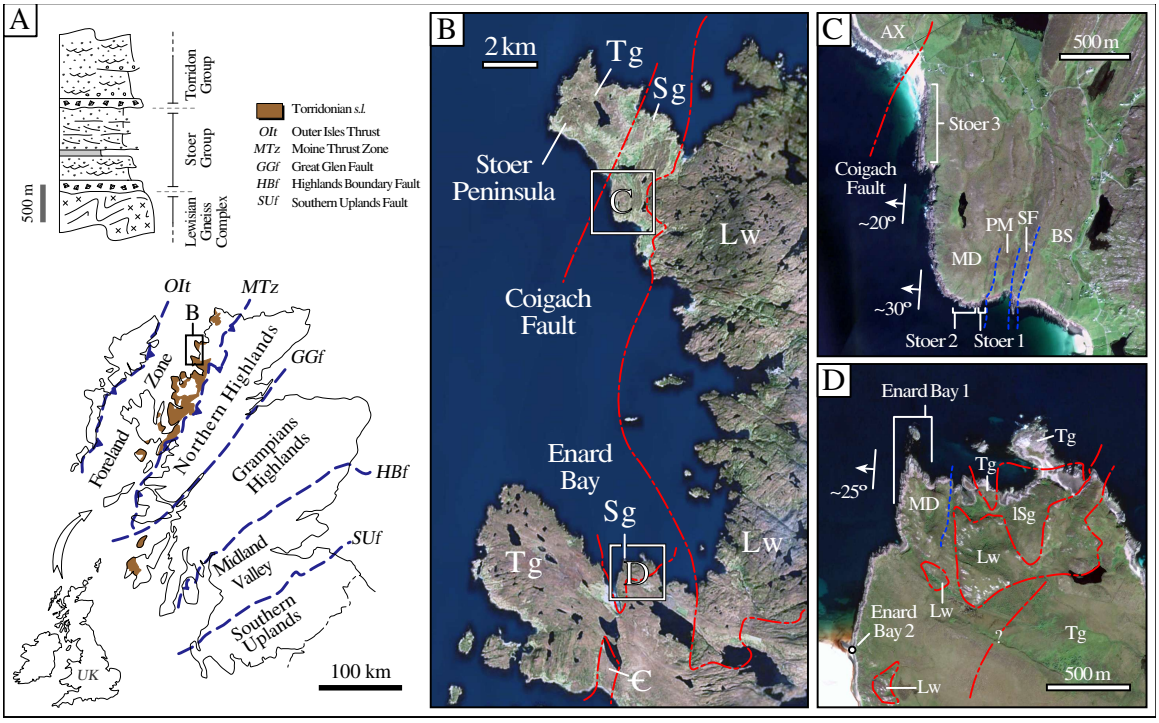

Figure 2-1: Regional map

A) Regional extent and stratigraphic development of the Torridonian succession of Scotland (stratigraphic column representative of the Foreland Zone), from Stewart (2002) and Leslie et al. (2008). Location of inset (B) is shown. B–D) Satellite views of the study area, including insets of Stoer Peninsula (C) and Enard Bay (D) showing the location of measured sections. Major regional boundaries are reported with red dashed lines. Abbreviations in (B): Lw, Lewisian Gneiss Complex; Sg, Stoer Group; Tg, Torridon Group; and C: Cambrian strata. Abbreviations in (C–D): BS, Bay of Stoer Formation; SF: Stac Fada Member; PM: Poll a'Mhuilt Member; MD, Meall Dearg Formation; AX, Applecross Formation; Lw, Lewisian Gneiss Complex; and Tg, undifferentiated Torridon Group. (For interpretation of the references to colour in this figure legend, the reader is referred to the web version of this article.)

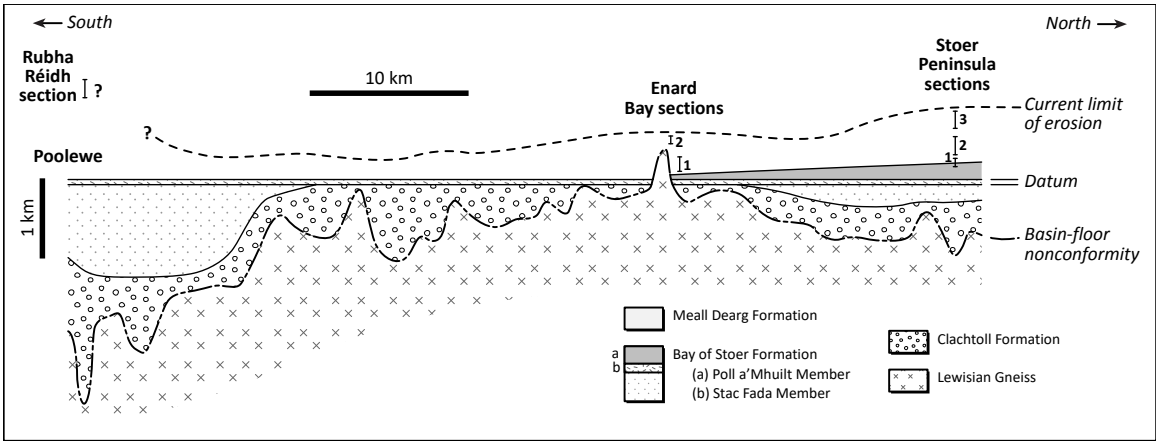

Figure 2-2: Regional transect

Regional transect showing the large-scale architecture of the Stoer Group strata, redrawn from Stewart (2002). Note basement high at Enard Bay. The location of measured sections is also reported.

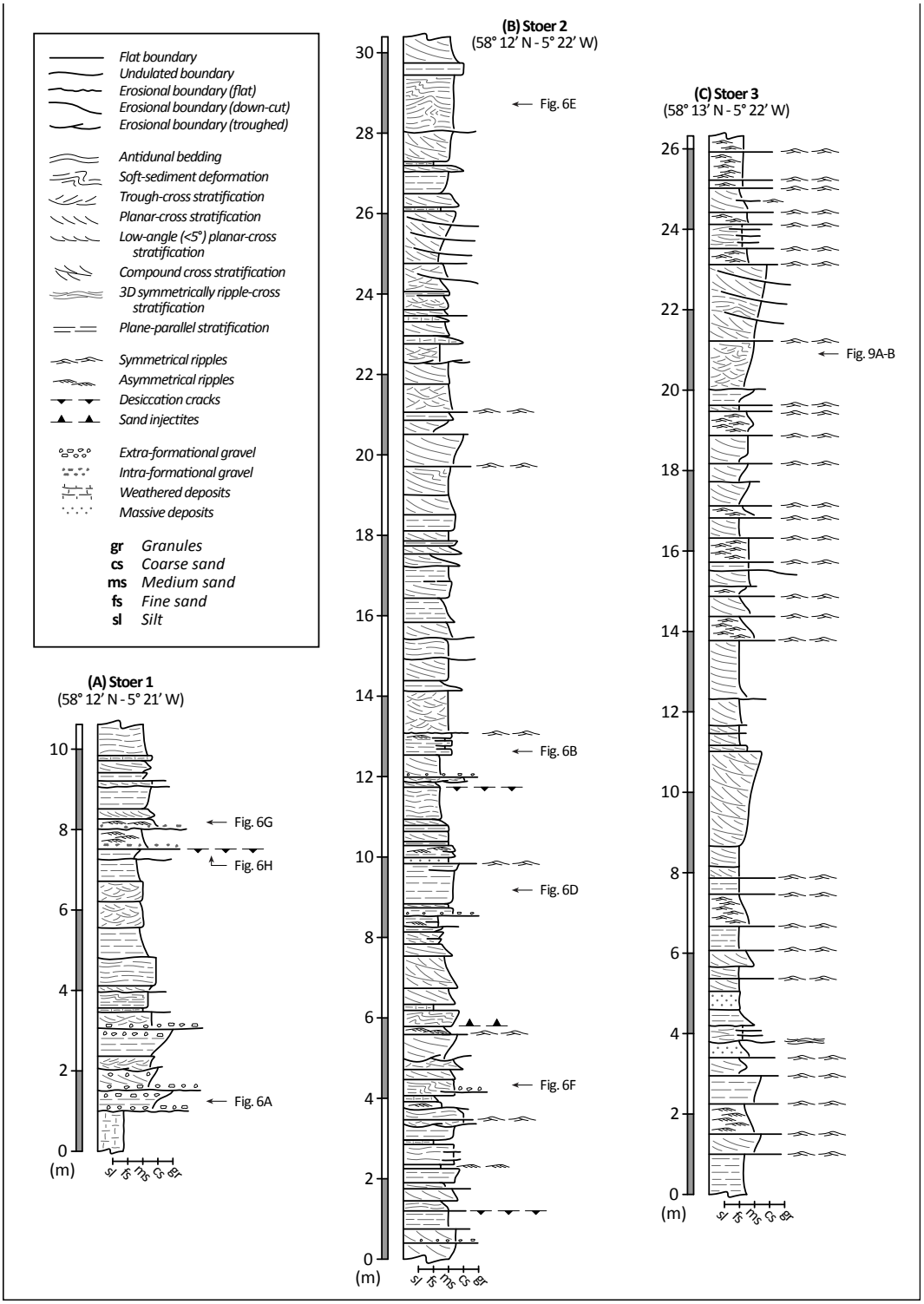

Figure 2-3: Stratigraphic log at Stoer Peninsula

Stratigraphic sections measured at Stoer Peninsula. See Figs. 1 and 2 for locations.

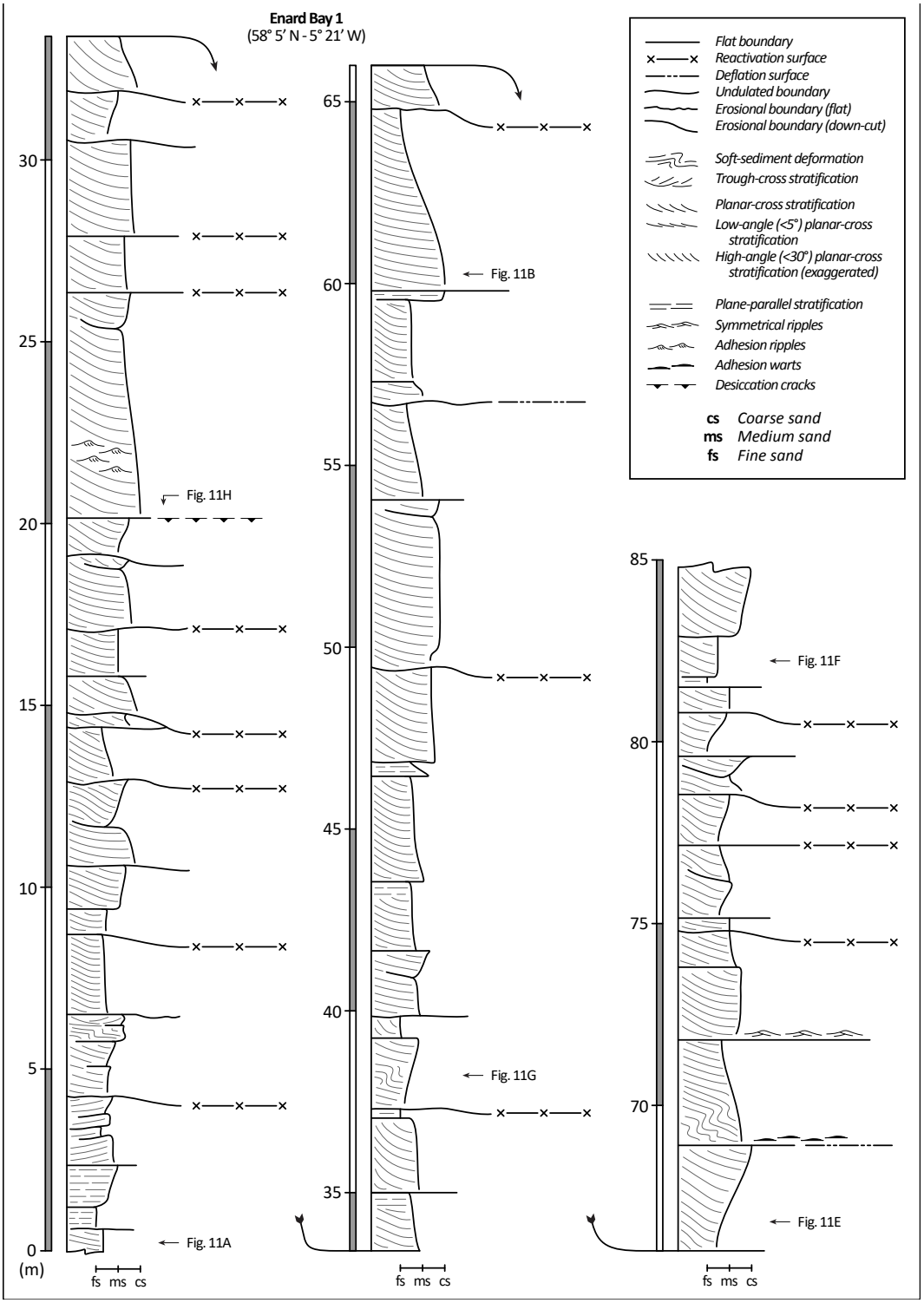

Figure 2-4: Stratigraphic log at Enard Bay

Stratigraphic section measured at Enard Bay 1. See Figs. 1 and 2 for location.

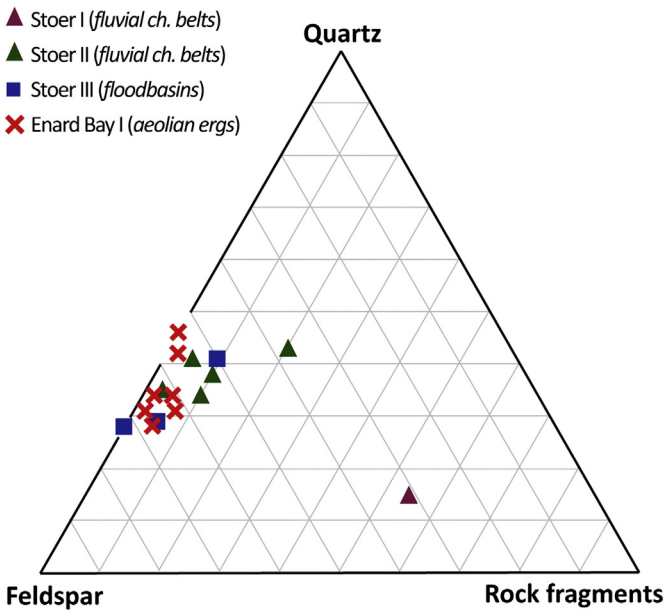

Figure 2-5: QFR petrographic diagram

Meall Dearg Formation thin-sectioned sandstone samples, colour-coded according to their facies association and plotted in a Quartz-Feldspar-Rock fragments space, using the approach of Folk (1968).

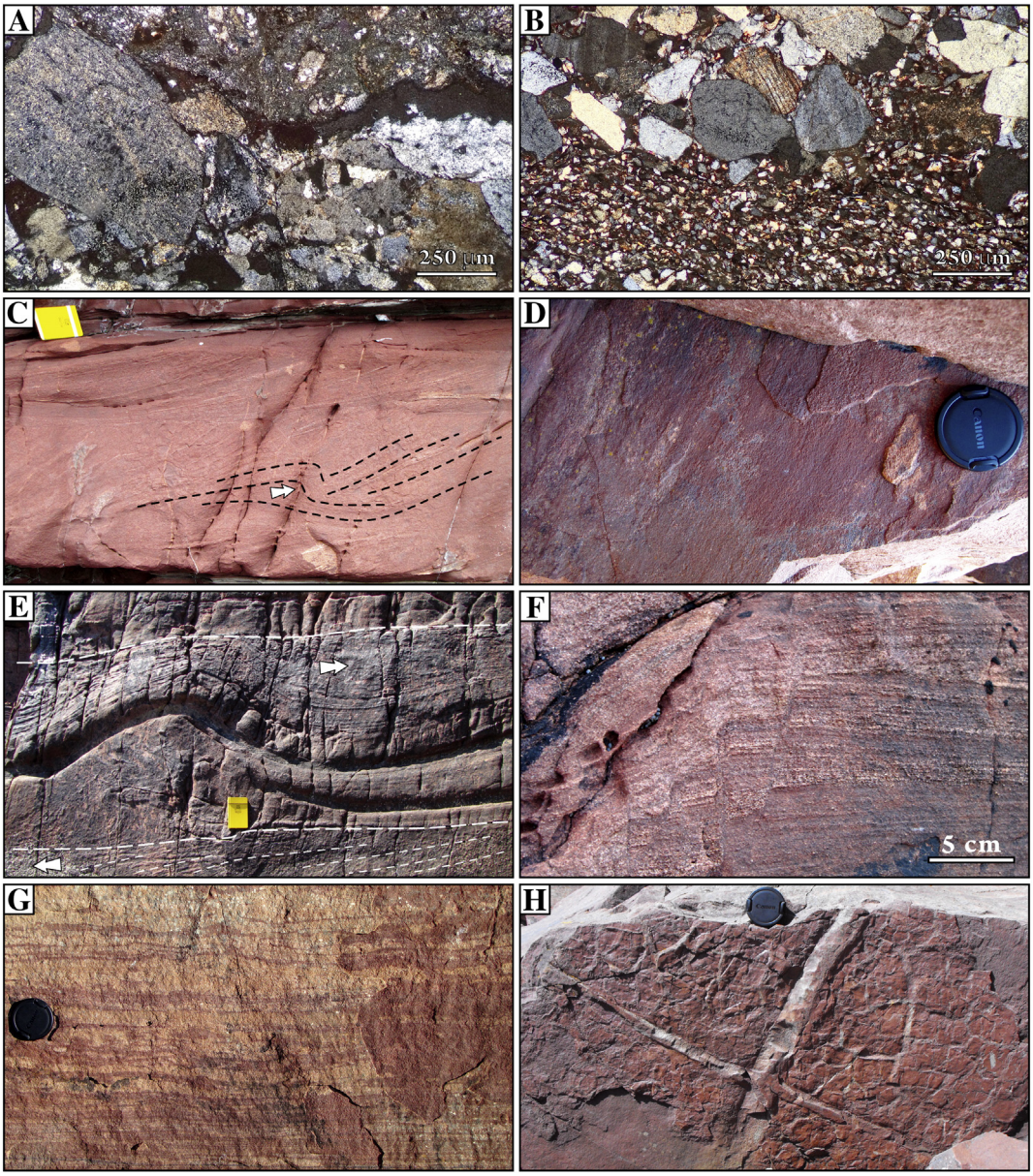

Figure 2-6: Sedimentary structures of the fluvial channel-belt facies association

Aspects of the fluvial channel-belt facies association. Field book in (C, E) is ~ 0.2 m wide; Lens cap (D, G, H) is ~ 50 mm across. A–B) Thin-section samples of fluvial sandstone observed under cross-polarised light, and representative of sections Stoer 1 (A) and 2 (B); note large irregular lithic grains (A) and low textural maturity defined by poor sorting and angular, poorly rounded grains (B). C) Sets of planar-cross bedded sandstone,

exhibiting curved foresets and (dashed lines) and small-scale antidune preserved therein (arrow pointing to antidune accretion). D) Plan view of plane-bedded sandstone, exhibiting primary current lineation. E) Large-scale antidune (within dashed lines) cored by soft-sediment deformed deposits; arrows indicate accretion of bedforms; note upstream accretion of the antidune with respect to the underlying cross-bed. F) Small-scale sin-depositional faulting associated to soft-sediment deformation. G) Sandstone exhibiting pervasive, low-relief ripple cross-lamination. H) Lower surface of a bed boundary showing well-preserved desiccation structures.

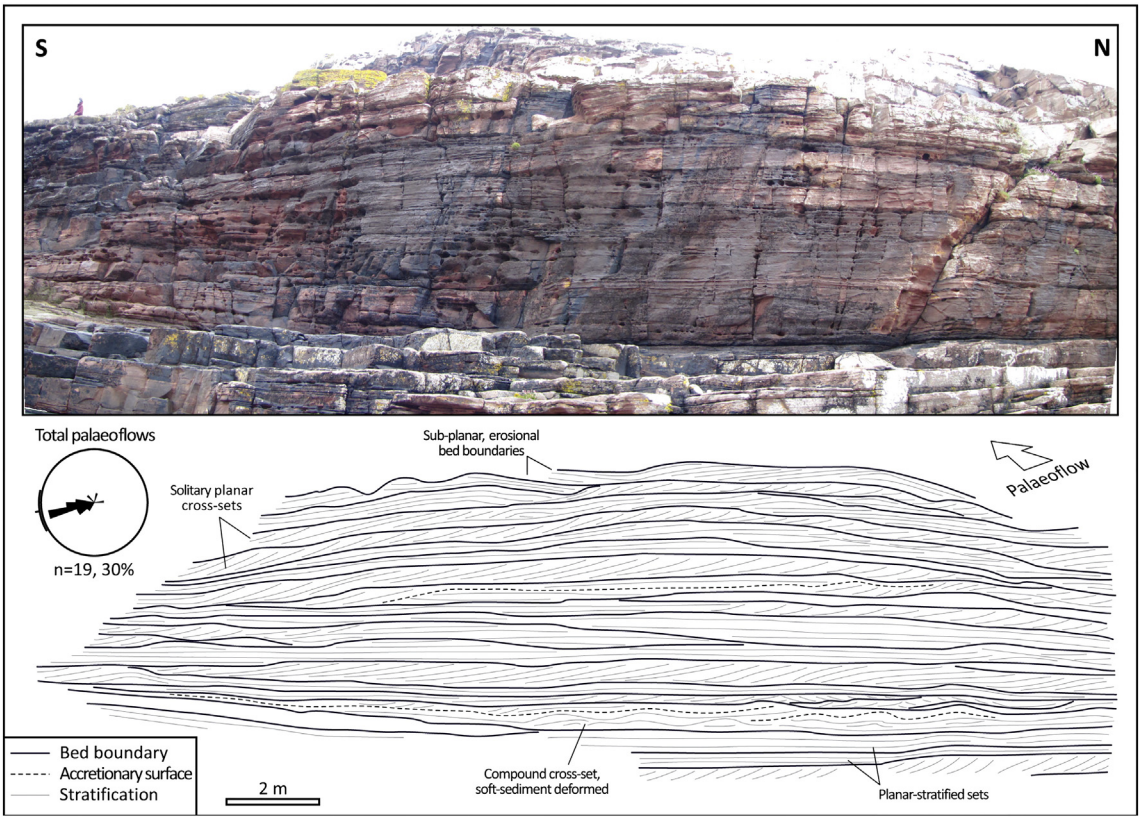

Figure 2-7: Architecture of lower fluvial channel-belt deposit

Field photo and interpretive line-drawing showing the architecture of fluvial deposits in the lower section of Stoer 2. Note planar beds bounded by irregular surfaces, and

abundance of solitary planar cross-sets and plane-bedded deposits.

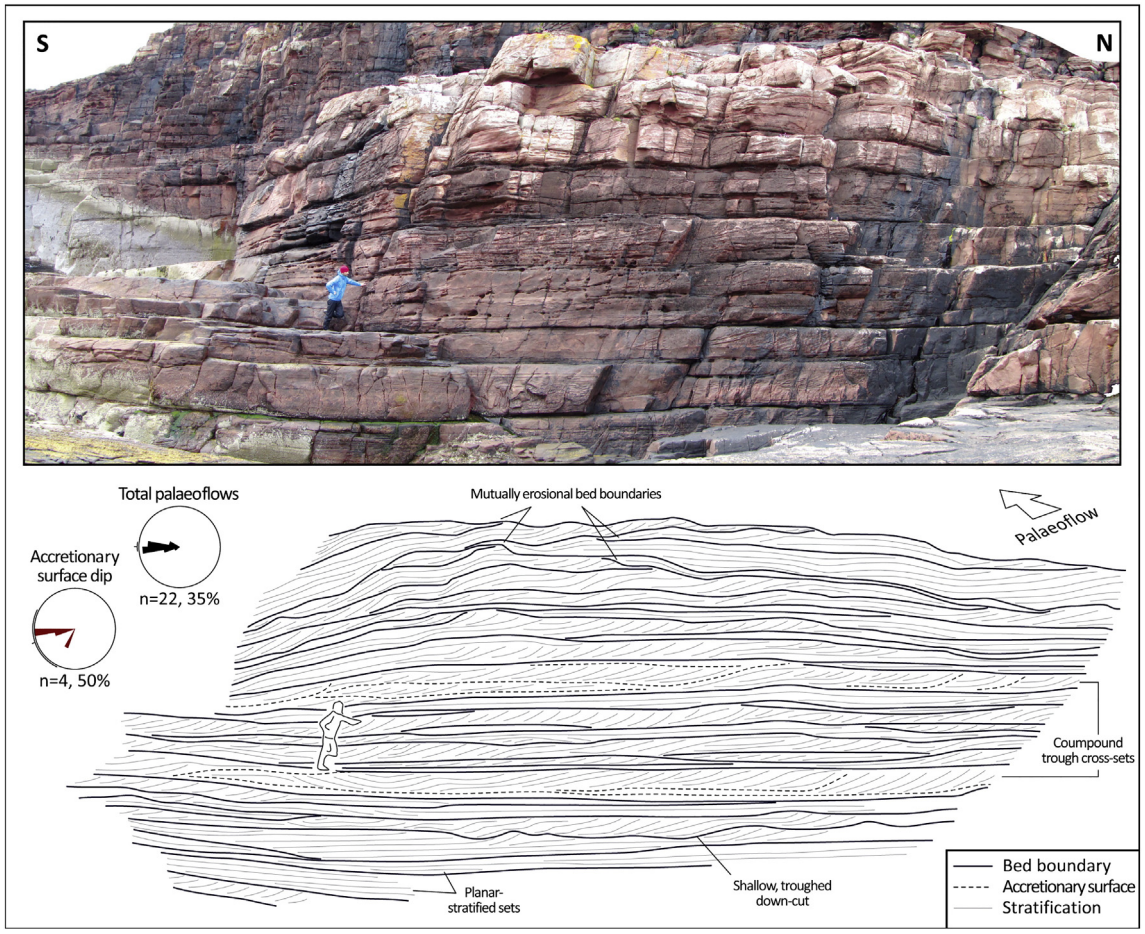

Figure 2-8: Architecture of upper fluvial channel-belt deposit

Field photo and interpretive line-drawing showing the architecture of fluvial deposits in the upper section of Stoer 2. Geologist is ~ 1.8 m tall. Note intervening compound cross-sets pointing to downstream accretion and migration of low-relief sediment bars, likely in shallow and wide channels.

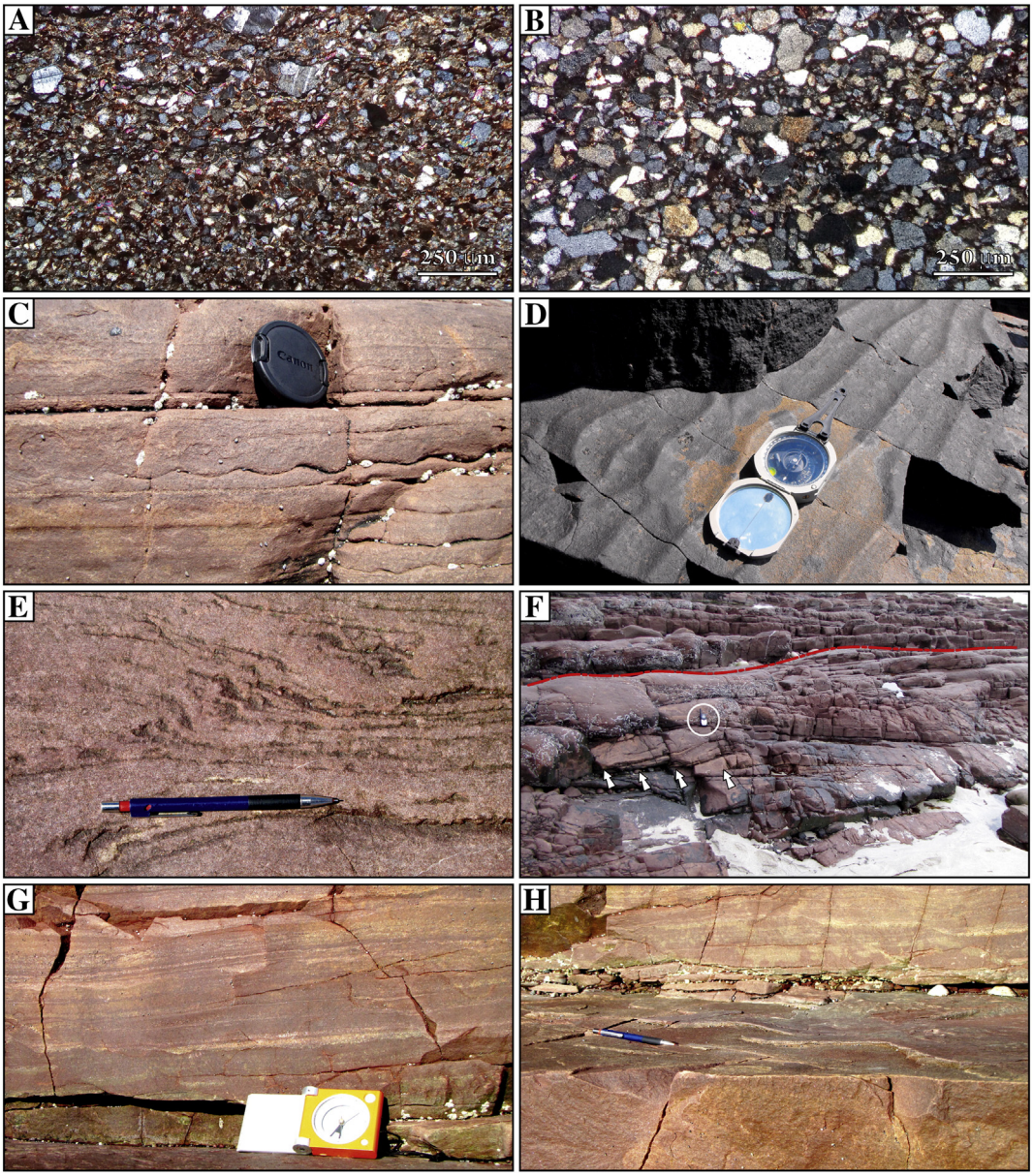

Figure 2-9: Sedimentary structures of the floodbasin facies association

Aspects of the floodbasin facies association. Pencil in (D, H) is ~0.15 m long. A–B) Thin-section samples of lacustrine sandstone observed under cross-polarised light, and representative of section Stoer 3; note occurrence of laminae dominated by either fine-grained (A) or medium-grained (B) sandstone, both with enhanced sorting, and moderate rounding and sphericity. C) Particular of wave ripple cross-laminated bed, with

symmetrical ripple crests exposed in section; lens cap is ~50 mm across. D) Boundary between individual beds, showing well-developed symmetrical ripples generated by oscillatory currents; compass is ~0.2 m wide. E) Localised soft-sediment deformation defined by small- scale slumping. F) Compound cross-set defined by inclined planar surfaces seldom floored by antidunal climbing sets (arrowed); hand-held radio (encircled) is ~0.1 m long. G) Tabular beds exhibiting plane-parallel and wavy lamination, the latter generated by the stacking of symmetrical ripples; compass is ~0.15 m long. H) Particular of low-relief, three- dimensional ripples pointing to combined oscillatory and unidirectional currents.

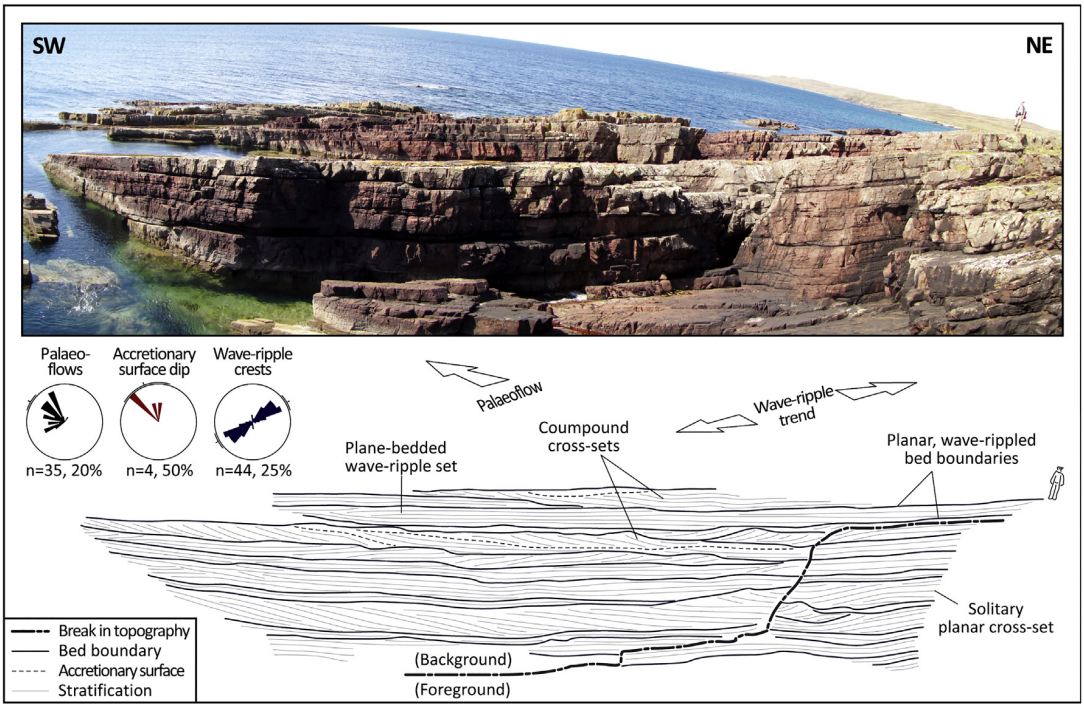

Figure 2-10: Architecture of floodbasin deposit

Field photo and interpretive line-drawing of floodbasin deposits, showing the stacking of tabular beds in places truncated by shallowly erosional surfaces. Geologist is ~1.6 m tall. Palaeoflow data and trends of wave-ripple crests are also reported.

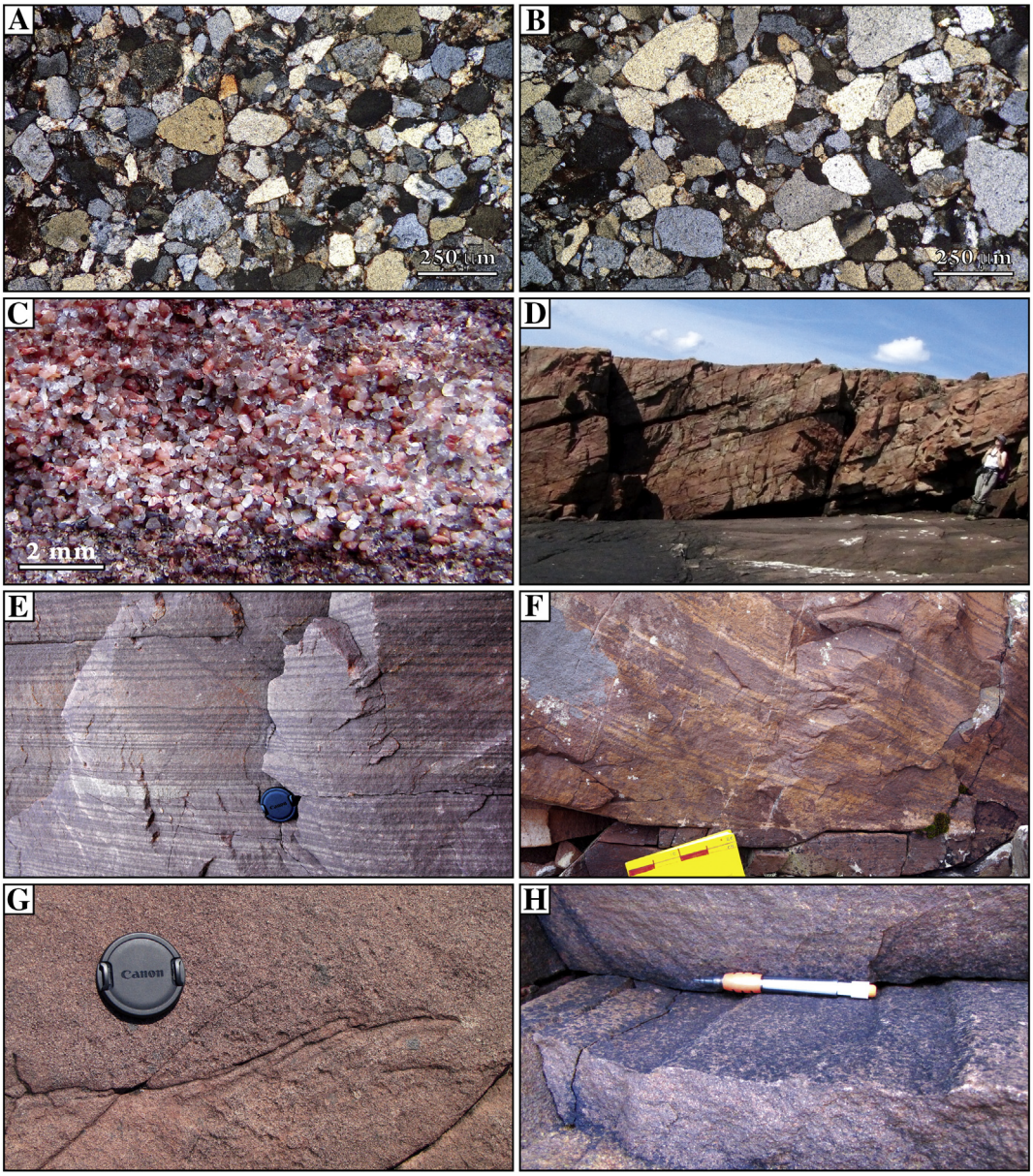

Figure 2-11: Sedimentary structures of the aeolian facies association

Aspects of the aeolian facies association. Lens cap in (E, G) is ~50 mm across. A–B) Thin-section samples of aeolian sandstone observed under cross-polarised light, and representative of section Enard Bay 1; note enhanced sorting compared to fluvial deposits, and moderate to good degree of sphericity. C) Close-up of aeolian laminae with closed packing due to strong compaction; note sharp grain size segregation, and very

good degree of sorting. D) Large-scale planar cross-bed with flat, high-angle foresets; Geologist is ~1.6 m tall. E) Well-sorted sandstone exhibiting sharp grain size segregation in between laminae, typical of pin-stripe lamination. F) Curved, pin-stripe laminated toesets, tangential with the bottom of a high-angle planar cross-set; field book is 0.2 m wide. G) Particular of localised soft-sediment deformation, in this case small-scale syn-depositional thrusting at the toe of a high-angle planar cross-set. H) Irregular bed boundary with faint desiccation structures preserved; pencil is 0.1 m long.

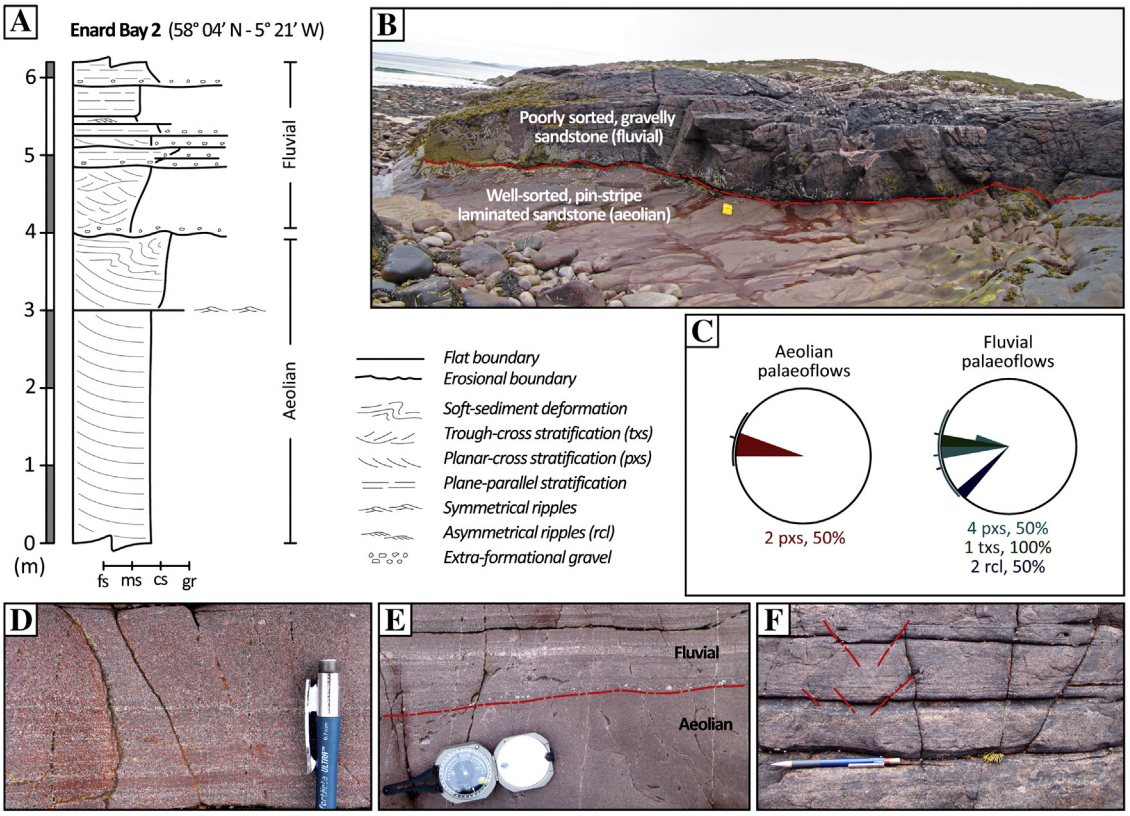

Figure 2-12: Sedimentary structures and stratigraphic log of fluvial-aeolian deposit

Stratigraphic section and field aspect of section Enard Bay 2, showing the interaction of fluvial and aeolian depositional systems. A) Stratigraphic log measured through the section. B) View of the section's top, showing fluvial deposits resting erosionally atop aeolian sandstone; field book is 0.2 m wide. C) Palaeoflow data showing the vectors of progradation of aeolian and fluvial bedforms (abbreviations: pxs, planar cross-set; txs, trough cross-set; rcl, ripple cross-lamination). D) Particular of aeolian facies, showing fine-grained, well-sorted and pin- stripe laminated sandstone; pen cap is 20 mm long. D) Close-up of the erosional boundary between fluvial and aeolian deposits; note local concentrations of granules and weaker degree of sorting in fluvial deposits. Compass is

~0.2 m wide. F) Small-scale extensional faults, likely due to sediment loading, developed in aeolian sandstone below the contact with fluvial deposits.

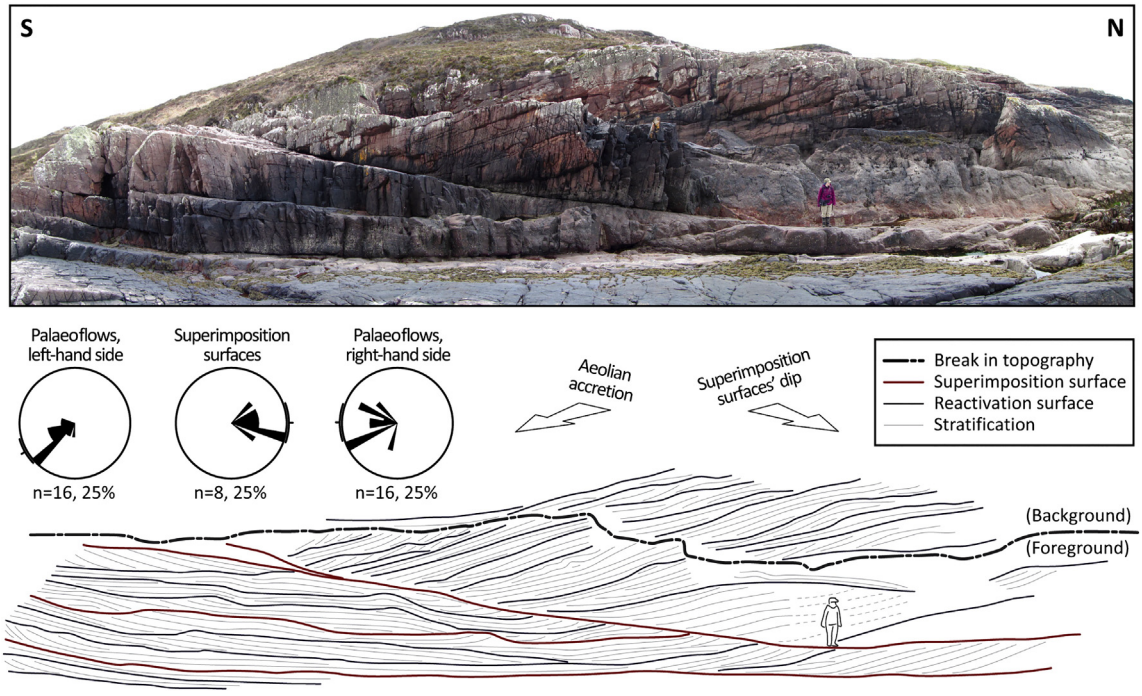

Figure 2-13: Architecture of aeolian deposit

Field sketch and interpretive line-drawing showing the architecture of aeolian deposits and bounding surfaces, lower section Enard Bay 1. Geologist is 1.6 m tall. Note large-scale planar cross-set climbing atop a superimposition surface. Palaeoflow data and attitude of superimposition bounding surfaces is also reported.

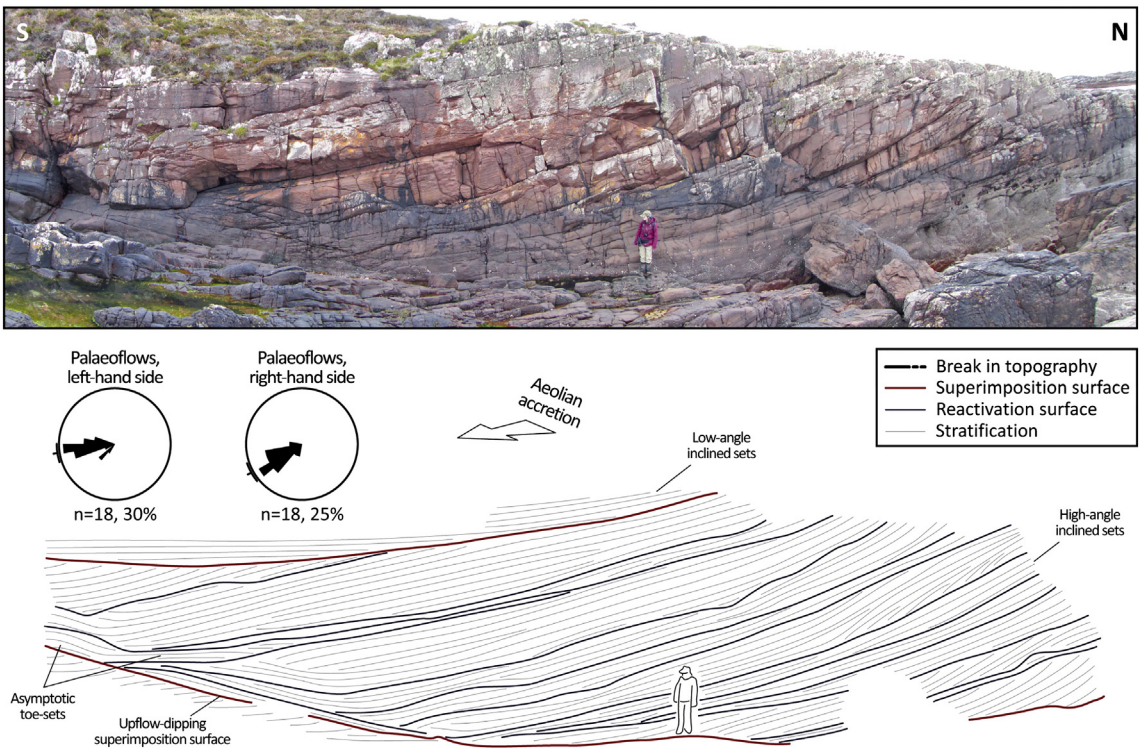

Figure 2-14: Architecture of aeolian deposit

Field sketch and interpretive line-drawing showing the architecture of a large-scale, tangentially based aeolian cross-set climbing obliquely atop a superimposition surface. Geologist is 1.6 m tall. Note the curved attitude of toesets and minor superimposition bounding surfaces.

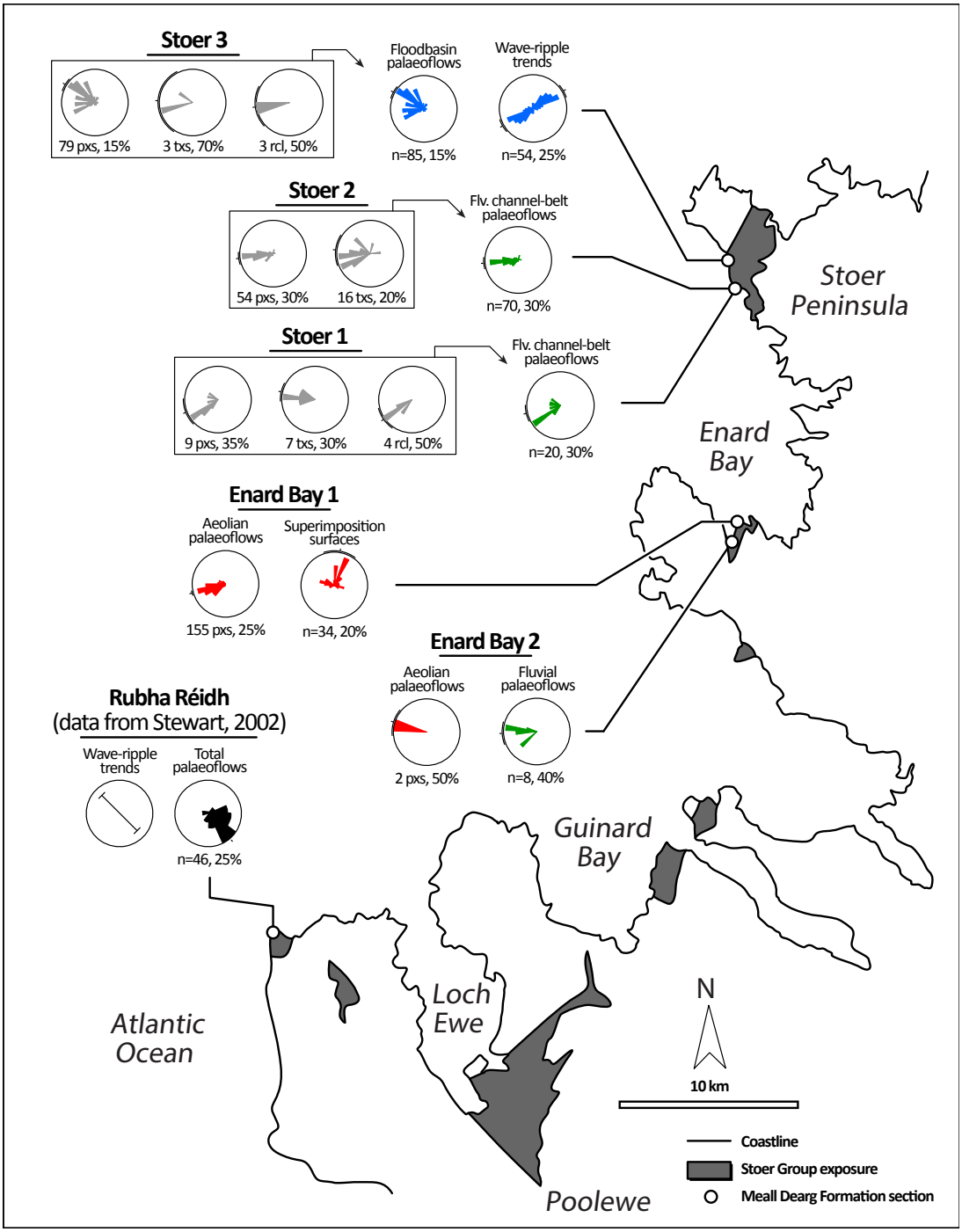

Figure 2-15: Palaeocurrent measurements

Palaeogeography of the Meall Dearg Formation, from analysis of sediment dispersal in fluvial channel-belt, floodbasin, and aeolian facies associations. Data from Stewart (2002) at Rubha Réidh is also reported for comparison. See text for discussion.

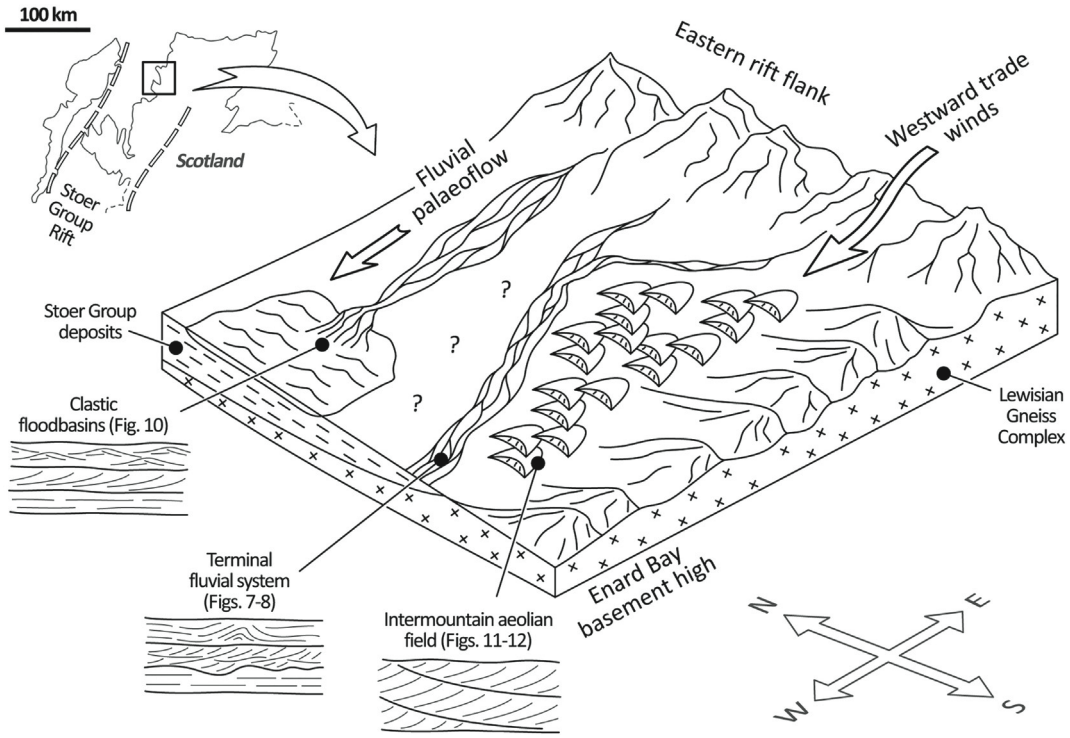

Figure 2-16: Depositional model

Depositional model inferred for the Meall Dearg Formation depicting the interplay of fluvial and aeolian depositional systems. See text for discussion. No scale is implied, and the geometry of aeolian dunes is purely graphical.

2.12 Tables

Table 2-1: fluvial channel-belt and floodbasin sedimentary facies

Summary of sedimentary facies deposited in fluvial environments, including channel-belts and floodbasins.

Fpb	**Planar-bedded sandstone.** Beds 10–80 cm thick of medium- to coarse- grained arkose (pebbly in places) with plane-parallel stratification and parting lineation preserved in planview.	Sediment bypass and aggradation of upper flow-regime traction carpets (Collinson et al., 2006).
Fpx	**Planar cross-bedded sandstone** Beds 10–85 cm thick of medium- to coarse-grained arkose (pebbly in places) with planar-cross stratification. Foresets often exhibit curved geometry and asymptotic bases.	Accretion and reworking of 2D dunes during poorly confined, tractional, lower to transitional upper-regime waterflows (Harms et al., 1975).
Fab	**Antidunal-bedded sandstone.** Beds 50-140 cm thick of medium- to coarse- grained arkose, exhibiting plane-parallel, low-relief undulatory bedding. Fully preserved antidune bedforms preserved in places.	Accretion and reworking of upper flow-regime antidunal beds during bedload-dominated events (Fielding, 2006).
Fcx	**Compound cross-bedded sandstone.** Bedsets 75–130 cm thick of medium- to coarse-grained arkose. Individual beds exhibiting planar-cross (rarely trough-cross) stratification and truncated by inclined surfaces.	Repeated accretion and reactivation of 2D (planar-cross) and 3D (trough-cross) dunes in relatively deep and confined, lower-regime waterflows (Rainbird, 1992).
Ftx	**Trough cross-bedded sandstone.** Beds 10–110 cm thick of medium- to coarse-grained arkose exhibiting trough-cross stratification.	Accretion and reworking of 3D dunes during confined, tractional, lower regime waterflows (Harms et al., 1975).
Fsd	**Soft-sediment deformed sandstone.** Beds 40–70cm thick of medium- to coarse-grained arkose exhibiting pervasive internal deformation, cm-scale sin-depositional faulting, and rare sand injection structures.	Flow-induced shearing and gravitative collapse of unconsolidated and water-saturated, cohesion-less sediment. Occasional sediment liquefaction and escape along pipes (Owen & Santos, 2014).

Frl	**Asymmetrically ripple cross-laminated sandstone.** Beds 10-50 cm thick of fine- to medium-grained arkose exhibiting unidirectional ripple forms, climbing in places.	Aggradation of ripple beds due to sediment traction and fallout in lower regime waterflows (Jopling and Walker, 1968). Ripple climbing during episodes of high bedload yield.
Fwr	**2D Symmetrically ripple cross-laminated sandstone.** Sets up to 5 cm thick of fine-to medium-grained arkose exhibiting wave-ripple forms, and flooring stratal bounding surfaces.	Sediment reworking by oscillatory waterflows in lower flow-regime, ripple-bed conditions (Clifton, 2006).
Fcr	**3D symmetrically ripple cross-laminated sandstone.** Fine- to medium-grained arkose exhibiting wave-ripple forms, in places flooring stratal bounding surfaces.	Accretion and reqorking of lower0flow regime bedforms under combined oscillatory and unidirectional conditions (Perillo et al., 2014).
Fms	**Massive sandstone.** Beds up to 5 cm thick of structure-less, ungraded coarse-grained arkose.	Depositional freezing of laminar, high-density flows (Reading and
Fwm	**Weathered mudstone.** Beds 5–100 cm thick of siltstone to fine-grained sandstone exhibiting blocky fabric and mottled rusty colouration.	Fine settling from suspensions or diluted, lower-regime waterflows. Repeated wetting-drying of mud-grade sediment. Iron-oxide precipitation in sub-aerial settings (Kraus and Gwinn, 1997).

Table 2-2: Aeolian sedimentary facies

Summary of the sedimentary facies deposited in aeolian environments.

Alx	**Large-scale planar cross-laminated sandstone**. Beds 10–500 cm thick of medium-grained arkose exhibiting planar-cross, pin-stripe lamination. Foresets dip at either high angles (<30^{o}) or low angles (<5^{o}).	Accretion and reworking of 2D transverse aeolian dunes. Sedimentation dominated by grain-fall in low-angle foresets during periods of strong wind; growth of high-angle foresets after mixed grain-flow, grain-fall, and wind- ripple migration during periods of weaker wind (Chakraborty, 1991).
Apb	**Planar-laminated sandstone.** Beds 10–115 cm thick of fine- to coarse- grained arkose, exhibiting sub-horizontal, plane-parallel pin-stripe lamination.	Accretion and migration of wind ripples atop sand sheets (Dal' Bó and Basilici, 2015), or in dry inter-dune settings (Chakraborty, 1991).
Asd	**Soft-sediment deformed sandstone.** Beds 10–350 cm thick of fine- to medium-grained arkose exhibiting either small-scale or large-scale contorted bedding.	Syn- to early post-depositional deformation of damp wind-blown sand (Horowitz, 1982). Small-scale deformation after gravitative collapse of moderately cohesive dune-lee slopes. Large-scale deformation after
Aar	**Adhesion-rippled sandstone.** Sets of inclined laminae up to 10 cm thick found within facies *Alcb*, and composed of medium- to coarse- grained arkose with	Accretion of wind-blown sand by adhesion onto damp, upwind facing ripples located on dune flanks (Kocurek & Fielder, 1982; Mountney, 2006).
Aaw	**Sandstone with adhesion warts.** Beds up to 5 cm thick of medium- grained arkose exhibiting irregular adhesion structures and irregular lamination in section. Found along	Accretion of wind-blown sand by adhesion onto damp, irregular bedforms during periods of frequently changing wind directions (Kocurek & Fielder, 1982; Mountney, 2006).
Awr	**Symmetrically rippled sandstone.** Beds up to 10 cm thick of medium- grained arkose exhibiting wave-ripple forms along flat stratal surface.	Reworking of wind-blown sand by oscillatory waves in shallow inter-dune ponds, recording periods of surfacing water table (Mountney et al., 2002).

Chapter 3

3. Detrital-zircon provenance of a Torridonian fluvial-aeolian sandstone: The 1.2 Ga Meall Dearg Formation, Stoer Group (Scotland)

Lorraine Lebeau [a*], Alessandro Ielpi [a], Maarten Krabbendam [b], William. J Davis [c]

[a] Harquail School of Earth Sciences, Laurentian University, Sudbury, Ontario P3E 2C6, Canada

[b] British Geological Survey, Lyell Centre, Research Avenue South, Edinburgh EH14 4AP, Scotland, UK

[c] Geological Survey of Canada, 601 Booth Street, Ottawa, Ontario K1A 0E8, Canada

3.1 Abstract

The Meall Dearg Formation is a 1.2 Ga fluvial-aeolian sandstone exposed in the north-western Highlands of Scotland. It is one of the least studied rock units in the Stoer Group (Torridonian succession), and little is known about the provenance and routing of its fluvial and aeolian detritus. Three hundred and nine detrital-zircons were analysed from the Meall Dearg Formation using sensitive high-resolution ion microprobe, allowing for its provenance to be resolved at the terrane scale. Ages range from c. 3,100 to c. 1,750 Ma, with dominant proportions between c. 2,900 and c. 2,650 Ma, and subordinate fractions are c. 2,500 Ma and c. 1,900 Ma in age. A total of eight studies that collected U-Pb protolith-zircon ages from across the Lewisian Gneiss Complex were compiled and compared to detrital age distributions of the Meall Dearg Formation. Strong similarities in age trends and palaeocurrent data confirm sedimentary provenance from the Lewisian

Gneiss Complex. Detritus was prevalently derived from the Rhiconich and Gruinard terranes, and subordinately from the Assynt, Gairloch (including the Loch Maree Group and Ard Gneiss), and Ialltaig terranes. Age distributions from the fluvial and aeolian samples were compared to test for sedimentary interaction. Near-matching distributions between the two indicates thorough sediment transfer between the adjacent depositional environments, and possible derivation from similar source rocks. The Meall Dearg Formation likely records the overfilling stage of the Stoer Group rift basin, representing an extensional basin-fill in a pre-Rodinian Laurentia setting. A relationship can be drawn between the Stoer Group and Gardar Rift of southern Greenland, based on patterns of rift basin development near the eastern flanks of Laurentia at c.1.2 Ga.

Keywords: Stoer Group, detrital-zircon geochronology, Lewisian Gneiss Complex, fluvial-aeolian interaction, Nuna/Columbia, Rodinia

3.2 Introduction

The Torridonian succession, located in northwestern Scotland, is a late Mesoproterozoic to early Neoproterozoic basin succession extensively exposed in the north-western Scottish Highlands. It has been a subject of study for almost 200 years (MacCulloch, 1819; Peach et al., 1907), and has spurred a large body of research in many sub-disciplines of geology including sedimentology (Stewart, 2002 and references therein; Williams and Foden, 2011; Owen and Santos, 2014; Ielpi & Ghinassi, 2015; Lebeau and Ielpi, 2017; and others), geochemistry and palaeoclimatology (Stewart, 1990; van de Kamp and Leake, 1997; Young, 1999; Stüeken et al., 2017), geochronology (Rainbird et al., 2001; Kinnaird et al., 2007; Krabbendam et al., 2017), palaeobiology (Prave, 2002; Brasier et al., 2016), and palaeomagnetics (Irving et al., 1957; Smith et al., 1983). Some

of the most significant research includes the understanding of life on land in the Proterozoic (Prave, 2002; Brazier et al., 2016), evidence of a Precambrian bolide impact event (Armor et al., 2007; Simms, 2015), and palaeocontinental reconstructions (Rainbird et al., 2001; Krabbendam et al., 2017). The Torridonian is subdivided into the lowermost Stoer, Sleat and uppermost Torridon groups — the Stoer Group separated by an angular unconformity from the above formations and is the focus of this study. The Stoer Group has thus far been interpreted to represent the fill of a Mesoproterozoic rift basin, possibly related to the incipient break-up of Supercontinent Columbia (also known as Nuna) (Rainbird et al., 2001). Parnell et al. (2011) has dated the Stoer Group with a depositional age of c.1.18 Ga, effectively placing the Stoer Group in the context of post-break up of Columbia and pre-assembly of Rodinia (e.g. Zhao et al. 2004).

The Stoer Group nonconformably lies atop the Archean to Palaeoproterozoic Lewisian Gneiss Complex (LGC), a metamorphic terrane that comprises multiple blocks with distinctive ages. Current consensus is that the Stoer Group was sourced from the LGC. However a limited number of enigmatic younger ages have been reported by Rainbird et al. (2001) in the Meall Dearg Formation (the uppermost unit of the Stoer Group), possibly pointing to distal provenance (outside the LGC) and warranting further investigation on its sedimentary provenance. The Meall Dearg Formation, the main unit analysed in this study, represents the later stages of rift basin fill of the Stoer Group. It is characterised by continental deposits of cross-bedded arkose associated with coeval fluvial and aeolian deposits (Lebeau & Ielpi, 2017). Specifically, the coeval depositional environments include fluvial channel-belt, floodbasin, and aeolian erg; however for the remainder of the paper floodbasin and fluvial channel-belt environments are grouped and

are referred to as “fluvial”. The Meall Dearg Formation is a critical unit of the Stoer Group for provenance studies because it represents the final stages of rifting.

This study aims to address the following questions: 1) Will a robust dataset of detrital-zircon ages resolve the provenance of the Stoer Group, and can it be used to test a rift-basin model for the Stoer Group? 2) Can detrital-zircon age distributions from coeval fluvial and aeolian deposits provide insight on fluvial-aeolian interaction in a pre-vegetation landscape? 3) Is the Stoer Group stratigraphically related to other pre-Rodinian sedimentary sequences? By addressing these questions, this study aims to advance our understanding of basin settings in the later Mesoproterozoic of Columbia, and test the utility of detrital-zircon geochronology as a tool to understand fluvial and aeolian dynamics in Precambrian sedimentary landscapes.

3.3 Geological Setting

3.3.1 The Torridonian succession, with an emphasis on the upper Stoer Group

The Torridonian succession of Scotland (see map in Figure 1 A&C) is one of the best-preserved Precambrian sedimentary records worldwide (Stewart, 2002), and includes fluvial, aeolian, and lacustrine deposits. The Torridonian succession is ~10 km thick, and covers an area of 200 by 40 km. It nonconformably overlies the Archean to Palaeoproterozoic Lewisian Gneiss Complex (LGC) and is unconformably covered by Cambrian nearshore-marine sedimentary rock. The succession as a whole underwent only minor deformation and very low grade metamorphism (Stewart, 2002). The Torridonian comprises three distinct units, the Stoer, Sleat, and Torridon groups. The Stoer Group, the oldest of the three and focus of this study, is separated from the Sleat and Torridon groups by a 30^{o} unconformity representing a gap in time of c. 200 million years. The

Stoer Group is interpreted as a late Mesoproterozoic rift setting (Stewart, 1982), whereas the Sleat and Torridon groups are interpreted as early Neoproterozoic syn-Grenvillian forelands (Krabbendam et al., 2017) (See stratigraphy in Figure 1B).

The Stoer Group is divided into the lowermost Clachtoll Formation, composed of basal breccia and alluvial-fan deposits interbedded with sandy sheet flood deposits (Stewart, 2002). The overlying Bay of Stoer Formation is composed of a lower mud-silt stone (Stac Fada Member), previously thought as volcanogenic in origin though recently recognised as a meteorite impact deposit (Stewart, 2002; Amor et al., 2007; Parnell et al., 2011; Simms, 2015), and an upper mudstone (Poll a' Mhuilt Member) interpreted as a lacustrine deposit– possibly marine influenced (Stewart, 2002; Parnell et al., 2015; Stüeken et al., 2017). The uppermost unit of the Stoer Group is the fluvial-aeolian Meall Dearg Formation (Lebeau & Ielpi, 2017), which represents the main stratigraphic target of this study. The regional stratigraphy of the Stoer Group is illustrated in Figure 2 in which the palaeo-topography of the formations is shown. Local geologic details of surface exposures at Stoer Peninsula and Enard Bay are illustrated in Figure 3.

The Meall Dearg Formation is composed of red beds exposed at Stoer Peninsula, Enard Bay, and Rubha Reidh (Stewart, 2002). The most representative sections, at Stoer Peninsula and Enard Bay, are up to 300 m thick, and include an assemblage of fluvial channel-belt, floodbasin, and aeolian erg facies (Lebeau and Ielpi, 2017). The lowermost and middle section on the Stoer Peninsula, interpreted as a fluvial channel-belt deposit, is composed of cross-bedded pebbly-lithic arkose fining upward to cross-bedded coarse- to medium grained arkose. The uppermost portions encompass ubiquitous symmetrically rippled fine-grained arkose associated with floodbasin deposits. In contrast, the Enard

Bay section comprises large-scale cross-bedded arkose associated with an intermountain aeolian erg environment, with evidence of fluvial interaction in its uppermost portions. The section at Rubha Reidh was not considered in this study, although is described in Stewart (2002) as a fluvial deposit. A Rb-Sr whole rock radiometric age of 1199 +/- 70 Ma has been inferred from a limestone bed in the upper Bay of Stoer Formation (Turnbull et al., 1996), immediately below the Meall Dearg Formation. Parnell et al. (2011) dates the lower Bay of Stoer, Stac Fada Member (impact deposit) more precisely based on $^{40}Ar/^{39}Ar$ dating of authigenic K-feldspar from fluid inclusions. Current consensus is that the Stoer Group detritus is derived for the most part from local erosion of the Archean – Palaeoproterozoic Lewisian Gneiss Complex, and a rift-related geodynamic setting is inferred (Rainbird et al., 2001; Stewart, 2002; Cawood, 2007). The rift-setting of the Stoer Group is interpreted by a number of evidences. This includes an extensional stress regime represented by extensional faults and dilatational cracks in the Clachtoll Formation, downwarping of the basin floor of the Bay of Stoer Formation, and compositional-textural immaturity of the sandstone (Rainbird et al., 2001; Stewart, 2002).

3.3.2 The Lewisian Gneiss Complex

The Lewisian Gneiss complex (LGC) is one of the world's most intensively studied Precambrian gneiss-terrane-complexes (see geologic map in Figure 1A). The LGC, like the Torridonian, has been studied for over a century, and its geological complexities and associated nomenclature have always been highly debated (Kinny et al., 2005). The nomenclature in this work will broadly follow that of Kinny et al. (2005). The Lewisian Gneiss Complex is the basement rock that underlies the Torridonian, and is mainly composed of deformed Archean tonalite-trondhjemite-granodiorite (TTG) that was

reworked throughout the Palaeoproterozoic. Its current outcrop includes the Outer Hebrides and a 30 x 100 km coastal strip west of the Moine thrust zone (Friend and Kinny, 2001). The LGC was originally described as a "contiguous block of Archaean crust" (Peach et al., 1907; Sutton and Watson, 1951), however, modern geochronological methods have since lead to its reappraisal. Current consensus interprets the LGC to represent multiple disparate terranes with distinct magmatic and metamorphic histories (Kinny and Friend, 1997; Friend and Kinny, 2001; Kinny 2005); although, the number of terranes and timing of amalgamation remains debated (Park, 2005; Goodenough et al., 2010).

3.3.3 LGC basement ages: protoliths, metamorphism, and intrusion

The Lewisian Gneiss Complex encompasses an assemblage of juxtaposed terranes with relatively distinct protolith ages and metamorphic events that make it ideal for attempting refined reconstructions of sedimentary provenance (Fig. 1A and Table 1). Along the north-western mainland, the northernmost Rhiconich Terrane (protolith c. 2840 - 2680 Ma) and Assynt Terrane (c. 3030-2960 Ma) comprise the northern and central districts (Friend and Kinny, 2001). To the south, the Gruinard (protolith c. 2840 Ma), Gairloch (Loch Maree Group >2000 Ma, Ard Gneiss c.1905 Ma), Ialltaig (c. 2000 Ma), and Rona (c. 3135 – 2889 Ma) terranes (Love et al., 2010) are exposed (see map in Figure 1A). In the Outer Hebrides, younger protolith ages are present, including the Ness and Roineabhal terranes (c. 1860 Ma and 1880 respectively), and other terranes with non-unique Archean ages similar to those on the mainland from 3125 Ma to 2750 Ma (Tarbert, Uist, and Bara terranes) (Friend and Kinny, 2001; Kelly et al., 2008).

The Lewisian Gneiss Complex can be generally divided into three metamorphic districts including a central granulite-facies unit (Assynt Terrane), which is surrounded by northern and southern amphibolite-facies units (Rhiconich and others) (Goodenough et al., 2010). The major metamorphic events affecting the LGC in chronologic order include the Inchinaian granulite-facies (c. 2730 Ma), Badcallian granulite-facies (c. 2490 Ma), Inverian amphibolite-facies (c. 2490-2400 Ma, 2500-2600 Ma), Laxfordian amphibolite-facies (c. 1740 Ma), and Somerledian (or: late Laxfordian) amphibolite-facies (c. 1670 Ma) (Friend and Kinny, 2001). Pegmatites, mafic dykes, and granite sheets were also intruded throughout the LGC (Love et al., 2010). The dominant intrusions include the early mafic Scourie dyke suite (2000 – 2400 Ma) (Heaman and Tarney, 1989; Waters et al., 1990; Goodenough, 2010), the Laxfordian granite sheets (1880-1854Ma), dioritic intrusions at 2680 Ma (Kinny and Friend, 1997), and pegmatites (1660-1694 Ma) (Shaw et al., 2016).

3.4 Analytical methods

3.4.1 Sampling and sample preparation

Four hand samples were collected from the Meall Dearg Formation for detrital-zircon geochronologic analysis (sample locations in Figure 3). Two samples were taken at Stoer Peninsula: sample LL-02 from the basal portions of the fluvial-channel-belt associated deposit, and sample LL-06 was collected up-section at the fluvial-floodbasin deposit. Samples LL-09 and LL-10 were taken from lower and upper portions of the aeolian erg deposit at Enard Bay, respectively. All samples were collected to include well-developed heavy-mineral bands to ensure a successful zircon yield. Also samples were collected in the lowermost portions of the largest cross-beds in the sections.

Samples were crushed and milled into fine- to medium-sand sized particles; crusher and mill were cleaned with a high-pressure air hose, steal wire-brush drill, and wiped down with alcohol between samples. Heavy minerals were then concentrated using a Wilfley table and placed under closed fume-hood for drying; the Wilfley table was also cleaned in the same manner between samples, excluding the wire-brush drill. Subsequent preparation and analysis was performed at the geochronology labs at the Geological Survey of Canada in Ottawa (Ontario, Canada). Continued heavy mineral separation was performed by means of passing dried-pulverised samples through methylene iodide, and the Franz isodynamic magnetic separator.

3.4.2 Imaging: photographs, cathodoluminescence (CL), and backscatter (BS)

Detrital-zircon grains were mounted and photographed under transmitted and reflected light for descriptions of grain morphology and colour. CL and BS imaging followed to 1) identify and avoid metamict grains, fractures, and inclusions for ion-microprobe analysis; 2) to date targeted core-mantle-rim domains within some complex grains; and 3) to analyse internal textures of the grains for interpretation of igneous or metamorphic sources.

3.4.3 Sensitive High Resolution Ion Microprobe (SHRIMP) analysis

SHRIMP analytical procedures followed those described by Stern (1997). Briefly, zircons were cast in 2.5 cm diameter epoxy mounts along with fragments of the GSC laboratory standard zircon (z6266, with 206Pb/238U age = 559 Ma, Stern and Amelin, 2003). The mid-sections of the zircons were exposed using 9, 6, and 1 μm diamond compound, and the internal features of the zircons (such as zoning, structures, alteration, etc.) were characterised in back-scattered electron mode (BSE) utilising a scanning electron

microscrope. Mount surfaces were evaporatively coated with 10 nm of high purity Au. Analyses were conducted using an ^{16}O- primary beam, projected onto the zircons at 10 kV. The count rates at eleven masses including background were sequentially measured over 5 scans with a single electron multiplier and a pulse counting system with deadtime of 21 ns. Off-line data processing was accomplished using SQUID version 2.50.11.10.15, rev. 15 Oct 2011 (Ludwig, 2009). The 1σ external uncertainties of $^{206}Pb/^{238}U$ ratios reported in the data table incorporate a ±1.5 % uncertainty in calibrating the 6266 zircon. Pb isotopic ratios were monitored by analyses of an in house zircon (1242) with a $^{207}Pb/^{206}Pb$ age of 2679.6 ± 0.3 Ma; no mass bias was applied to the data based on a measured value of 2676 ± 3 Ma during the session. Common Pb correction utilised the Pb composition of the surface blank (Stern, 1997). Sm-Nd was not a plausible analytical method to augment this provenance study because of a lack of mudstone in the Meall Dearg Formation; however Sm-Nd has been undertaken on the lower Poll a M'huilt Member in the Stoer Group (Turnbull et al., 1996).

3.5 Sample description

Sixteen samples were collected and thin sectioned for petrographic assessment, only four of which were further analysed for detrital-zircon geochronology. Nine samples were collected from the lower to upper portions of the Stoer Peninula section, and seven were collected bottom to top from Enard Bay. Stoer Peninsula and Enard Bay are adjacent to one another and the samples from both locations are from comparable stratigraphic levels. Samples were relatively small (<0.5 kg), and were selected along heavy mineral layering. A point count was performed and plotted on a QFR ternary diagram in Lebeau and Ielpi (2017). Of sixteen samples, fourteen were classified as fine- to medium-grained

arkose, one as feldspathic litharenite, and another as lithic arkose. The feldspathic litharenite and lithic arkose sandstones were collected in the lower and middle sections at Stoer Peninsula. Petrographic descriptions of the four samples analysed for detrital-zircon geochronology are presented in Table 2.

3.6 Results

3.6.1 Sedimentology

Lebeau & Ielpi, (2017) presented a detailed facies analysis and depositional environment interpretation of the Meall Dearg Formation, and recognised three facies associations (illustrated in sedimentary log in Figure 4): Facies 1) erosively bounded, cross-stratified-dominated arkose and lithic arkose — associated with the basal to middle section of Stoer Peninsula; Facies 2) wave-ripple-bounded, cross-stratified-dominated arkose — characterising the uppermost portions of the Stoer Peninsula section; and Facies 3) large-scale, tangential cross-stratified-dominated arkose— describing the entirety of the section at Enard Bay. Facies (1) incorporates key sedimentary structures such as planar- and cross-beds, primary current lineation, antidunal forms, symmetrical and assymetrical ripples. This assemblage of structures is related to a fluvial channel-belt environment with supercritical- to sub-critical- flows in shallow-wide channels and limited flow confinement. Facies (2) comprises ubiquitous symmetrical ripples between most stratal boundaries, planar-cross and trough-cross beds, three-dimensional and low-relief symmetrical ripples, and minor assymetrical ripples. This array of structures is associated with a sand-rich floodbasin environment as a product of bedload-dominated flows feeding splay complexes. Facies (3) is characterised by large-scale planar laminated cross-beds (1 - 5 m thick), planar-laminated sandstone, minor adhesion ripples and warts,

symmetrically rippled sandstone, and some poorly sorted fluvial lag deposits. This collection of structures points to an aeolian erg environment with intermittent damp conditions and evidence of contemporaneous fluvial and aeolian interaction. Palaeocurrent measurements of unidirectional air and water flows point generally westward (See Figure 4, rose diagram a, c, d). Bidirectional flows measured from symmetrical ripples of the floodbasin unit point NE-SW (Figure 4, rose diagram b), and a secondary crosswind points NNE measured from aeolian reactivation surfaces (Figure 4, rose diagram e).

3.6.2 Detrital-zircon data and morphology

U-Pb dating from detrital-zircon in combination with the analysis of internal textures was undertaken to gain insight of the metamorphic or magmatic nature of possible sedimentary source areas. In general, the highest proportions of zircon originate from felsic igneous rock as primary magmatic or xenocrystic; smaller amounts of zircon may develop during subsequent metamorphism, either recrystallised igneous or newly grown metamorphic zircon (Corfu et al., 2003). Metamorphic reworking of zircon is typically represented as recrystalised domains or as rims in zircon that can be abraded and removed during sedimentary transport. This results in a tendency towards magmatic zircon-forming events being better represented in detrital-zircon datasets than metamorphic.

A primary method of displaying detrital-zircon data sets is the probability density diagram (PDD), wherein taller and narrower peaks represent higher precision data (i.e. dates most repeated in the dataset— used as a proxy for density without bandwidth limitations) (Vermeesch, 2012). U-Pb detrital-zircon data analysed by SHRIMP is

presented in (Appendix A - D), and a summary of detrital-zircon age distribution data is represented in Table 4.

Grain morphology and internal textures were also evaluated to provide insight about source rock magmatic and metamorphic histories, as well as sedimentary pathways. Attributes such as crystal face development and internal textures may help correlate grains to source areas affected by certain metamorphic facies aiding in source provenance interpretations (Fedo et al., 2003). Furthermore, attributes in grain morphology can help infer distance of transport and energy of sedimentary transport (Gartner et al. 2013). Using cathodoluminescence and backscatter images, dated detrital-zircon grains were classified into four groups guided by Corfu's "atlas of zircon textures" (2003): group 1) well-preserved oscillatory zoning with limited overgrowths or reworking— reconciled with igneous zircon (Figure 5A); group 2) moderately-preserved oscillatory zoning, may have blurring and overgrowths— associated with amphibolite metamorphic zircon (Figure 5B); group 3) convoluted and chaotic textures, minor oscillatory zoning to none present, may have overgrowths— associated with granulite-facies metamorphic zircon (Figure 5C); and group 4) homogeneous, may have faint patchy textures— can be igneous or metamorphic (Figure 5D, see Table 5 for morphological summary of each sample).

LL-02 (Stoer Peninsula, Lower Unit – Fluvial facies)

Eighty-two grains were sampled and dated, showing a variety of morphologies and internal textures. Crystals are mainly clear to light beige in colour, generally equant, anhedral and rounded to well-rounded. Subordinate variations include dark-brown to dark-purple colours that are elongate with faceted and fragmented edges, and one grain is

considered euhedral. Grain sizes range from 60 to 200 μm, with most in the range of 90-120 μm. Forty-five percent of grains are fractured (not including annealed), one grain is metamict, and inclusions are rare. Internal textures can be divided into four subgroups with 37% containing very poorly defined to no oscillatory zones with blurry, convoluted, and chaotic textures (group 3), 25% are homogeneous to slightly patchy (group 4), 22% have moderately defined oscillatory zoning with some blurring and bright overgrowths (group 2), and 16% had perfectly preserved oscillatory zones with no overgrowths (group 1).

Out of 82 grains analysed, 79 grains are concordant within 5% concordance (i.e., 96% of grains are concordant). Figure 4A shows a dominant peak extending between c. 2670-2900 Ma (74% of data), the tallest peak at c. 2800 Ma. Flanking the c. 2670-2900 Ma peak are several subordinate older and younger peaks at c. 2900-3000 Ma (6% of data), and c. 2460-2670 Ma (11% of data) respectively. Only one grain is dated pre-3000 Ma at 3144 ± 41 Ma. The youngest date (1826 ± 8 Ma) is part of the youngest group of zircons ranging from c.1800 to 2000 Ma that makes up 9% of the data as small contiguous peaks.

LL-06 (Stoer Peninsula, Upper Unit – Fluvial facies)

Eighty grains were sampled and dated. Crystals are mainly clear and subordinately grey-brown in colour, none are purple/brown. Crystal morphology is dominantly faceted with some rounding most of which are elongate, with a secondary population of rounded to well-rounded equant grains. A minor component is subrounded to angular and fragmented, 8 grains are euhedral. Grain size is generally larger than the LL-02 sample, maximum range is between 60 to 200 μm though dominantly between 120 – 150 μm.

Sixty-five percent of grains are fractured (not including annealed) many with inclusions, 5 grains are metamict. Internal textures were subdivided in a similar manner into four subgroups showing similar patterns to LL-02 but in different proportions: 33% contain very poorly developed to no oscillatory zones with convoluted-penetration textures (group 3), 27% have moderately defined oscillatory zonation with bright rims and overgrowths (group 2), 25% are generally homogeneous (group 4), and 8% have pristine oscillatory zonation with no overgrowths (group 1).

Eighty-nine percent of grains are concordant (within 5% concordance). Figure 4B shows a dominant population between c. 2725 – 2925 Ma (65% of total population) with the tallest peak at c. 2800 Ma, similar to sample LL-02. Subordinate younger peaks flank the dominant age fraction from c. 2725 to 2400 Ma encompassing 26% of the data. Only two pre-3000 Ma grains were dated including 3076 ± 9 Ma represented by a discordant narrow-isolated peak, and one dated at 3638 ± 10 Ma – possibly the oldest zircon ever dated in the Stoer Group (not shown in histogram). The youngest dates reside as three isolated peaks at c. 1750 Ma, c. 1950 Ma, and c. 2150 Ma, the youngest dated grain is 1736 ± 24 Ma.

LL-09 (Enard Bay, Lower Unit – Aeolian facies)

Sixty-nine grains were sampled and dated. Crystal colours are dominantly clear to beige with some grey-brown and purple. Crystal face development is mainly anhedral and equant. Most of these grains are fragmented showing both rounded edges on one side and angular-sharp edges on the other. The majority of grains are faceted to subrounded, and a secondary population is rounded to well-rounded. Grain size is significantly larger than LL-02 and LL-06 fluvial samples, with a maximum range between 60 to 400 μm (almost

double the size of previous samples) and a dominant range between 150 – 180 μm. Seventy percent of grains are fractured with minor inclusions, one is metamict. Internal textures were again subdivided into four groups: 36% have moderately well preserved oscillatory zonation with blurring and overgrowths (group 2), 32% are homogeneous to patchy (group 4), 24% have little to no oscillatory zoning with convoluted-chaotic textures and sector zoning present (group 3), 8% with perfectly preserved oscillatory zonation (group 1).

Out of 69 grains, 91% are concordant (within 5% concordance). Figure 4C shows a dominant age fraction between c. 2650-2850 Ma (60% of data) where the tallest peak is dated at c. 2800 Ma. Pre- 2850 Ma there is a subordinate and contiguous population between c. 2850-3000 Ma (15% of data), and one zircon dated at 3368 ± 13 Ma. Post-2650 Ma fractions have three peaks from c. 2550-2650 Ma (6% of data), c. 2400-2500 Ma (17%), and the youngest zircon a single zircon dated at 1864 ± 24 Ma at 1σ.

LL- 10 (Enard Bay, Upper Unit– Aeolian facies)

Seventy-eight grains were sampled and dated. Crystal colour is dominantly clear to beige with subordinate grey, grey-brown colours, few are purple. Crystal face development is mainly anhedral and equant with some subhedral grains, only 4 are euhedral and elongate. Grains are dominantly subrounded to rounded to well-rounded, a second significant population of angular fragmented grains are also present. Grain size ranges from 60 to 320 μm and most grains fit between a 120 to 150 μm range — notice both aeolian samples have larger grains than the fluvial populations. Thirty-eight percent of grains are fractured (not including annealed) with minor inclusions, four are metamict. Internal textures were subdivided, 35% are homogeneous with slight patchy textures

(group 4), 32% have moderately preserved oscillatory zoning with overgrowths (group 2), 27% have little to no oscillatory zoning with convoluted chaotic textures (group 3), 6% have well-preserved oscillatory zoning (group 1).

Ninety-five percent of grains are concordant out of 78 grains. Figure 4D shows a dominant grouping between c. 2700 – 2850 Ma comprising 51% of data, where the tallest peaks are c. 2800 Ma. Pre-2850 Ma grains (11% of total data) mostly constitutes separated isolated and narrow peaks at c. 3050 Ma, 3150 Ma, and 3200 Ma, with the oldest grain dated at 3214 ± 5 Ma. Post-dating 2700 Ma, are contiguous – non-distinct – peaks up to c. 2300 Ma (33 % of data) and a separate peak at c. 1900 Ma (5% of data). The youngest grain is 1869 ± 15 Ma.

3.6.3 Statistical analysis

Four statistical methods were used including probability density diagram (Figure 4), the cumulative distribution function (Figure 6A), the Kolmogorov-Smirnov test, and the kernel density estimate (Figure 6B). The probability density diagram was constructed by AgeDisplay (Sircombe, 2004), and other diagrams by using "R" software, guided by Vermeesch et al. (2016). The cumulative distribution function illustrates the comparison among the four samples with input uncertainties of 1σ (Vermeesch et al., 2016). Figure 6A illustrates that the age distributions from the four samples are relatively similar pre-2500 Ma but diverge post-2500 Ma. The separation post-2500 Ma could be the result of different source areas, different proportions from the same source areas, or possibly the result of facies control (shown by the coupling of fluvial from aeolian curves). However, there is a smaller number of post-2500 Ma, relative to pre-2500 Ma grains and this separation could be an artifact of sample bias and can not be over interpreted. To

quantitatively test the hypothesis of a facies-controlled distribution, a two-sample Kolmogorov-Smirnov (K-S) test was undertaken. The K-S test assigns a *p*-value to sample pairs based on the similarity of their cumulative distribution functions as seen in Figure 6. A high *p*-value (>0.05) indicates a statistically significant likelihood that the two samples were derived from sources with the same zircon age distributions (Press et al., 1986; Szwarc et al., 2014). In addition, the K-S test is accompanied by the D statistic, where the closer the value is to 0 the more likely it is that the sample pairs are of the same provenance. A summary of *p*-values and D statistics are shown in Table 3. The fluvial pair (LL-02 vs LL-06) has a *p*-value =0.9985, and D = 0.0507, suggesting a very strong similarity of provenance. The aeolian pair (LL-09 vs LL-10) has a *p*-value = 0.5961, and D = 0.1262, suggesting that provenance is still similar although with slight differences. The fluvial-aeolian comparison (LL-02 vs LL-09) yield a *p*-value = 0.8125, and D= 0.10315, and (LL-02 vs LL-10) a *p*-value 0.5098, and D=0.1279. Comparison of fluvial sample LL-06 was not done because both fluvial distributions are highly similar. All fluvial and aeolian detrital-zircons were also compared (LL-02, LL-06 vs. LL-09, LL-10) yielding a p-value of 0.3027, and D = 0.1088. Comparing all the fluvial and aeolian samples, they are both statistically speaking from the same provenance, although a *p*-value of 0.3027 has the lowest degree of similarity. A lower *p*-value is expected comparing all four samples because of an increase in the number of grains evaluated, which influences the statistic. Nonetheless, the K-S test quantitatively confirms that there is a degree of facies-control regarding detrital-zircon distributions of the samples. This is most evident in the high similarity of the fluvial pairs (*p*-value = 0.9985). A high similarity between the fluvial and aeolian samples (LL-02 vs, LL-06, p-values =0.8125),

could either indicate that provenance is very similar (disproving a facies-controlled provenance) or possibly that the two sedimentary systems had a high degree of sediment transfer.

The kernel density estimate (Figure 6B) is used to smoothen probability density distribution curves (Figure 4) and to better interpret statistically significant age fractions. These curves (using bandwidth 25 for all samples) show a consistent peak at c. 2800 Ma through all samples. The Lower Enard Bay LL-09 trend shows a distinction of possibly four age fractions: 1) c. 2400 Ma, 2) 2750 Ma, 3) the dominant c. 2800 Ma, and 4) a subtle fraction at c. 2900 Ma. Up stratigraphic section the Upper Enard Bay LL-10 distribution preserves the dominant c. 2800 Ma, the c. 2750 Ma peak is reduced, and the c. 2900 Ma is non-existent. New peaks include a young age fraction c. 1800 Ma and c. 2500 Ma. The Lower and Upper Stoer LL-02, LL-06 trends show a migration of the c. 1800 Ma peak toward c. 1900 Ma, a decreasing c. 2500 Ma peak that was prominent in the aeolian samples, whereas the c. 2750 Ma peak reappears as more prominent. The c. 2800 Ma peak also remains present.

3.7 Discussion

The study of sedimentary provenance is widely used to characterise the nature of sediment source areas, dispersal pathways by which sediment is transported, and the nature of the palaeocontinent (e.g., palaeoclimate, topography, catchment area size) (Haughton et al., 1991). In the following, sedimentary provenance of the Meall Dearg Formation will be discussed and compared to ages of the Lewisian Gneiss Complex basement. When referring to zircons collected from the LGC (by previous literature) the term “protolith-zircon” is used. Similarly, when referring to zircons collected from the

Meall Dearg Formation (by this study) the term "detrital-zircon" is used. Fluvial and aeolian interactions are also discussed in terms of what can be revealed from detrital-zircon age distributions from these coeval environments. Lastly, the basin setting of the Stoer Rift is described followed by its context within supercontiental assembly and comparisons to the Gardar Rift.

3.7.1 Provenance interpretations

Protolith-zircon from the Lewisian Gneiss Complex

Over the past few decades, the Lewisian Gneiss Complex has been extensively dated using U-Pb zircon geochronology. To date, approximately eighteen papers have used zircon geochronology to refine the LGC regarding timing of terrane amalgamation, and of metamorphic events (events summarised in Table 1, including Rhinnian Complex) (Friend & Kinny, 2001; Whitehouse & Kemp, 2010; Love et al., 2010; Goodenough et al., 2013). Unsurprisingly, such extensive research gave rise to contentious interpretations, partly because of the different methods used (e.g., SIMS vs. TIMS) (Friend et al., 2007). Nonetheless, the high number of zircon grains that have been analysed combined with the fact that the LGC is composed of disparate crustal blocks with relatively distinct ages warrants a sedimentary provenance study at the terrane scale.

In this study, literature that reports U-Pb zircon analyses by ion-microprobe (e.g., SIMS, and SHRIMP) were compiled to compare age distributions with those of the Meall Dearg Formation. Works using TIMS methods were not included and deemed incomparable with the SHRIMP data acquired for this study. A total of eight studies were compiled (summarised in Table 6), and protolith-zircon ages were plotted in a kernel density estimate curve (n=1301) (grey, opaque curve in Figure 7A). The trends of the protolith-

zircon ages represented in the LGC compilation curve of Figure 7A are geologically relevant, although the height of the peaks is not reliable because of inherent sample bias. In Figure 8, areas sampled in the LGC's mainland and Outer Hebrides are shown. Areas of intense sampling would be represented in the curve with much higher peaks then areas with fewer samples (e.g., large portions of the Outer Hebrides). Consequently, peak height in this curve is not necessarily representative of protolith-zircon age proportions throughout the Lewisian Gneiss Complex. A second bias exists because the compilation comprises protolith-zircon from present-day exposure and not the exposure at the time of erosion and deposition in the Stoer Group: large areas of LGC exposed during the Mesoproterozoic are now covered by the later Torridon Group or hidden in the sea. LGC basement exposure east of the Stoer Group is mostly reworked and covered by younger rocks now exposed along the Moine Thrust Zone.

Four main peaks can be recognised in the LGC protolith-zircon age compilation curve including a broad peak ranging from c. 2,900 to c. 2,600 Ma, and three narrow peaks at c. 2,500, c. 1,875 Ma, and c. 1,675 Ma. Older secondary populations are also recorded between 3,200 Ma and 2,900 Ma. From oldest to youngest, these populations will be discussed in terms of geological events and terranes in the following.

The oldest populations from c. 2,900 – 3,200 Ma are related to protoliths from migmatites of the Roineabhal Terrane (Friend & Kinny, 2001), trondhjemitic gneiss from the Gruinard and Assynt terranes (Love et al., 2004; McDonald et al., 2015), and banded tonalitic gneiss from the Rona Terrane (Love et al., 2010). Ages within this range have also been documented in the Tarbert and Corodale Gneiss in the Outer Hebrides although not by ion-microprobe (Love et al., 2010).

The broad peak c. 2,900 - 2,600 Ma is a non-Gaussian curve with a multimodal trend. The peak can be related to TTG protolith formation, intrusion, high-grade metamorphism, and meta-sedimentary packages. More specifically, the curve has distinguishable populations at c. 2,850, c. 2,730, and c. 2,640 Ma. The c. 2,850 Ma fraction mostly coincides with protolith formation in the mainland Rhiconich and Gruinard terranes, and the Outer Hebrides Roineabhal, Tarbert, and Ness terranes. Whitehouse and Kemp (2010) collected samples from the Assynt with estimated protolith age of c.2.85 Ga, this will not be considered due to severe Pb-loss complications in the study. Further events related to this date include high-grade metamorphism in the Tarbert (Kelly et al., 2008) and the Gruinard terranes (c.2,800 Ma) (Whitehouse et al., 1997) recorded in metamorphic rims. The smaller c. 2,730 Ma portion is related to granulite-facies metamorphism and intrusion across the Gruinard, Gairloch, and Tarbert terranes (Love et al., 2004; Kelly et al., 2008; Love et al., 2010). Lastly the c. 2,640 Ma population is most likely an artefact of Pb-loss from c.2.8 Ga protolith affected by c.2.5 Ga Badcallian metamorphism (Whitehouse et al., 1997; Whitehouse & Kemp 2010). It is of course possible that zircons with Pb-loss are also present in the detrital-zircon population in the Meall Dearg formation.

The c. 2,500 Ma peak is only related to high-grade metamorphism from the Assynt Terrane. This event has been recorded in metamorphic rims (c.2,482 Ma) of TTG gneiss (MacDonald et al., 2015), and from protolith-zircon rims of granulite-facies tonalitic gneiss (Whitehouse & Kemp, 2010). This same event was also recognised as isotopic disturbances at c.2,480 Ma in trondhjemite sheets (Love et al., 2004). Authors named this event the Badcallian-Inverian granulite-facies metamorphism.

The c. 1,875 Ma peak is related to plutons, metamorphic events, and meta-sedimentary packages. Along the mainland, the Rhiconich Terrane has granitic sheets dated at 1,850 and 1,880 Ma (Friend & Kinny, 2001; Goodenough et al., 2013) and the Ialltaig Terrane has protolith-zircon metamorphic rims dated at c. 1,877 Ma (Love et al., 2010). In the Outer Hebrides' - Roineabhal Terrane, the c. 1,875 Ma peak is related to the Leverburgh and Langavat meta-sedimentary belts with ages spanning 2,780 to 1,880 Ma and granulite-facies metamorphism c. 1,880 Ma (Friend & Kinny, 2001).

The youngest c. 1,675 Ma peak is related to the Roineabhal Terrane's granite sheet intrusions and pegmatites across the Langavat Shear Zone (Friend & Kinny, 2001; Kelly et al., 2008). At a regional scale, this peak coincides with the second phase of Laxfordian metamorphism. The first phase of Laxfordian metamorphism (c. 1,790-1,740 Ma) is not represented in the distribution with a peak, possibly because previous studies did not sample the areas affected by it.

Provenance of the Meall Dearg Formation

Detrital-zircon dated from all four samples of the Meall Dearg Formation were compiled into a kernel density estimate curve (red curve in Figure 7A) to represent statistically significant age populations (n=309). A direct comparison with the Lewisian Gneiss Complex curve can be made because both the "protolith" zircon and the "detrital" zircon were analysed by ion-microprobe techniques (e.g., SHRIMP or SIMS). Unlike the LGC curve, the relative peak heights of the Meall Dearg Formation (MDF) curve remain proportionally correct without significant sample bias. The LGC curve of protolith-zircon and the MDF curve of detrital-zircon share three of the four main peaks. Overlapping peaks comprise the tallest peak between c. 2,900 and c. 2,600 Ma, and two smaller peaks

at c.2,475 and c.1,900 Ma. Although peaks may not align exactly, they are within the range of the same geological events. Differences in peak height between the curves are not considered due to sample bias in the LGC curve as explained above. The high similarity between the LGC and MDF curves suggests that today's zircon ages across the LGC (i.e. the lower crust) are similar to those during timing of deposition (i.e. the upper crust). Provenance analyses based on the detrital-zircon Meall Dearg Formation curve are detailed as follows.

The tallest peak of the Meall Dearg Formation curve is between 2,900 and 2,600 Ma. Thus, crust within this age bracket was the most important source of sediment during timing of deposition. This peak corresponds almost perfectly with the tallest peak of the protolith-zircon ages from the LGC, confirming that comparisons of source rock to deposit can be drawn. Crustal blocks with such protolith ages include the mainland, Rhiconich, Gruinard terranes, and the Outer Hebrides Roineabhal, Tarbert and Ness terranes. These terranes likely supplied igneous and metamorphic zircon as a result of high-grade metamorphism and intrusion. Internal textures of zircon from the Meall Dearg Formation within the 2900-2600 Ma age bracket include igneous growth zones in grain "d", and metamorphic textures including blurry texture (grain a), bright rims (grains b and e), sector zoning (grain c), homogenisation (grain f) (Figure 9A). A source in the Rhiconich, Gruinard terranes is compatible with the measured palaeocurrents.

The second tallest peak of the detrital-zircons at c. 2,475 Ma represents a subordinate source that contributed to the deposit. This peak, which is also present in the LGC protolith-zircon curve, corresponds to age ranges of the Badcallian – Inverian granulite facies metamorphism. This event has only been recorded in zircon metamorphic rims in

the Assynt Terrane. Zircon internal textures are for the most part highly convoluted (Figure 9B-grain c), a texture that is associated with granulite-facies metamorphic events (Corfu et al., 2003). Palaeoflow is consistent with the Assynt terrane as a source rock.

The smallest detrital-zircon peak broadly spans c. 2,000 to c. 1,750 Ma and represents a minor component of detrital-zircon supply. This peak corresponds to a wide range of crustal ages in the Lewisian Gneiss Complex including intrusions from the Rhiconich Terrane, metamorphism in the Ialltaig and Ard Gneiss (c. 1,900 Ma), and meta-sedimentary packages of the Loch Maree (>2000 Ma), and Leverburgh-Langavat groups (2,780 – 1,880 Ma). Northwestern and southeastern pointing palaeoflow measurements from the Meall Dearg Formation suggest protolith-zircon supply from the northern Rhiconich Terrane, and from the southern Ialltaig and Gairloch terranes (Ialltaig gneiss, Ard gneiss, Loch Maree Group). However, input from the Rhiconich intrusions is less likely because detrital-zircon with well-defined growth zones are not documented (as expected from an intrusive source) (Figure 9C). This is supported by the observation of wel00defined zoning in protolith-zircon from the granitic pegmetites in the Rhiconich Terrane (Goodenough et al., 2013).

Mismatches between the LGC and Meall Dearg Formation curves include the c. 1,675 Ma peak and the oldest populations from 3,200 to 2,900 Ma. The c. 1,675 Ma peak is present in the LGC, but these protolith-zircon ages are absent in the detrital population in the Meall Dearg Formation, probably because c. 1,675 ma intrusions did not cover a significant surface area for erosion. The older 3,200 – 2,900 Ma fractions represent protolith ages of the oldest terranes, mainly the Assynt, Rona, Tarbert terranes and Corodale Gneiss. Therefore, these terranes likely did not provide sediment. This is

inconsistent however with the presence of the c. 2,475 Ma peak that is only associated with the Assynt Terrane. It is likely that the Assynt has younger crustal portions that are near c. 2,800 Ma (Love et al., 2004) without c. 2,475 Ma metamorphic rims.

In summary, assuming that the relative proportion of detrital-zircon ages is representative of volumetric sediment budgets, the most sediment that accumulated in the Meall Dearg Formation was derived from the Rhiconich, and Gruinard terranes (largest peak), with minor components originating from the Assynt and Gairloch (Loch Maree, Ard Gneiss) terranes. The Rhinnian Complex (south of the LGC), might have been a plausible source area but its c. 1,800-1,750 Ma ages are not reflected in the Meall Dearg Formation distribution.

3.7.2 Fluvial and aeolian interaction based on detrital-zircon age distributions

Sediment entrainment by aeolian and fluvial systems differ in that wind-blown sediment may source from 10's to 1000's of kilometres away, whereas water transport is channel-confined and sediment is eroded from the local highlands. Differences in transport mechanisms of the two environments imply that their detrital-zircon age distributions may be dissimilar to some degree by means of different provenance. However, coeval fluvial and aeolian environments can interact, effectively mixing their detrital-zircon and resulting in similar detrital-zircon age distributions. Hence, dissimilarities of age distributions point to differences in provenance and limited sediment mixing, whereas their similarities suggest related provenance and sediment mixing. Sediment mixing can occur in many ways including bulk sediment delivery to aeolian systems via fluvial processes upwind (Mountney and Russell, 2004); interdune flooding of fluvial incursions (Mountney and Russell, 2006); and aeolian deflation of dried river-beds (Bullard et al.,

2002). Aeolian processes can also selectively entrain smaller grained zircons over larger ones, thus the full spectrum of provenance may not be reflected in age distributions. Below comparisons of detrital-zircon age distributions are discussed regarding the coeval fluvial and aeolian systems of the Meall Dearg Formation.

It is expected that the detrital-zircon age distributions of the fluvial and aeolian deposits will differ because the aeolian deposit has an additional south-westerly palaeowind with respect to the regional westward water and air flows (see rose diagrams in Figure 8). However, as seen in the probability density diagrams in Figure 7B, the two curves follow the same trends with distinctions by population proportions (i.e., peak height). This could be the result of different sample numbers (i.e., fluvial, n=162 and aeolian, n=147), or possibly slight differences in provenance.

The main dissimilarities are observed at the c. 2,500 and c. 1,900 Ma peaks. The aeolian samples have a higher higher proportion of c. 2,500 Ma detrital-zircon than the fluvial deposit, whereas the opposite is the case for the 1,900 Ma peak. The c. 2,500 Ma detrital-zircons are associated with the Assynt Terrane (Badcallien-Inverian high grade metamorphism), which presently surrounds the fluvial but not the aeolian deposit of the Meall Dearg Formation (see map in Figure 8). A higher proportion of aeolian c. 2,500 Ma zircon could suggest that the present LGC exposure is different than during the time of deposition (although speculative), and possibly indicates a degree of sediment mixing. Regarding the c. 1,900 Ma peak, the fluvial curve spans c. 1,650 - 2,000 Ma, whereas the aeolian is narrow and spans c. 1,800 - 2,000 Ma. These corresponds to protolith-zircon ages from intrusions of the Rhiconich Terrane, to the Ialltaig and Gairloch terranes (including Ard Gneiss and Loch Maree), and the South Harris Igneous Complex (SHIC).

Because the fluvial curve has higher detrital-zircon proportions here, it is interpreted the fluvial catchment area incorporated the Ialltaig and Gairloch terranes and there were high degrees of fluvial-aeolian sediment mixing. Provenance from the Rhiconich intrusions and the SHIC is unlikely because of a lack of igneous textured detrital-zircons and by a lack of palaeoflow from the west, respectively (refer to Figure 9C, and textures from Goodenough et al. (2013), Fig. 4 sample LX7).

In summary, the catchment area of the fluvial deposit likely eroded into bedrock with ages spanning from c. 2,900 to c. 1,650 Ma. Terranes associated with these ages are the northern Rhiconich, and central Gruinard, Gairloch, and Ialttaig terranes. Provenance from the oldest southern Rona Terrane is unlikely because of >2,900 Ma ages in that terrane (Love et al., 2010), and neither from the Outer Hebrides due to a lack of palaeoflow measurements from the west (Figure 8). Aeolian contributions show no evidence of foreign/distal wind-blown grains, and the fluvial and aeolian age distributions are highly similar. It is likely that provenance of both systems were supplied by the same terranes despite differences in palaeoflow, and that there was a high degree of fluvial-aeolian interaction. Interbedded fluvial and aeolian deposits exposed at Enard Bay also provide evidence of interaction and likely sediment transfer.

3.7.3 The Stoer Group: pre-Rodinian rifting in east Laurentia

The Stoer Group represents a fault-bounded rift basin, however detailed discussion of its sediment fill in relation to rift evolution requires further study. In short, a rift basin is characterised by episodic subsidence and creation of accommodation space, followed by drawn out periods of basin filling and final tectonic quiescence (Prosser, 1993; Martins-Neto & Catuneau, 2009). Rift-basin fill can be considered in three stages: (1) the

lowermost “underfilled” facies of fluvial and fault scarp breccia (rift initiation); (2) the “filled” facies of sub-aqueous mud/silt (rift climax); and (3) the “overfilled” facies of terrestrial deposits (post-rift) (Prosser, 1993; Martins-Meto & Catneau, 2009). Within the Stoer Group in this rift-basin framework, the lowermost Clachtoll Formation represents an “underfilled” rift initiation phase, the Bay of Stoer Formation represents the “filled” rift climax stages, and the Meall Dearg Formation is associated with the “overfilled” post-rift quiescent stage (See phases of sediment fill in Figure 10). Specifically, the Clachtoll Formation is composed of conglomerate interbedded with trough-cross bedded sandstone interpreted as alluvial fan deposits (Stewart, 2002). The Bay of Stoer is characterised by muddy sandstone (Stac Fada Member) and interbedded mud-silt stone with limestone (Poll a’ Mhuilt Member) reconciled with maximum submergence of the basin in a lacustrine, possibly marine influenced environment (Ielpi et al., 2016). Finally, the uppermost Meall Dearg Formation comprises fluvial and aeolian deposits with little evidence of syn-tectonic activity (Stewart, 2002).

Extension of pre-Rodinian Laurentia is believed to have occurred from the mid- to late-Mesoproterozoic and carried on until the Grenville Orogeny (Davidson, 2008). In addition to the Stoer Group, the c. 1,270 Ma Mackenzie Dyke Swarm, the c. 1100 Ma Abitibi Dyke Swarm, and the flood basalts in the Coppermine River Group among other rock formations all attest to igneous activity as a result of extension in Laurentia (Davidson, 2008). Concerning rift-related sedimentary sequences, the coeval Gardar Rift may be the only one comparable to the Stoer Group (Upton et al., 2003). The Gardar Rift and the Stoer rift-basin both existed contemporaneously along the eastern flank of Laurentia c. 1,180 Ma, and presently remain unmetamorphosed and undeformed (see

Figure 11) (Stewart, 2002; Upton, 2003). The Gardar Rift's clastic sequence is named the Eriksjord Formation, a ~3.4 km thick package of subaerial lavas and interbedded continental fluvial-aeolian deposits (Anderson, 2003; Upton et al., 2003). Compared to the Stoer Group, both sequences comprise lowermost conglomeritic (rift-initiation?) units and fine upward to fluvial-aeolian deposits — the one main distinction being the Eriksfjord is interbedded with lavas, which are absent in the Stoer Group. Regarding sedimentary provenance, both sequences were locally derived (Anderson, 2003). Anderson (2003) undertook detrital-zircon analysis of the Eriskfjord Formation, with dominant age signatures from the northern Archean and Nagssugtoquidian cratons, and lesser from the surrounding Ketilidian basement (see Figure 11). Evidence pointed to a predominance of local sources from within Greenland — very similar to this study with the Stoer Basin likely being sourced from within north-western Scotland. Here it is suggested that the Stoer Group is related to the Gardar Rift in terms of timing of rifting along the eastern margin of Laurentia in a pre-Grenville and hence pre-Rodinia setting.

3.8 Conclusion

U-Pb detrital-zircon geochronologic data was collected from the c. 1.2 Ga fluvial-aeolian Meall Dearg Formation, the upper sandstone unit of the Stoer Group (Torridonian succession of Scotland). Detrital-zircon ages were plotted in kernel density estimates and compared to a compilation of protolith-zircon ages previously collected from across the Lewisian Gneiss Complex. A combination of westerly and south-easterly palaeocurrent measurements, detrital-zircon internal textures, and age distributions confirm provenance from the Lewisian and allowed for the inference of provenance at the terrane scale. Detrital-zircon ages from the Meall Dearg Formation that overlapped with protolith ages

from the Lewisian Gneiss Complex comprise a dominant peak spanning c. 2,900 to 2,600 Ma — likely derived from metamorphic and igneous textured zircon of the Rhiconich (c. 2,840-2,680 Ma), and Gruinard (c. 2,840 and c. 2,730 Ma) terranes. Subordinate detrital-zircon populations span from c. 2,000 to c. 1,750 Ma most probably derived from the Assynt Terrane (3,030-2,960 Ma), Ialltaig Terrane (c. 2,000 – 1,875 Ma) and Gairloch terrane's Ard Gneiss (c. 1,900 Ma) and meta-sedimentary Loch Maree Group (>2,000 Ma).

The Meall Dearg Formation is interpreted to represent coeval fluvial and aeolian depositional environments. Detrital-zircon age distributions from fluvial and aeolian samples were compared in order to semi-quantitatively test for sedimentary interaction between the two environments. The fluvial and aeolian detrital-zircon age distributions demonstrated to be nearly identical, suggesting either provenance from similarly aged source rock, a high degree of sediment transfer, or a combination of the two.

The continental fluvial-aeolian fill of the Meall Dearg Formation is best related to an overfilled, late- to post-rift succession within the Stoer Group. This inference supports the current understanding of the Stoer Group as a fault-bounded rift basin found along the margin of pre-Rodinian Laurentia at c.1.2 Ga. Finally, based on similar patterns of rifting and basin development, the Stoer Group can be related to the coeval Gardar Rift of southern Greenland.

3.10 References

Amor, K., Hesselbo, S.P., Porcelli, D., Thrackrey, S., Parnell, J., 2007. A Precambrian proximal ejecta blanket from Scotland. Geology 36, 303-306.

Anderson, T., 2013. Age, Hf isotope and trace element signatures of detrital-zircons in the Mesoproterozoic Eriksfjord sandstone, southern Greenland: are detrital-zircons reliable guides to sedimentary provenance and timing of deposition? Geological Magazine 3, 426-440.

Bingen, B., Andersson, J., Söderlund, U., Möller, C., 2008. The Mesoproterozoic in the Nordic countries. Episodes 31, 29-34.

Brasier, A.T., Culwick, T., Battison, L., Callow, R.H.T., Brasier, M.D., 2016. Evaluating evidence from the Torridonian Supergroup (Scotland, UK) for eukaryotic life on land in the Proterozoic. In: Brasier, A.T., McIlroy, D., McLoughlin, N. (Eds.), Earth Systems Evolution and Early Life: a Celebration of the Work of Martin Brasier, vol. 448. Geological Society Special Publication, pp. 121-144.

Bullard, J., Livingstone, I., 2002. Interactions between aeolian and fluvial systems in dryland environments. Area 34, 8-16.

Cawood, P.A., Nemchin, A.A., Strachan, R., Prave, T., Krabbendam, M., 2007. Sedimentary basin and detrital-zircon record along East Laurentia and Baltica during assembly and breakup pf Rodinia. Journal of the Geological Society of London 164, 257-275.

Corfu, F., Hanchar, J.M., Hoskin, P.W.O., Kinny, P., 2003. Atlas of Zircon Textures. Reviews in Mineralogy and Geochemistry 53, 469-500.

Daly, J.S., 1996. Pre-caledonian history of the annagh gneiss complex North- Western Ireland, and correlation with Laurentia-Baltic. Irish J. Earth Sci. 15, 5-18.

Davidson, A., 2008. Late Palaeoproterozoic to mid-Neoproterozoic history of northern Laurentia: An overview of central Rodinia. Precambrian Research 160, 5-22.

Fedo, C. M., Sircombe, K. N., & Rainbird, R. H., 2003. Detrital-zircon analysis of the sedimentary record. Reviews in Mineralogy and Geochemistry 53, 277-303.

Friend, C.R.L., Kinny, P.D., 2001. A reappraisal of the Lewisian Gneiss Complex: geochronological evidence for its tectonic assembly from disparate terranes in the Proterozoic. Contributions to Mineralogy and Petrology 142, 198–218.

Friend, C.R.L., Kinny, P.D., Love, G.J., 2007. Timing of magmatism and metamorphism in the Gruinard Bay aea of the Lewisian Gneiss Complex: comparison with the Assynt Terrane and implications for terrane accretion — reply. Contributions to mineralogy and petrology 153, 489-492.

Gärtner, A., Linnemann, U., Sagawe, A., Hoffman, M., Ullrich, B., Kleber, A., 2013. Morphology of zircon crystal grains in sediments — characteristics, classifications, definitions. Geologica Saxonica 59, 65-73.

Goodenough, K.M., Park, R.G., Krabbendam, M., Myers, J.S., Wheeler, J., Loughlin, S.C., Crowley, Q.G., Friend, C.R.L., Beach, A., Kinny, P.D., Graham, R.H., 2010.

The Laxford Shear Zone: an end-Archaean terrane boundary? In: Law, R.D., But- ler, R.W.H., Holdsworth, R.E., Krabbendam, M., Strachan, R.A. (Eds.), Continental Tectonics and Mountain Building, vol. 335. Geological Society, London.

Goodenough, K.M., Crowley, Q.G., Krabbendam, M., Parry, S.F., 2013. New U-Pb age constraints for the Laxford Shear Zone, NW Scotland: Evidence for tectono-magmatic processes associated with the formation of a Paleoproterozoic supercontinent. Precambr. Res. 233, 1–19.

Haughton, P.D.W., Todd, S.P., Morton, A.C., 1991. Sedimentary provenance studies. In: Morton, A.C., Todd, A.C., Haughton, P.D.W. (Eds.), Developments in sedimentary provenance studies, vol. 57. Geological Society Special publication, pp. 1-11.

Heaman, L.M., Tarney, J., 1989. U Pb baddeleyite ages for the Scourie Dyke Swarm, Scotland: evidence for two distinct intrusion events. Nature 340, 705–708.

Ielpi, A., Ghinassi, M., 2015. Planview style and palaeodrainage of Torridonian channel belts: Applecross Formation, Stoer Peninsula, Scotland. Sedimentary Geology 325, 1–16.

Ielpi, A., Ventra, D., Ghinassi, M., 2016. Deeply channelled Precambrian rivers: remote sensing and outcrop evidence from the 1.2 Ga Stoer Group of NW Scotland. Precambrian Research 281, 291–311.

Irving, E., 1957. The origin of the palaeomagnetism of the Torridonian sandstones of north-west Scotland. Philisophical Transactions of the Royal Society A 250, 100-110.

Kelly, N.M., Hinton, R.W., Harley, S.L., Appleby, S.K., 2008. New SIMS U-Pb zircon ages from the Langavat Belt, South Harris, NW Scotland: implications for the Lewisian terrane model. Journal of the Geological Society of London 165, 967-981.

Kinnaird, T.C., Prave, A.R., Kirkland, C.L., Horstwood, M., Parrish, R., Batchelor, R.A., 2007. The late Mesoproterozoic-early Neoproterozoic tectonostratigraphic evolution of NW Scotland: the Torridonian revisited. Journal of the Geological Society of London 164, 541-551.

Kinny, P.D, Friend, C.R.L., 1997. U-Pb isotopic evidence for the accretion of different crustal blocks to form the Lewisian Complex of Northwest Scotland. Contributions to Mineralogy and Petrology 129, 326-340.

Kinny, P.D., Friend, C.R.L., Love, G.J., 2005. Proposal for a terrane-based nomenclature for the Lewisian Gneiss Complex of NW Scotland. Journal of the Geological Society of London 162, 175-186.

Krambbendam, M., Bonsor, H., Hortswood, M.A.S., River, T., 2017. Tracking the evolution of the Grenvillian foreland basin: Constraints from sedimentology and detrital-zircon and rutile in the Sleat and Torridon groups, Scotland. Precambrian Research, 195, 67-89.

Lebeau, E.L., Ielpi, A., 2017. Fluvial channel-belts, floodbasins, and aeolian ergs in the Precambrian Meall Dearg Formation (Torridonian of Scotland): Inferring climate regimes from the pre-vegetation clastic rock records. Sedimentary Geology 357, 53-71.

Love, G.J., Kinny, P.D., Friend, C.R.L., 2004. Timing of magmatism and metamorphism in the Gruinard Bay area of the Lewisian Gneiss Complex: comparisons with the Assynt Terrane and implications for terrane accretion. Contributions to Mineralogy and Petrology 146, 620–636.

Love, G.J., Friend, C.R.L., Kinny, P.D., 2010. Palaeoproterozoic terrane assembly in the Lewisian Gneiss Complex on the Scottish mainland, south of Gruinard Bay: SHRIMP U-Pb zircon evidence. Precambrian Research 183, 89-111.

Ludwig, K., 2009. SQUID 2: A user's manual, rev. 12 Apr, 2009. Berkeley Geochron. Ctr. Special Publication. 5, 110 p.

Ludwig, K.R., 2003. User's manual for Isoplot/Ex rev. 3.00: a Geochronological Toolkit for Microsoft Excel. Special Publication, 4, Berkeley Geochronology Center, Berkeley, 70 p.

MacCulloch, J., 1819. A description of the Western Islands of Scotland, including the Isle of Man comprising an account of their geological structure; with remarks on their agriculture, scenery and antiquities, Hurst, Robinson, and Co., London (UK) (585 pp.).

Martins-Neto, M. A., O. Catuneanu., 2012. Rift sequence stratigraphy. Marine and Petroleum Geology. 58-70.

Mason, A.J., Parrish, R.R., Brewer, T.S., 2004. U-Pb geochronology of Lewisian orthogneisses in the Outer Hebrides, Scotland: implications for the tectonic setting

and correlation of the South Harris Complex. Journal of the Geological Society of London 161, 44-54.

MacDonald, J.M., Goodenough, K.M., Wheeler, J., Crowley, Q., Harley, S., Mariani, E., Tathan, D., 2015. Temperature-time evolution of the Assynt Terrane of the Lewisian Gneiss Complex of Northwestern Scotland from zircon U-Pb dating and Ti thermometry. Precambrian Research 260, 22-75.

Owen, G., Santos, M.G.M., 2014. Soft-sediment deformation in a pre-vegetation river system: the Neoproterozoic Torridonian of NW Scotland. Proceedings of the Geologists' Association 125, 511–523.

Mountney, N.P., Russell, A.J., 2004. Sedimentology of cold-climate aeolian sandsheet deposits in the Askja region of northeast Iceland. Sedimentary Geology 166, 223-224.

Mountney, N.P., Russell, A.J., 2006. Coastal aeolian dune development, Solheimasandur, southern Iceland. Sedimentary Geology 192, 167-181.

Park, R.G., 1991. The Lewisian complex. In: Craig, G.Y. (Ed.), The Geology of Scotland, 3rd Edition. The Geological Society of London, pp. 25–64.

Park, R.G., 2005. The Lewisian terrane model: a review. Scott. J. Geol. 41, 105–118.

Parnell, J., Mark, D., Fallick, A.E., Boyce, A., Thackery, S., 2011. The age of the Mesoproterozoic Stoer Group sedimentary and impact deposits, NW Scotland. Journal of the Geological Society, London 168, 349–358.

Parnell, J., Spinks, S., Andrews, S., Thayalan, W., Bowden, S., 2015. High molybdenum availability for evolution in a Mesoproterozoic lacustrine environment. Nature communications 6, 6996.

Peach, B.N., Horne, J., Gunn, W., Clough, C. T., Hinxman, L.W., Teal, J.J.H., 1907. The geological structure of the north-west Highlands of Scotland. Memoirs of the Geological Survey of Great Britain, Hedderrick & sons, ltd., Glasgow (UK) (825 p.).

Prave, A.R., 2002. Life on land in the Proterozoic: evidence from the Torridonian rocks of northwest Scotland. Geology 30, 811–814.

Press, W.H., Flannery, B.P., Teukolsky, S.A., and Vetterling, W.T., 1986, Numerical Recipes, The Art of Scientific Computing. Cambridge, UK, Cambridge University Press, 186 p.

Prosser, S., 1993. Rift-related linked depositional systems and their seismic expression. In: Williams, G.D., Dobb, A. (Eds.), Tectonics and seismic sequence stratigraphy, vol. 71. Geological Society Special Publication, pp. 35-66.

Rainbird, R.H., Hamilton, M.A., Young, G.M., 2001. Detrital-zircon geochronology and provenance of the Torridonian, NW Scotland. Journal of the Geological Society of London 158, 15-27.

Scanlon, R., Daly, J.S., Whitehouse, M., 2003. The c. 1.8 Ga Stanton Banks Terrane, offshore western Scotland, a large juvenile Palaeoproterozoic crustal block within the accretionary Lewisian complex. In EGS-AGU-EUG Joint Assembly.

Shaw, R.A., Goodenough, K.M., Roberts, N.M.W., Hortswood, M.S.A., Chenery, S.R., Gunn, A.G., 2016. Petrogenesis of rare-metal pegmatites in high-grade metamorphic terranes: A case study from the Lewisian Gneiss Compex of north-west Scotland. Precambrian Research 281, 338-362.

Simms, M.S., 2015. The Stac Fada impact ejecta deposit and the Lairg gravity low: Evidence for a buried Precambrian impact crater in Scotland? Proceedings of the Geologist's Association 126, 742-761.

Smith, R.L., Stearn, J.E.F., Piper, J.D.A., 1983. Palaeomagnetic studies of the Torridonian sediments, NW Scotland. Scottish Journal of Geology 19, 29-45.

Soper, N.J. and England, R.W., 1995. Vendian and Riphean rifting in NW Scotland. Journal of the Geological Society 152. 11-14.

Stern, R.A., 1997. The SC sensitive high resolution ion microprobe (SHRIMP): analytical techniques of zircon U-Th-Pb age determinations and performance evaluation. Radiogenic age and isotopic studies, Report 10. Current Research 1997-F Geological Survey of Canada, 1-31.

Stern, R.A., and Amelin, Y., 2003. Assessment of errors in SIMS zircon U-Pb geochronology using a natural zircon standard and NIST SRM 610 glass; Chemical Geology 197, 111-146.

Stewart, A.D., 1982. Late Proterozoic rifting in NW Scotland: the genesis of the 'Torridonian'. J. Geol. Soc. London 139, 413–420.

Stewart, A.D., 1990. Geochemistry, provenance and climate of the Upper Proterozoic Stoer Group in Scotland. Scottish Journal of Geology 2, 89-97.

Stewart, A.D., 2002. The later Proterozoic Torridonian rocks of Scotland: Their sedimentology, geochemistry, and origin. Geological Society, London, Memoir vol. 24, 136 p.

Stüeken, E.E., Bellefroid, E.J., Prave, A., Asael, D., Planavsky, N.J., Lyon, T.W., 2017. Not so non-marine? Revisiting the Stoer Group and the Mesoproterozoic biosphere. Geochemical Perspectives Letters 3, 221-229.

Sutton, J., Watson, J., 1951. The pre-Torridonian metamorphic history of the Loch Torridon and Scourie areas in the North-West Highlands and its bearing on the chronological classification of the Lewisian. Quarterly Journal of the Geological Society of London 106, 241–296.

Szwarc, T.S., Johnson, C.L., Stright, L.E. and McFarlane, C.M., 2015. Interactions between axial and transverse drainage systems in the Late Cretaceous Cordilleran foreland basin: evidence from detrital-zircons in the Straight Cliffs Formation, southern Utah, USA. GSA Bulletin 127, 372-392.

Turnbull, M.J.M., Whitehouse, M.J., Moorbath, S., 1996. New isotopic age determinations for the Torridonian, NW Scotland. J. Geol. Soc. London 153, 955–964.

Upton, B.G.J., Emeleus, C.H., Heaman, L.M., Goodenough, K.M. and Finch, A.A., 2003. Magmatism of the mid-Proterozoic Gardar Province, South Greenland:

chronology, petrogenesis and geological setting. Lithos 68, 43-65.

van de Kamp, P.C., Leake, B.E., 1997. Mineralogy, geochemistry, provenance, and sodium metasomatism of Torridonian rift basin clastic rocks, NW Scotland. Scottish Journal of Geology 33, 105-124.

Vermeesch, P., 2012. On the visualization of detrital age distributions. Chemical Geology 312-313, 190-194.

Vermeesch, P., Resentini, A., Garzanti, E., 2016. An R package for statistical provenance analysis. Sedimentary Geology 336, 14-25.

Waters, F.G., Cohen, A.S., O'Nions, R.K., O'Hara, M.J., 1990. Development of Archaean lithosphere deduced from chronology and isotope chemistry of Scourie Dykes. Earth Planet. Sci. Lett. 97, 241–255.

Whitehouse, M.J., 1993. Age of thre Corodale Gneisses, South Uist. Scottish Journal of Geology 29, 1-7.

Whitehouse, M.J., Claesson, S., Sunde, T., Vestin, J., 1997. Ion microprobe U-Pb zircon geochronology and correlation of Archean gneisses from the Lewisian Gneiss Complex of Gruinard Bay, northwestern Scotland. Geochimica et Cosmochimica Acta 61, 4429-4438.

Whitehouse, M.J., Bridgwater, D., 2001. Geochronological constrains on Palaeoproterozoic crustal evolution and regional correlations of the northern Outer Hebridean Lewisian complex, Scotland. Precambrian Research 105, 227–245.

Whitehouse, M., Kemp, A.I.S., 2010. On the difficulty of assigning crustal residence, magmatic protolith and metamorphic ages to Lewisian granulites: constraints from combined in-situ U-Pb and Lu-Hf isotopes. In: Law, R.D., Butler, R.W.H., Holdsworth, R.E., Krabbendam, M., Strachan, R.A. (Eds.), Continental Tectonics and Mountain Building: The Legacy of Peach and Horne, vol. 335. The Geological Society Special publication. pp. 81-101.

White, R.W., Palin, R.M., Green, E.C.R., 2017. High-grade metamorphism and partial melting in Archean composite grey gneiss complexes. Journal of Metamorphic Geology 35, 181-195.

Williams, G.E., Foden, J., 2011. A unifying model for the Torridon Group (early Neoproterozoic), NW Scotland: product of post Grenvillian extensional collapse. Earth- Science Reviews 108, 34-49.

Young, G.M., 1999. A geochemical investigation of palaeosols developed on Lewisian rocks beneath the Torridonian Applecross Formation, NW Scotland. Scottish Journal of Geology 35, 107-118.

Zhao, G., Sun, M., Wilde, S.A., Li, S., 2004. A Paleo-Mesoproterozoic supercontinent: assembly, growth and breakup. Earth-Science Reviews 67, 91-123.

3.11 Figures

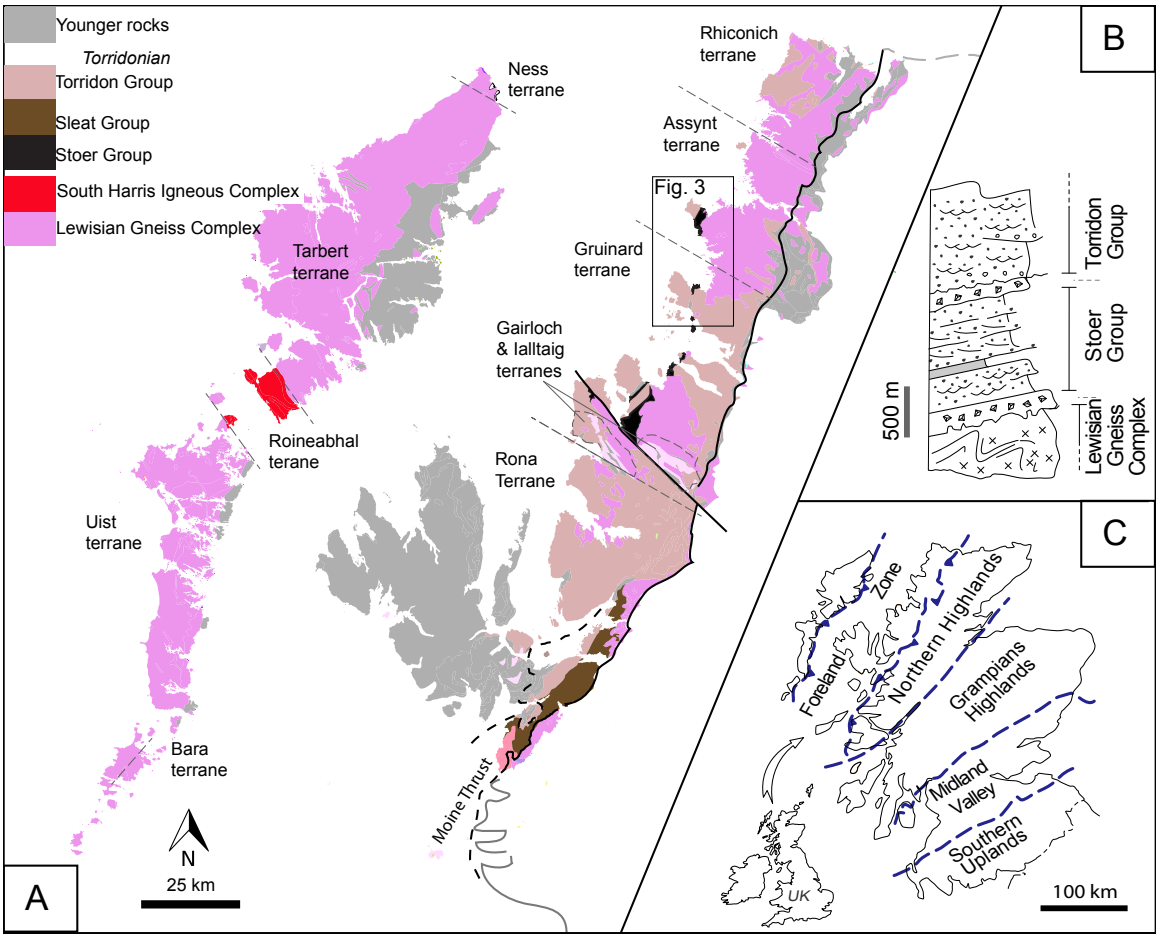

Figure 3-1: Regional map

Geological setting. A) Regional geologic map of northwestern Scotland, including mainland and Outer Hebrides, illustrating the extent of the Torridonian succession and Lewisian Gneiss Complex. B) General stratigraphy of the Torridonian. Notice the Sleat Group is not part of this log because the relationship between the Stoer and Sleat Group are unknown. Where the Sleat Group is exposed, it conformably underlies the Torridon (Stewart, 2002). C) Inset map of northwestern Scotland, thick blue-hatched lines represent major tectonic-fault zones.

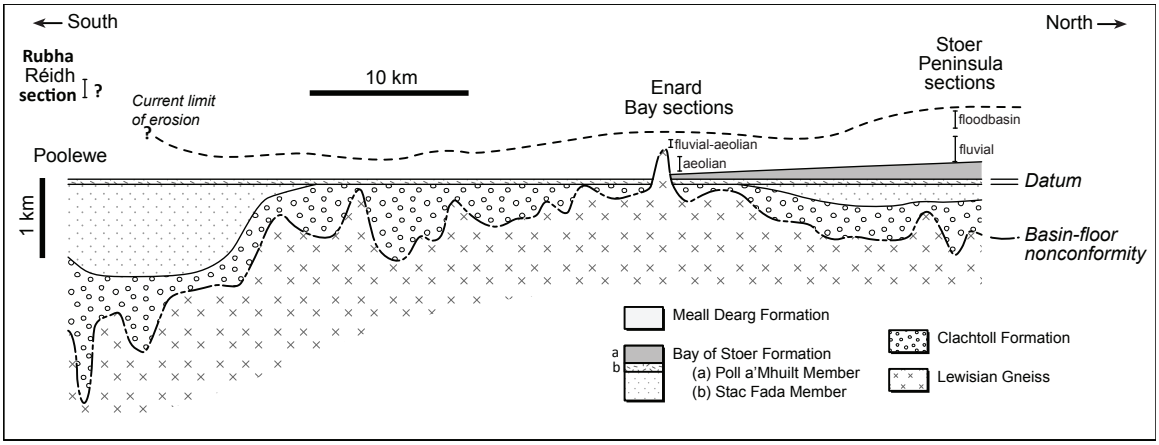

Figure 3-2: Regional transect

Geologic setting. Regional transect of the Stoer Group from Stoer Peninsula and across Enard Bay, illustrating stratigraphy and palaeotopography. The fluvial/floodbasin and aeolian sections are indicated in the Meall Dearg Formation.

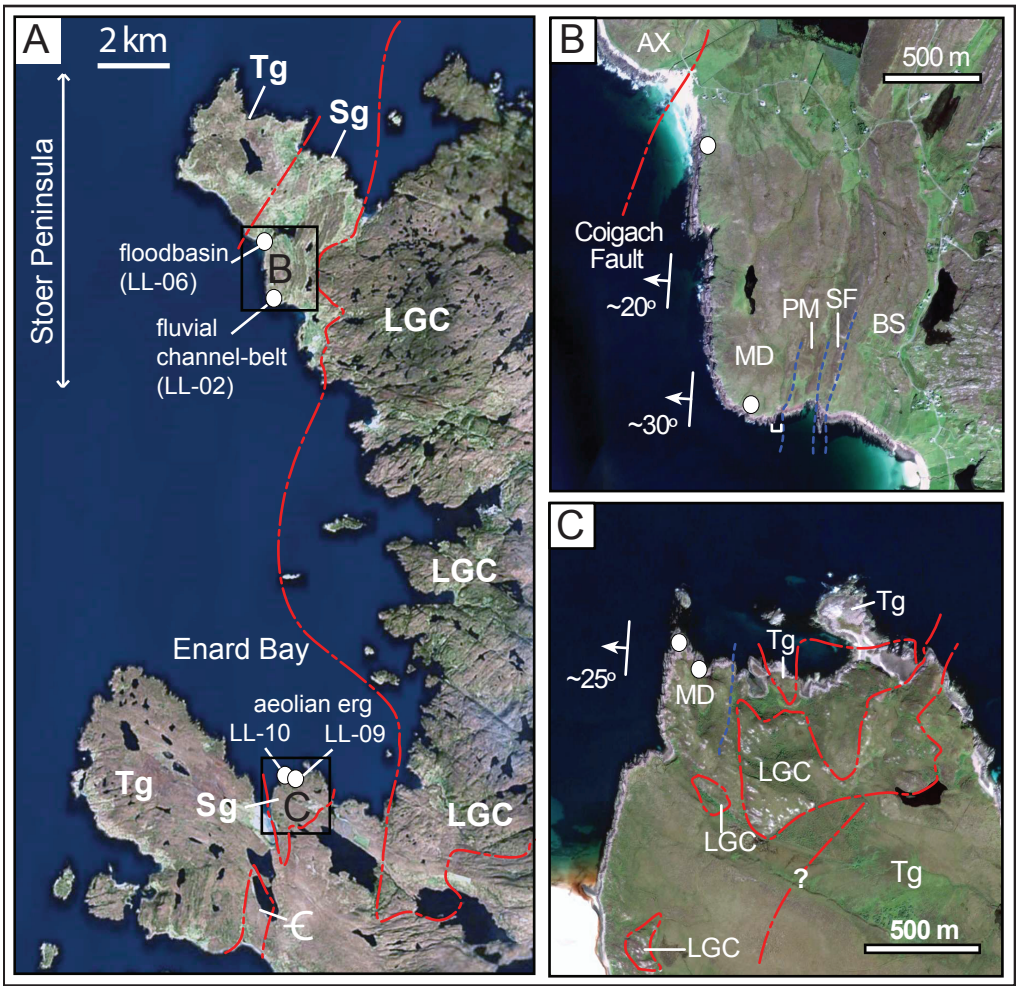

Figure 3-3: Field area

Geological setting. A) Satelite Imagery of Stoer Peninsula and Enard Bay, northwestern Scotland. Including inset of Stoer Peninsula (B) and Enard Bay (B). White dots represent areas sampled for detrital-zircon analysis. Major regional boundaries are shown as red dashed lines. Abbreviations in (A): LGC, Lewisian Gneiss Complex; Sg, Stoer Group; Tg, Toridon Group; C, Cambrian strata. Abbreviations in (B-C): BS, Bay of Stoer Formation; SF, Stac Fada Member; PM, Pol a' Mhuilt Member; MD, Meall Dearg Formation; Ax, Applecross Formation; LGC, Lewisian Gneiss Complex.

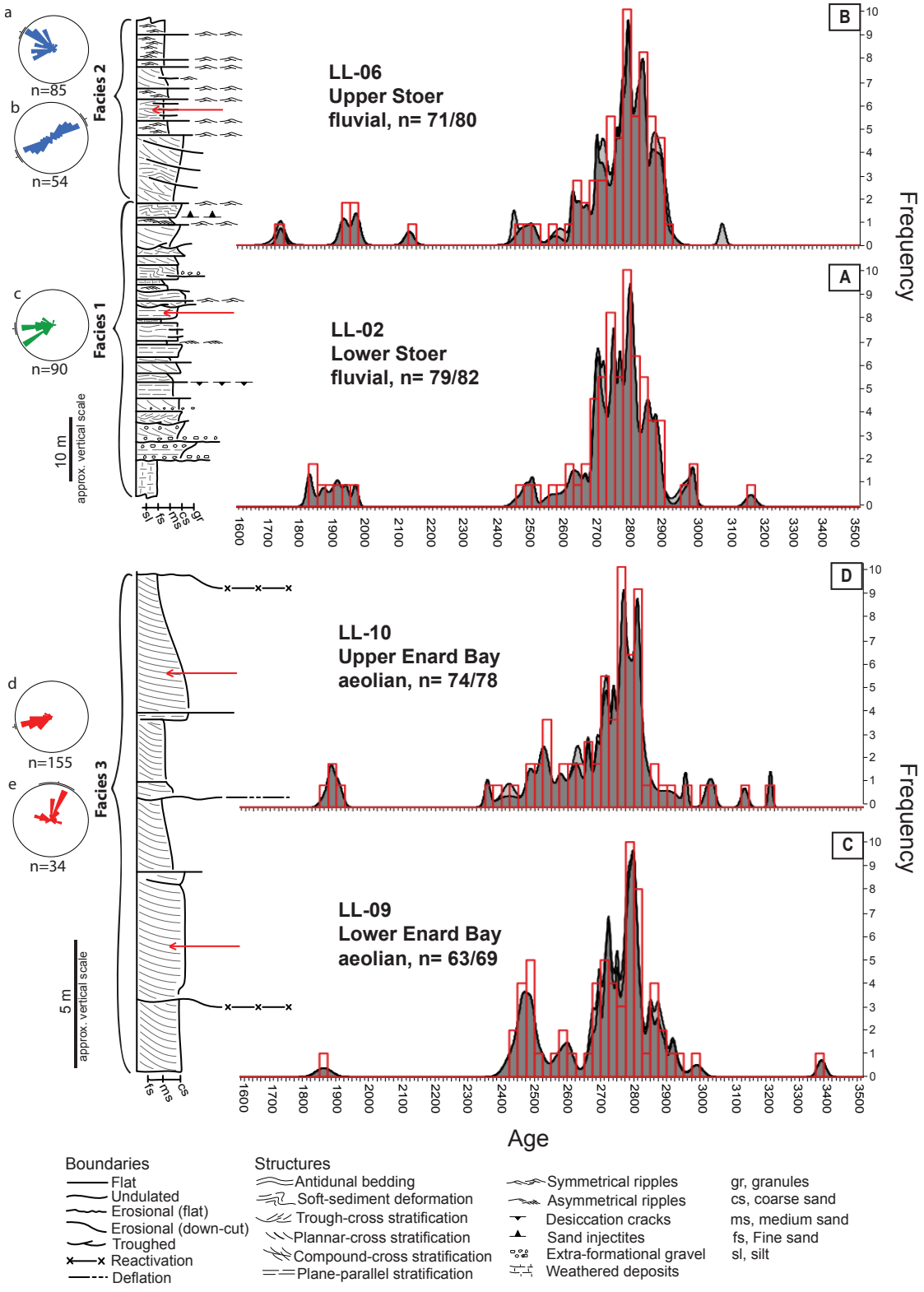

Figure 3-4: Detrital-zircon probability density diagrams

Detrital-zircon age probability density diagrams (grey opaque curve) with combined histograms (red bars). Red arrows point to approximate locations sampled from the Meall Dearg Formation's stratigraphy. Concordant data is represented in dark grey, and discordant in light grey. Sedimentary logs are representative sketches encompassing all three facies of the Meall Dearg Formation. Facies 1: Erosively bounded, cross-stratified-dominated arkose and lithic arkose. Facies 2: wave-ripple-bounded, cross-stratified-dominated arkose. Facies 3: Large-scale, tangential cross-stratified-dominated arkose. Rose diagrams (a, c) incorporate unidirectional flow structures (e.g., planar-cross, trough-cross, and ripple-cross laminations); (b) bidirectional wave-ripple trends; (d) planar-cross stratification; (e) superimposition surfaces (e.g., reactivation surfaces). The top of the page represents north for rose diagrams.

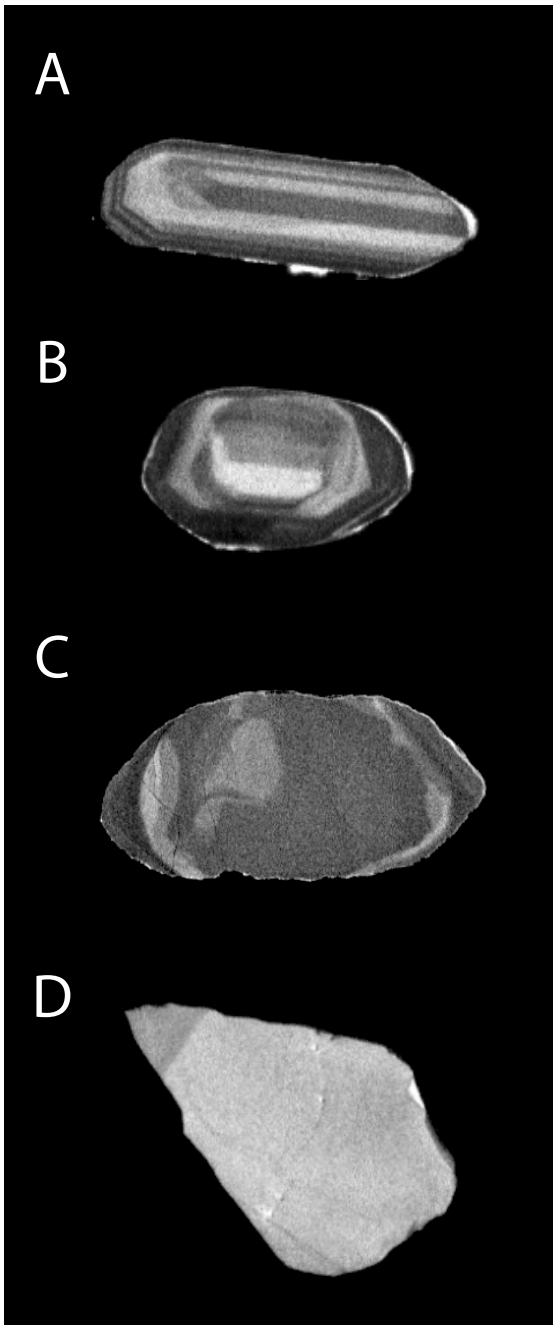

Figure 3-5: Representative internal textures of detrital-zircon grains

Results. Representative internal textures of detrital-zircon grains collected from the Meall Dearg Formation. A) well-preserved oscillatory zoning with no overgrowths or reworking— reconciled with igneous zircon. B) moderately-preserved oscillatory zoning, may have blurring and overgrowths— associated with amphibolite metamorphic zircon.

C) convoluted and chaotic textures, minor oscillatory zoning to none present, may have overgrowths— associated with granulite-facies metamorphic zircon. D) homogeneous, may have faint patchy textures— can be igneous or metamorphic.

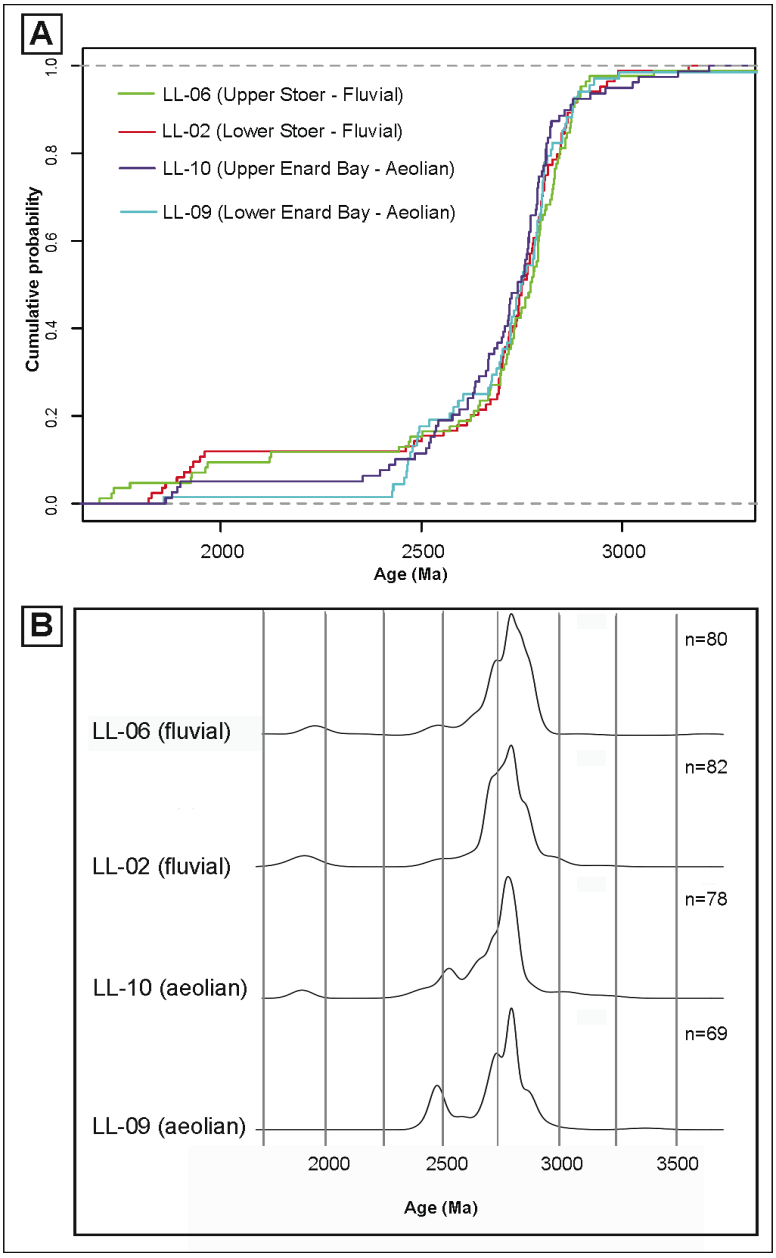

Figure 3-6: Cumulative distribution function and kernel density estimate Results. A) Cumulative distribution functions for all four samples collected from the Meall Dearg Formation. 1σ error loaded. B) Kernel density function for four samples collected from the Meall Dearg Formation. 1σ error loaded, 25 bandwidth.

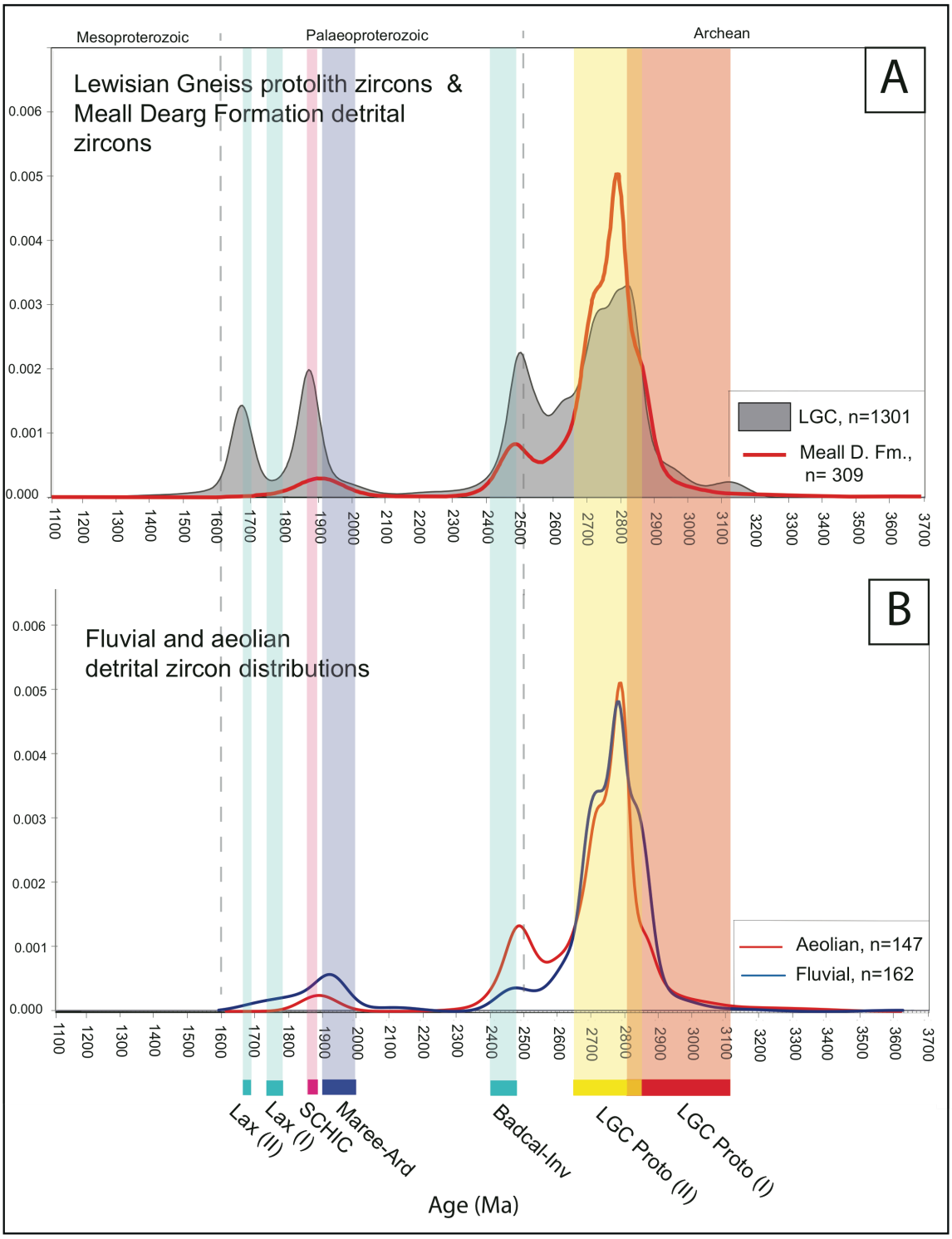

Figure 3-7: Probability density diagrams, Lewisian Gneiss Complex, Meall Dearg Formation, fluvial-aeolian

Discussion. Detrital-zircon age distributions (using kernel density estimates) and overlaid geological events. A) Comparing zircon age distributions of the Lewisian Gneiss Complex (grey) and Meall Dearg Formation (red). B) Comparing zircon ages derived from the fluvial and aeolian deposits.

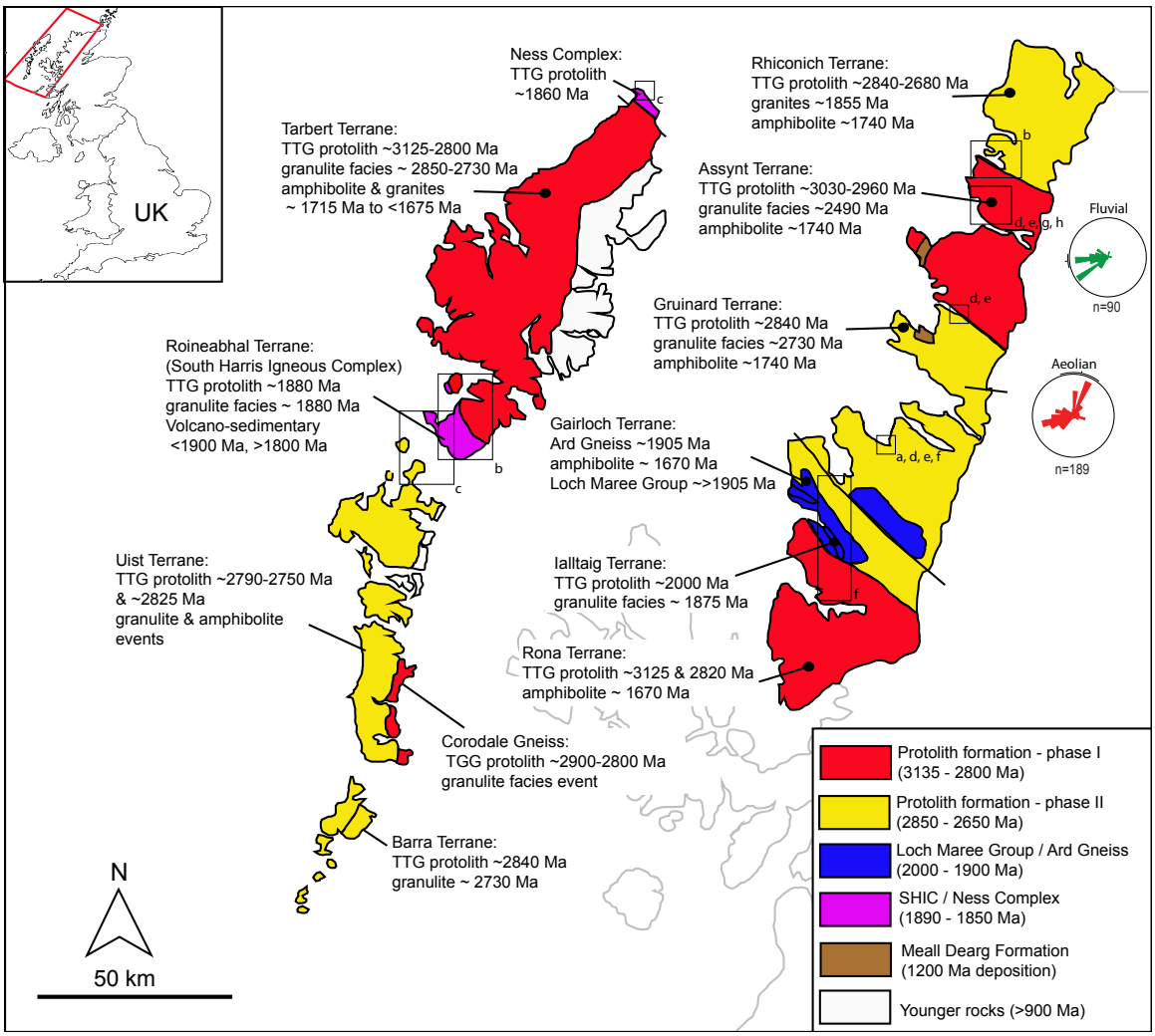

Figure 3-8: Sketch map of Lewisian Gneiss Complex zircon protolith ages

Discussion. Sketch map of the Lewisian Gneiss Complex with its mainland and Outer Hebrides exposures, NW Scotland (Modified from Kelly et al., 2008; Love et al., 2010; Goodenough et al., 2013). Terrane divisions are delineated according to the model of Friend & Kinny (2001) and protolith/metamorphic ages described from (ages reffered from Whitehouse, 1993; Love et al., 2004; Mason et al., 2004; Kinny et al., 2005; Love et al., 2010; Kelly et al., 2008; Goodenough et al., 2013). Note these are dates from all analyses types (e.g., TIMS and SIMS). The boxed areas "a" to "h" are regions of sample

collection for ion microprobe zircon dating analysis from previous literature, summarised in Table 6. a) Whitehouse et al., 1997; b) Friend & Kinny, 2001; c) Whitehouse & Bridgwater, 2001; d) Love et al., 2004; e) Kelly et al., 2008; f) Love et al., 2010; g) Whitehouse & Kemp 2010; h) MacDonald et al., 2015. A compilation of zircon dates from these areas are represented in a kernel density curve in Figure 2 (A).

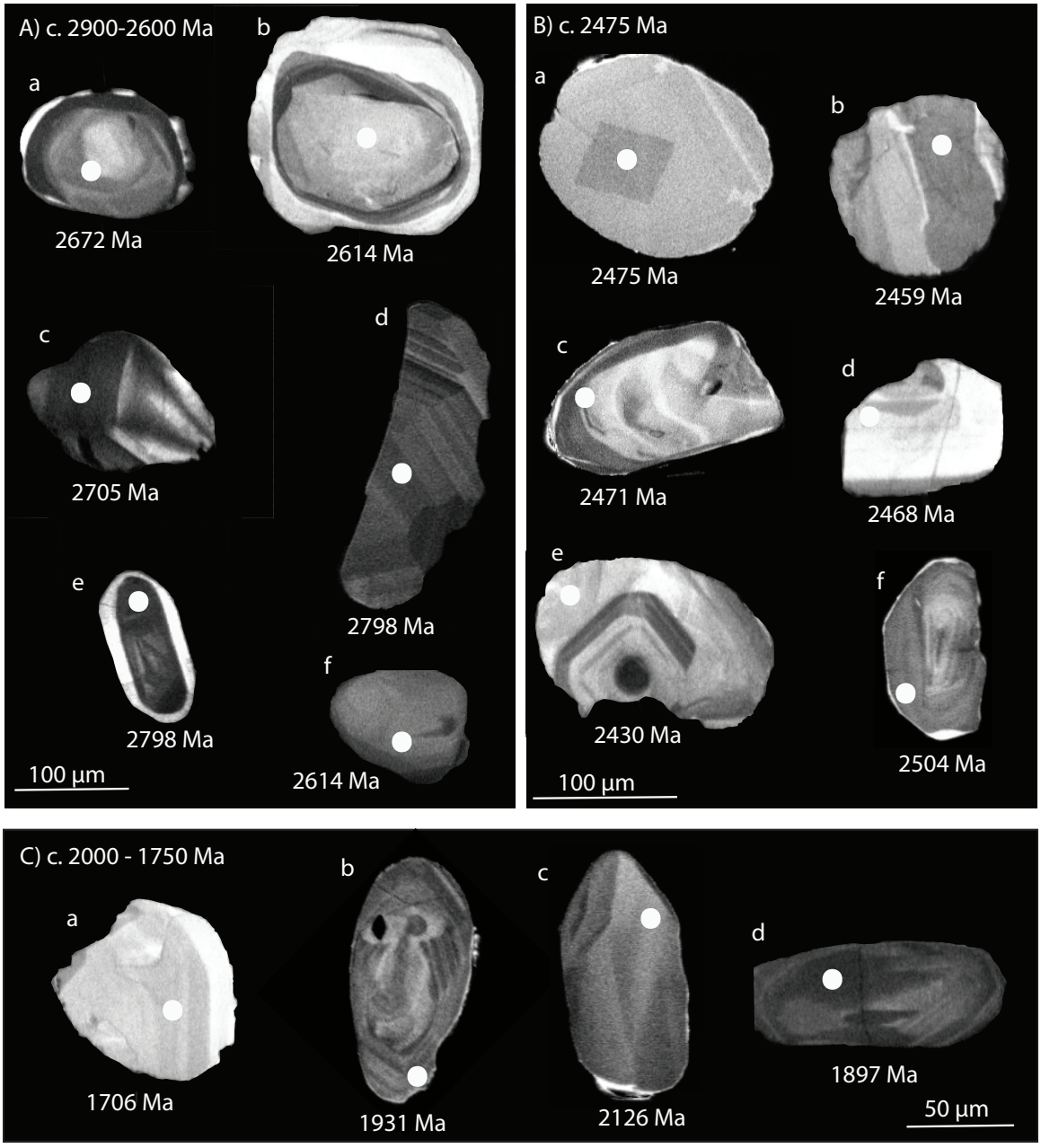

Figure 3-9: Detrital-zircon internal textures

Discussion. Detrital-zircon textures from four samples of the Meall Dearg Formation classified by age ranges. White dots on each zircon represents areas sampled (not to scale) with associated dates below each grain.

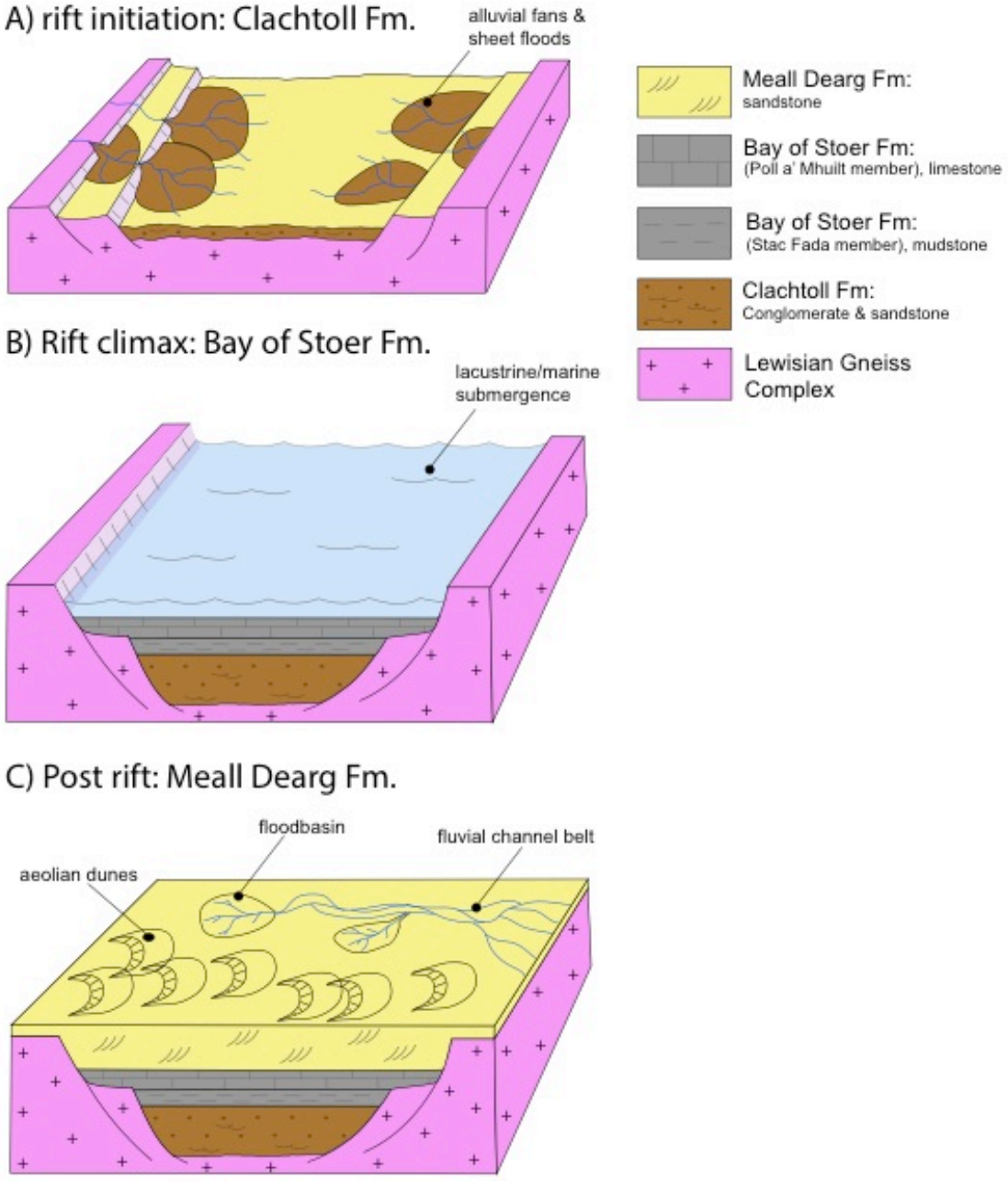

Figure 3-10: Depositional sequence of Stoer Group

Discussion. Depositional sequence of the Stoer Basin in response to A) rift initiation, B) Rift climax, and C) post rift. Rift initiation (underfilled facies) is represented as the Clachtoll Formation's alluvial fan conglomerate and trough cross-bedded sheet flood sandstone. See text for discussion.

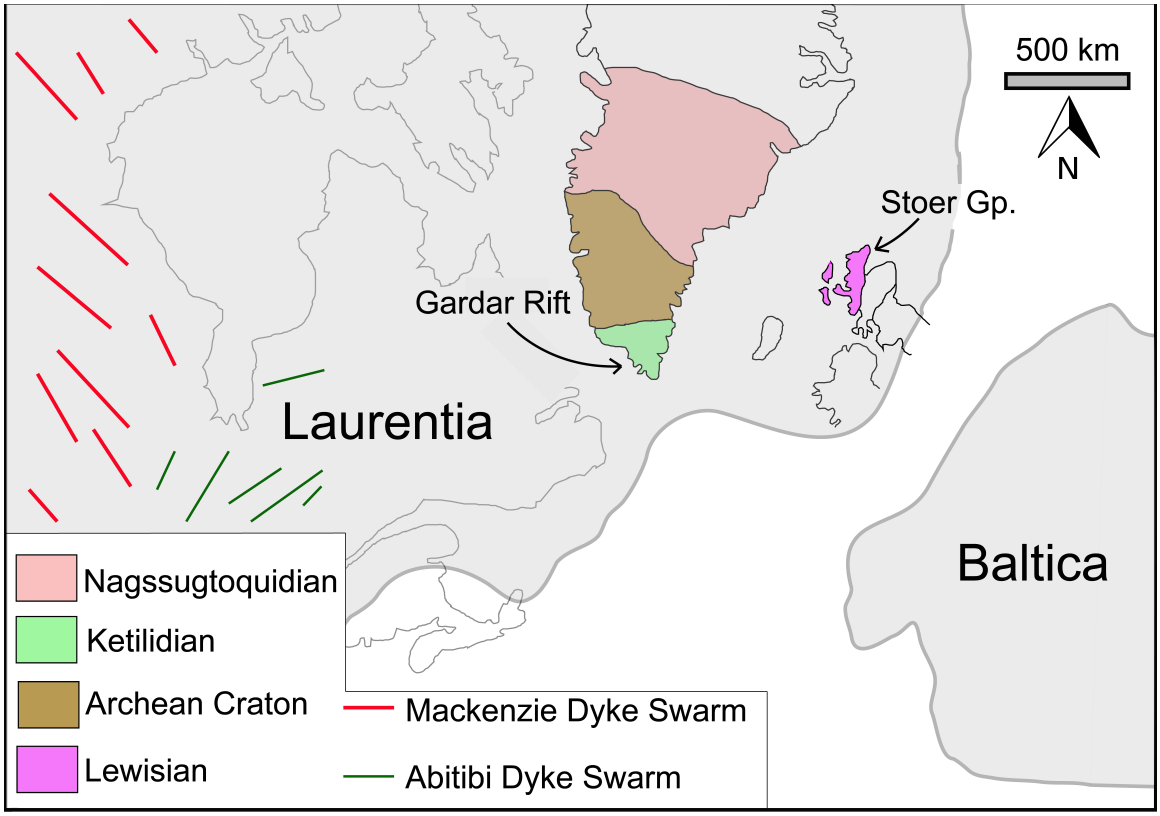

Figure 3- 11: Stoer and Gardar rifts, pre-Rodinian Laurentia

The Stoer and Gardar rifts in relation to Laurentia, Baltica, and Amazonia at c. 600 Ma after opening of Iapetus Ocean (Modified from Cawood et al., 2007). Gardar rift basin received detritus locally from Ketilidian, Archean Craton, and Nagssugtoquidian regions in Greenland (Anderson, 2003). The Stoer Basin received detritus from the Lewisian Gneiss Complex, NW Scotland. Both rifts are of comparable basin settings.

3.12 Tables

Table 3-1: Geological events in Lewisian Gneiss Complex

Intrusive and metamorphic events in the Lewisian Gneiss Complex, and the Rihnnian Complex. Events mainly after Friend & Kinny (2001) and Kiny et al. (2005), additions after Mason et al (2004); Goodenough et al (2013); MacDonald et al (2015). For Rhinnian: Daly et al. (1996); Scanlon et al (2003).

Age range (Ma)	Name	Description and notes	Short Name
LEWISIAN GNEISS COMPLEX			
>3150		Older inherited zircons	
3135-2800	Protolith formation – phase I	Intrusive event, forming older terranes, e.g. Assynt, Rona and Tarbert terranes	LGC proto I
2850-2650	Protolith formation – phase II	Intrusive event, forming younger terranes, e.g. Rhiconich, Gruinard and Barra terranes. Metamorphism in older terranes.	LGC proto II
c. 2730-2600	Protracted burial	Granulite-facies metamorphism in some terrane / Pb-loss / protracted burial	
2480-2400	Badcallian + Inverian	Granulite-and amphibolite facies metamorphism, with some partial melting; pegmatite intrusion.	Badcal-Inv
2400-2000	Scourie Dykes	Intrusion of mafic dyke swarm (main swarm at c. 2400 Ma); little/no production of zircons.	
2000-1900	Loch Maree Group / Ard Gneiss	Ialtaig gneiss intrusion at c. 2000 Ma Ard Gneiss intrusion at c. 1905 Ma, volcano-sedimentary sequence	Maree-Ard
1890-1850	South Harris Igneous Complex / Ness / Rubha Ruadh granites /	Tonalite, diorite intrusion and granulite-facies metamorphism (South- Harris, Northern Lewis); granite intrusion on mainland. Localised.	SHIC
c. 1790-1740	Laxfordian I	Amphibolite-facies metamorphism, pegmatite intrusions; localised granite sheets.	Lax I
1690-1670	Laxfordian II	Amphibolite-facies metamorphism, pegmatite intrusion. Widespread. Locally granite sheet intrusion, e.g. Harris granite complex. 'Somerledian' of Kinny et al. 2005	Lax II
RHINNIAN COMPLEX			
1800-1750	Rhinnian	Granite, syenite, granodirotie intrusions; metamorhism, Rhinns Complex; Annagh Gneiss Complex; Stanton Banks; Rockall Bank. Likely related to the Ketilidian Orogeny in south Greenland.	Rhinns

Table 3-2: Petrographic descriptions

Petrographic descriptions of four samples collected for detrital-zircon analysis.

Polycrystaline quartz included in quartz (%).

Sample	Lithology/texture	Framework	Cement/matrix	Other features
Stoer Peninsula				
LL-02-DZ	Medium- to coarse-grained, subangular to subrounded, moderately sorted lithic arkose	Quartz (28%), feldspar (25%), cement (18%), lithic fragments (13%), fine ground mass (13%)	Quartz, feldspar, and oxide cement, fine matrix	Finely laminated, sericitised, undulose quartz, deformation twins in feldspar, sutures, grain alignment
LL-06-DZ	Medium- to coarse-grained, subangular to subrounded, very well sorted arkose	Feldspar (51%), quartz (22%), cement (16%), lithic fragments (4%), ground mass (6%)	Quartz, feldspar, and oxide cement, fine matrix	Finely laminated, sericitised, undulose quartz, deformation twins, stylolites
Enard Bay				
LL-09-DZ	Medium- to coarse-grained, subrounded to rounded, moderately to well sorted arkose	Feldspar (40%), quartz (20%), cement (8%), lithic fragments (5%)	Quartz, feldspar cement	Massive, sericitised, undulose quartz, deformation twins, sutures
LL-10-DZ	Medium- to coarse-grained, subrounded to rounded, well sorted arkose	Feldspar (56%), quartz (24%), cement (15%), lithic fragments (4%), mica (1%)	Quartz, feldspar cement	Massive, sericitised, undulose quartz, deformation twins, sutures

Table 3-3: Kolmogorov-Smirnov *p*-values and D-statistics

Summary of Kolmogorov—Smirnov test for statistical comparison of facies types. P--values and D statistics are presented.

Sample	(LL-02) vs (LL-06)	(LL-09) vs (LL-10)	(LL-02) vs (LL-09)	(LL-02) vs (LL-10)	(LL-02, LL-06) vs (LL-09, LL-10)
Environment	fluvial vs fluvial	aeolian vs aeolian	fluvial vs aeolian	fluvial vs aeolian	fluvial vs aeolian
p-value	0.9985	0.5961	0.8125	0.5098	0.3027
D statistic	0.0507	0.1262	0.10315	0.1279	0.1088

Table 3-4: Summary of U-Pb dates

U-Pb dates collected from four samples by SHRIMP, dates are in millions of years (Ma).

Sample	Youngest grain	Youngest group	Younger populations	Dominant populations	Older populations	Oldest grain	Concordant/total (n)
Stoer Peninsula							
LL-02-DZ	1826 ± 8	1800-2000	2460-2670	2670-2900	2900-3000	3144 ± 41	79/82
LL-06 -DZ	1736 ± 24	1750, 1950, 2150	2400-2725	2725-2925	3076 ± 9	3638 ± 10	71/80
Enard Bay							
LL-09-DZ	1864 ± 24	2400-2500	2550-2650	2650-2850	2850-3000	3368 ± 13	63/69
LL-10-DZ	1869 ± 15	1900	2300	2700-2850	3050, 3150, 3200	3214 ± 5	74/78

Table 3-5: Summary of Internal textures and morphology

Samples	Colour	Morphology	Dominant size range, max size (μm)	Fracture	Internal textures
Stoer Peninsula					
LL-02 (82 grains)	clear/ beige	anhedral, equant, rounded to well-rounded	90-120, 200	45%	37% - convoluted/chaotic 25% - homogeneous 22% - moderate growth zones 16% - pristine growth zones
LL-06 (80 grains)	clear/ beige	anhedral, equant, rounded to well-rounded, minor angular/fragmented	120-150, 200	65%	33% - convoluted/chaotic 27% - moderate growth zones 25% - homogeneous 8% - pristine growth zones
Enard Bay					
LL-09 (69 grains)	clear/ beige	anhedral, equant, rounded and angular/fragmented grains	150-180, 400	70%	36% - moderate growth zones 32% - homogeneous 24% - convoluted/chaotic 8% - pristine
LL-10 (78 grains)	clear/ beige	anhedral, equant, rounded to well rounded and high population of angular/fragmented grains	120-150, 320	38%	35% - homogeneous 32% - moderate growth zones 27% - convoluted/convoluted 6% - pristine growth zones

Table 3-6: Literature compilation of Lewisian Gneiss Complex

Compilation of literature reporting zircon dates collected by ion-microprobe from across the Lewisian Gneiss Complex.

Article	Sample localities (terrane)	Rock types	Analysis type, (# zircon dated)
Whitehouse et al., 1997	Gruinard Bay (Gruinard)	Banded tonalite, hornblendite, trondhjemite	Ion microprobe (51)
Friend & Kinny, 2001	Fanagmore, Laxford Brae (Rhiconich); North Harris (Tarbert); South Harris (Roineabhal)	Granodioritic gneiss, tonalitic gneiss, granite sheets, migmatitic gneiss, metasediments	SHRIMP (244)
Whitehouse & Bridgewater, 2001	Butt of Lewis (Ness Complex); South Harris (Roineabhal); Berneray (Uist)	Diorite, tonalite, psammite,	Ion microprobe (134)
Love et al., 2004	Gruinard Bay (Gruinard), Badcall Bay, Lochinver (Assynt)	Trondhjemitic gneiss, tonalitic granulite, trondhjemite sheet, tonalitic gneiss	SHRIMP (190)
Kelly et al., 2008	Gruinard Bay (Gruinard), Badcall Bay, Lochinver (Assynt)	Tonalitic granulite, trondhjenitic gneiss, deformed trondjemite, tonalitic gneiss, trondjemitic gneiss	Ion microprobe (149)
Love et al., 2010	Gruinard Bay, Loch Ewe (Gruinard); Loch Gairloch (Gairloch & Ialltaig – Ard Gneiss & Loch Maree); Diabaig (Rona)	Tonalitic gneiss, Ard gneiss granodiorite	SHRIMP (185)
Whitehouse & Kemp, 2010	Kylestrome, Scouriemore (Assynt)	Tonalitic gneiss	SIMS (76)
MacDonald et al., 2015	Badcall Point, Duartmore Point, Sithean Mor (Assynt)	TTG gneisses, meta-sedimentary rock	Ion microprobe (98)

Chapter 4

4. Concluding statements

4.1 Conclusions

This thesis investigated the sedimentology, geochronology, and sedimentary provenance of the Meall Dearg Formation, the uppermost part of the Stoer Group. The formation was, prior to this thesis, one of the last units in the Torridonian succession of Scotland that lacked a modern sedimentologic framework. In this thesis, a reappraisal of the Meall Dearg Formation is provided in terms of its sedimentology and its inferred depositional environments. In addition, the sedimentary provenance of the formation was investigated in higher detail than before, based on the age distributions of detrital-zircons therein. Two main stratigraphic sections, at Stoer Peninsula and Enard Bay, were the main focus of sedimentologic field work and rock sampling.

4.1.1. Sedimentology

Mesoproterozoic terrestrial environments were discussed in Chapter 2. The Meall Dearg Formation represents a record of fluvial channel-belt, floodbasin, and aeolian erg environments based on facies analysis and petrography. Fluvial channel-belt deposits are represented by abundant transitional- to upper-flow regime structures (e.g., cross-beds, and plane-beds, and antidunal beds) associated with a low-sinuosity, ephemeral style system. The floodbasin deposit consists of plane- and cross-beds ubiquitously bounded by symmetrical wave ripples associated with splay complexes in temporary flooded depressions. The aeolian erg deposit represented by large-scale, pin-stripe-laminated cross-beds suggests intermountain dune fields.

The three facies deposit types were present along comparable stratigraphic levels and are inferred to have been coeval with one another. The uppermost section at Enard Bay exposed fluvial-lag deposits juxtaposed with aeolian, pin-stripe-laminated cross-beds, and occasional interaction between fluvial and aeolian depositional processes is thus inferred. This inference is corroborated by petrographic evidence that shows no remarkable difference between the composition and mineralogical maturity of fluvial and aeolian sandstones.

Comparisons of palaeoclimate indicators amongst three coeval depositional environments from the Meall Dearg Formation provided a rare opportunity to disentangle local climate indicators from environmental signatures in a pre-vegetation setting. The record of fluvial channel-belts with ubiquitous upper-flow regime structures is typically associated with "flashy" ephemeral style rivers in arid environments. Yet environmental factors like a small catchment can also yield the same sedimentary record. The aeolian record mostly showed evidence of aridity (e.g., only a few adhesion structures and wave ripples), indicating again an arid climate. However, the aeolian erg was located along a topographic high and therefore even a high ground water table (associated with humid climates) would not have reached the substrate surface at such elevations. Only the floodbasin deposit having a clastic fill rather than evaporitic or carbonate fill relates the system more confidently in a local humid climate regime.

4.1.2. Detrital-zircon geochronology

Three hundred and nine zircons were collected from the Meall Dearg Formation (>117 grains must be collected for statistical significance, Vermmesch, 2004). Previously, only 18 grains had been analysed, from which a local rift-basin setting was interpreted (also based on complementary evidence; Rainbird et al., 2001). Using a statistically significant

number of zircons, it is confirmed with a higher degree of confidence that the sediment from the Meall Dearg Formation is derived from the local Lewisian Gneiss Complex, again supporting a local rift-basin setting.

The detrital-zircon age distributions from the fluvial and aeolian deposit derived samples were compared. Considering the high similarities in age signatures, combined with sedimentological evidence of interbedded fluvial and aeolian deposits exposed along Enard bay, it is highly likely that sediment transfer had occurred while these environments were active. Further, it appears likely that a broad stratigraphic correlation can existed between the Stoer Group and the Gardar Rift (southern Greenland), based on similar timing of rifting along the eastern margin of Laurentia.

4.2 Future work

Chapter 2 concluded that the Meall Dearg Formation represents a fluvial-aeolian continental setting that persisted in a humid local climate regime in a pre-vegetation setting. This work however prompted for caution when discussing palaeoclimate indicators solely based on an individual depositional environment, due to possible overprinting by other environmental signatures. Future work that will integrate analysis of chemical index of alteration (CIA; Nesbitt and Young, 1982) could provide an independent test for palaeoclimate analysis, and allow for a higher degree of confidence in these kind of analyses.

Chapter 3 concluded that the sediment from the Meall Dearg Formation is derived from the local Lewisian Gneiss Complex basement. Furthermore, it represents a period of tectonic quiescence at the post-rift stages of the Stoer Group. To date, all units of the Stoer Group have now been studied using detrital-zircon geochronology for provenance

studies (Rainbird et al., 2001; Krabbendem et al., 2017). What still remains unknown about the Stoer Group is the reason for rifting (Cawood et al., 2007) and the location of the rift margins (Stewart, 2002), and as such should be future research targets.

4.3 References

Cawood, P.A., Nemchin, A.A., Strachan, R., Prave, T., Krabbendam, M., 2007. Sedimentary basin and detrital-zircon record along East Laurentia and Baltica during assembly and breakup pf Rodinia. Journal of the Geological Society of London 164, 257-275.

Krabbendam, M., Bonsor, H., Hortswood, M.A.S., River, T., 2017. Tracking the evolution of the Grenvillian foreland basin: Constraints from sedimentology and detrital-zircon and rutile in the Sleat and Torridon groups, Scotland. Precambrian Research, 195, 67-89.

Nesbitt, H.W., Young, G.M., 1982. Early Proterozoic climates and plate motions inferred from major element chemistry of lutites. Nature 299, 715-717.

Rainbird, R.H., Hamilton, M.A., Young, G.M., 2001. Detrital-zircon geochronology and provenance of the Torridonian, NW Scotland. Journal of the Geological Society of London 158, 15–27.

Stewart, A.D., 2002. The later Proterozoic Torridonian rocks of Scotland: Their sedimentology, geochemistry, and origin. Geological Society, London, Memoir vol. 24, 136 p.

Vermeesch, P., 2004. How many grains are needed for a provenance study? Earth and Planetary Sciences Letters 224, 441-451.

4.4 Appendices

Appendix A: Sample LL-02 U-Pb SHRIMP data

U, Th, Yb, Hf, $^{206}Pb^*$, are in parts per million (ppm)

										Atomic Ratios							Model Age (Ma)						
Spot name	**U**	**Th**	**Th/U**	**Yb**	**Hf**	**$^{204}Pb/^{206}Pb$**	% err	**f(206) 204**	**$^{206}Pb^*$**	**$^{208}*Pb/^{206}*Pb$**	% err	**$^{207}*Pb/^{235}U$**	% err	**$^{206}*Pb/^{238}U$**	% err	**Corr Coeff**	**$^{207}*Pb/^{206}*Pb$**	% err	**$^{206}Pb/^{238}U$**	**$\pm^{206}Pb/^{238}U$**	**$^{207}Pb/^{206}Pb$**	**$\pm^{207}Pb/^{206}Pb$**	**Disc. %**
LL-02, Meall Dearg Fm. (Lower Stoer)																							
12084-003.1	56	34	0.64	82	9505	3.6E-5	58	0.06	26.0	0.171	2.8	14.820	1.9	0.5440	1.8	0.949	0.1976	0.6	2800	40	2806	10	+0
12084-007.1	112	318	2.94	175	11547	1.2E-5	71	0.02	50.6	0.836	0.9	13.383	1.7	0.5275	1.7	0.968	0.1840	0.4	2731	37	2689	7	-2
12084-008.1	35	192	5.68	40	11137	1.7E-4	33	0.29	16.9	1.579	2.7	15.744	9.4	0.5633	9.1	0.972	0.2027	2.2	2880	212	2848	36	-1
12084-011.1	122	116	0.98	142	9654	5.6E-6	100	0.01	57.2	0.282	1.5	14.694	1.7	0.5439	1.6	0.972	0.1959	0.4	2800	37	2793	6	0
12084-012.1	202	230	1.18	87	9107	2.8E-5	33	0.05	97.5	0.335	1.0	15.833	3.1	0.5614	2.9	0.925	0.2045	1.2	2872	67	2863	19	0
12084-013.1	33	44	1.39	119	9336	2.2E-4	32	0.38	15.8	0.399	2.6	15.217	2.9	0.5584	2.0	0.681	0.1977	2.1	2860	46	2807	35	-2
12084-015.1	111	72	0.67	211	10092	3.8E-5	41	0.07	52.4	0.185	3.9	14.851	1.7	0.5469	1.7	0.968	0.1970	0.4	2812	38	2801	7	0
12084-016.1	39	39	1.02	95	10275	4.8E-5	58	0.08	21.4	0.267	2.6	18.842	2.4	0.6354	1.9	0.799	0.2151	1.4	3171	47	2944	23	-10
12084-018.1	141	235	1.72	114	10367	4.6E-5	33	0.08	63.7	0.474	1.1	13.606	1.7	0.5263	1.6	0.972	0.1875	0.4	2726	36	2720	7	0
12084-019.1	142	50	0.36	197	11412	-1.0E-5	71	-0.02	69.6	0.101	2.3	16.392	1.7	0.5724	1.6	0.976	0.2077	0.4	2918	38	2888	6	-1
12084-020.1	104	74	0.74	102	10942	2.9E-14	9999	0.00	45.9	0.205	2.0	12.882	1.7	0.5163	1.7	0.964	0.1809	0.5	2684	37	2662	8	-1
12084-022.1	59	53	0.94	135	11083	7.3E-5	41	0.13	27.2	0.254	5.1	14.796	1.9	0.5405	1.8	0.946	0.1985	0.6	2786	40	2814	10	+1
12084-023.1	38	77	2.13	104	10836	-4.2E-5	71	-0.07	16.5	0.584	2.0	13.016	2.1	0.5114	1.9	0.924	0.1846	0.8	2663	42	2694	13	+1
12084-024.1	53	19	0.38	173	8529	2.4E-5	71	0.04	26.7	0.105	3.7	17.499	2.0	0.5841	1.8	0.883	0.2173	1.0	2966	43	2961	15	0
12084-025.1	31	19	0.64	156	10429	7.2E-5	58	0.13	15.0	0.181	4.0	16.284	2.2	0.5665	2.0	0.922	0.2085	0.8	2894	47	2894	14	+0

12084-026.1	65	35	0.55	191	8995	7.8E-5	38	0.13	30.5	0.146	3.0	15.357	1.9	0.5468	1.8	0.949	0.2037	0.6	2812	40	2856	10	+2
12084-027.1	114	8	0.07	100	13308	5.3E-5	32	0.09	61.4	0.018	18.4	21.364	1.9	0.6286	1.7	0.867	0.2465	1.0	3144	41	3163	15	+1
12084-028.1	91	43	0.48	396	11639	2.3E-5	71	0.04	27.5	0.138	3.1	5.787	1.8	0.3502	1.7	0.926	0.1198	0.7	1936	29	1954	12	+1
12084-028.2	209	61	0.30	565	11824	-1.6E-5	58	-0.03	65.3	0.088	2.6	6.041	1.7	0.3632	1.6	0.960	0.1206	0.5	1997	28	1966	8	-2
12084-029.1	287	89	0.32	205	10205	2.1E-5	45	0.04	79.1	0.091	2.3	4.939	1.6	0.3210	1.6	0.965	0.1116	0.4	1795	25	1826	8	+2
12084-030.1	268	110	0.42	351	12843	7.2E-4	16	1.26	91.2	0.113	4.9	10.084	2.0	0.3954	1.6	0.798	0.1850	1.2	2148	29	2698	20	+24
12084-033.1	50	22	0.46	58	11017	-5.9E-14	9999	-0.00	22.9	0.119	3.7	14.235	1.9	0.5325	1.8	0.944	0.1939	0.6	2752	41	2775	11	+1
12084-034.1	15	22	1.52	100	10283	2.0E-4	50	0.34	6.9	0.435	3.7	13.751	2.8	0.5266	2.4	0.871	0.1894	1.4	2727	54	2737	22	+0
12084-036.1	228	179	0.81	171	12863	9.7E-22	9999	0.00	111.8	0.226	1.2	17.380	1.7	0.5703	1.6	0.961	0.2210	0.5	2909	37	2988	7	+3
12084-037.1	65	38	0.61	248	9996	8.8E-5	35	0.15	29.7	0.169	2.7	14.224	1.9	0.5362	1.8	0.949	0.1924	0.6	2768	40	2763	10	0
12084-038.1	225	114	0.52	219	10734	1.9E-5	41	0.03	105.1	0.146	1.6	14.895	1.6	0.5441	1.6	0.982	0.1986	0.3	2800	36	2814	5	+1
12084-041.1	32	38	1.23	78	9176	1.4E-4	45	0.25	12.8	0.349	3.1	10.442	2.3	0.4713	2.0	0.880	0.1607	1.1	2489	42	2463	18	-1
12084-042.1	295	72	0.25	141	9535	2.4E-5	30	0.04	137.6	0.067	3.3	14.791	1.6	0.5433	1.6	0.971	0.1974	0.4	2797	36	2805	6	+0
12084-043.1	86	135	1.63	249	8005	8.6E-6	100	0.01	37.8	0.439	1.5	13.156	1.8	0.5136	1.7	0.959	0.1858	0.5	2672	37	2705	8	+1
12084-044.1	58	131	2.34	65	9719	9.8E-5	35	0.17	26.6	0.657	1.5	14.436	2.0	0.5362	1.8	0.880	0.1952	1.0	2768	40	2787	16	+1
12084-045.1	56	69	1.27	158	10864	4.9E-5	50	0.09	26.2	0.349	2.0	14.787	1.9	0.5428	1.8	0.947	0.1976	0.6	2795	41	2806	10	+0
12084-047.1	298	172	0.60	187	13437	2.9E-5	29	0.05	137.6	0.167	1.3	14.266	1.6	0.5370	1.6	0.986	0.1927	0.3	2771	36	2765	4	0
12084-048.1	155	162	1.08	141	11354	1.3E-4	21	0.22	70.4	0.238	1.5	14.326	1.8	0.5287	1.6	0.928	0.1965	0.7	2736	36	2798	11	+3
12084-050.1	27	16	0.59	87	8728	3.6E-4	29	0.63	11.6	0.150	5.6	11.544	2.4	0.4930	2.1	0.853	0.1698	1.3	2584	44	2556	21	-1
12084-051.1	108	139	1.34	239	9731	3.5E-5	45	0.06	48.9	0.369	1.5	13.518	1.7	0.5294	1.7	0.964	0.1852	0.5	2739	37	2700	8	-2
12084-052.1	81	50	0.64	35	11126	4.3E-5	50	0.07	32.6	0.180	4.1	10.527	1.8	0.4692	1.7	0.944	0.1627	0.6	2480	36	2484	10	+0
12084-054.1	91	52	0.59	122	10480	3.3E-14	9999	0.00	46.2	0.167	2.3	17.881	1.9	0.5902	1.7	0.897	0.2197	0.8	2990	41	2979	14	0
12084-055.1	99	14	0.15	53	9560	-2.2E-5	58	-0.04	45.9	0.042	7.0	14.591	1.7	0.5384	1.7	0.965	0.1965	0.5	2777	38	2798	7	+1
12084-056.1	96	35	0.38	77	10068	-2.2E-5	58	-0.04	46.3	0.106	4.6	16.006	1.7	0.5632	1.7	0.966	0.2061	0.5	2880	39	2875	7	0
12084-057.1	28	26	0.96	82	10383	1.7E-4	41	0.29	12.0	0.275	3.5	12.181	2.3	0.5024	2.0	0.892	0.1759	1.0	2624	44	2614	17	0

12084-061.1	36	48	1.36	103	11133	-1.0E-4	45	-0.17	16.4	0.383	2.4	13.740	2.1	0.5242	1.9	0.923	0.1901	0.8	2717	43	2743	13	+1
12084-063.1	95	85	0.93	95	7817	6.6E-5	35	0.11	39.3	0.269	1.9	11.556	2.4	0.4833	1.7	0.717	0.1734	1.6	2542	36	2591	28	+2
12084-065.1	42	131	3.19	30	8205	7.0E-5	50	0.12	18.9	0.916	1.5	13.814	7.8	0.5199	2.1	0.265	0.1927	7.5	2699	46	2765	124	+3
12084-066.1	54	45	0.86	85	9579	1.3E-5	100	0.02	24.6	0.237	2.5	14.133	1.9	0.5309	1.8	0.946	0.1931	0.6	2745	40	2769	10	+1
12084-068.1	20	98	0.50	107	12289	2.8E-5	35	0.05	90.1	0.137	1.7	13.605	1.6	0.5188	1.6	0.980	0.1902	0.3	2694	35	2744	5	+2
12084-070.1	2110	52	0.49	92	11242	6.5E-6	100	0.01	51.4	0.138	4.5	14.593	1.7	0.5418	1.7	0.969	0.1953	0.4	2791	38	2788	7	0
12084-071.1	83	109	1.34	91	11208	-2.5E-5	58	-0.04	38.7	0.376	4.5	14.554	1.8	0.5400	1.7	0.962	0.1955	0.5	2784	39	2789	8	+0
12084-072.1	149	154	1.07	161	9314	3.6E-5	35	0.06	71.8	0.305	1.3	15.458	1.7	0.5607	1.6	0.976	0.2000	0.4	2869	38	2826	6	-2
12084-074.1	40	49	1.28	124	11159	1.9E-5	100	0.03	18.0	0.354	4.3	13.810	2.1	0.5291	1.9	0.931	0.1893	0.8	2737	43	2736	12	0
12084-076.1	198	59	0.31	127	11463	1.7E-5	58	0.03	58.8	0.094	2.6	5.654	1.7	0.3454	1.6	0.958	0.1187	0.5	1913	27	1937	9	+1
12084-076.2	320	134	0.43	216	11040	2.2E-5	41	0.04	96.0	0.128	1.8	5.684	1.6	0.3489	1.6	0.969	0.1182	0.4	1929	26	1929	7	0
12084-077.1	75	60	0.82	37	11089	7.2E-5	38	0.12	32.1	0.225	2.3	12.105	1.8	0.4962	1.7	0.947	0.1769	0.6	2597	37	2624	10	+1
12084-078.1	89	63	0.73	282	9196	-3.4E-5	50	-0.06	42.5	0.199	2.2	15.579	1.8	0.5575	1.7	0.961	0.2027	0.5	2856	39	2848	8	0
12084-079.1	34	14	0.41	46	12869	1.1E-4	58	0.19	9.8	0.121	6.2	5.258	2.5	0.3353	2.0	0.815	0.1137	1.4	1864	32	1860	26	0
12084-079.2	68	29	0.43	97	12258	3.4E-5	71	0.06	19.2	0.123	3.9	5.048	2.0	0.3265	1.8	0.894	0.1121	0.9	1822	28	1834	16	+1
12084-080.1	131	48	0.38	98	11231	-1.6E-5	58	-0.03	62.7	0.105	2.3	15.801	1.7	0.5557	1.7	0.975	0.2062	0.4	2849	38	2876	6	+1
12084-082.1	291	35	0.13	193	11678	5.7E-5	21	0.10	123.5	0.032	6.2	12.772	1.6	0.4949	1.6	0.984	0.1872	0.3	2592	34	2717	5	+6
12084-083.1	46	33	0.74	103	11160	6.5E-5	50	0.11	21.5	0.213	3.0	14.028	2.0	0.5405	1.9	0.933	0.1882	0.7	2786	42	2727	12	-3
12084-084.1	27	95	3.64	41	12761	2.5E-4	32	0.44	12.2	0.950	4.9	13.197	3.5	0.5257	2.0	0.584	0.1821	2.8	2723	45	2672	47	-2
12084-085.1	78	28	0.37	79	10473	3.9E-14	9999	0.00	33.8	0.106	3.2	12.512	1.8	0.5074	1.7	0.956	0.1788	0.5	2645	38	2642	9	0
12084-086.1	234	152	0.67	216	9813	8.1E-5	25	0.14	67.5	0.176	1.9	5.425	1.7	0.3357	1.6	0.952	0.1172	0.5	1866	26	1914	9	+3
12084-088.1	47	36	0.78	139	9409	-1.4E-5	100	-0.02	23.6	0.207	2.8	16.448	1.9	0.5833	1.8	0.946	0.2045	0.6	2962	44	2863	10	-4
12084-089.1	29	48	1.73	121	10176	1.8E-4	38	0.31	13.3	0.487	2.5	13.885	2.3	0.5377	2.0	0.902	0.1873	1.0	2774	46	2718	16	-3
12084-090.1	49	35	0.73	39	7759	7.8E-5	45	0.14	21.9	0.208	2.9	13.108	2.0	0.5154	1.8	0.932	0.1845	0.7	2680	40	2693	12	+1
12084-092.1	44	48	1.13	231	8866	5.0E-5	58	0.09	20.8	0.317	2.4	15.467	2.0	0.5548	1.9	0.937	0.2022	0.7	2845	43	2844	11	0

12084-093.1	50	49	1.01	284	9158	7.1E-5	45	0.12	23.3	0.298	2.3	14.470	1.9	0.5400	1.8	0.939	0.1943	0.7	2783	41	2779	11	0
12084-094.1	132	79	0.62	176	9717	1.1E-5	71	0.02	60.9	0.174	1.8	14.329	1.7	0.5379	1.6	0.973	0.1932	0.4	2775	37	2770	6	0
12084-096.1	110	37	0.35	166	10608	1.9E-5	58	0.03	53.2	0.101	2.6	15.586	1.7	0.5615	1.7	0.969	0.2013	0.4	2873	39	2837	7	-2
12084-097.1	70	44	0.65	92	10868	2.1E-5	71	0.04	30.9	0.180	2.6	13.257	1.8	0.5166	1.7	0.952	0.1861	0.6	2685	38	2708	9	+1
12084-098.1	118	75	0.66	162	13579	2.0E-5	58	0.04	55.1	0.187	2.0	14.784	1.7	0.5449	1.7	0.967	0.1968	0.4	2804	38	2800	7	0
12084-099.1	46	27	0.61	171	9132	1.2E-4	35	0.20	22.5	0.164	3.3	15.718	2.0	0.5627	1.8	0.938	0.2026	0.7	2878	43	2847	11	-1
12084-100.1	46	39	0.87	156	7780	6.6E-5	50	0.12	20.5	0.232	2.8	13.230	2.0	0.5191	1.9	0.931	0.1848	0.7	2696	41	2697	12	+0
12084-101.1	130	171	1.36	143	11090	1.8E-5	58	0.03	52.3	0.386	1.3	10.662	1.7	0.4700	1.6	0.965	0.1645	0.4	2484	34	2503	7	+1
12084-102.1	76	16	0.22	63	10868	3.0E-5	58	0.05	33.3	0.061	7.7	12.934	1.8	0.5084	1.7	0.953	0.1845	0.6	2650	38	2694	9	+2
12084-103.1	164	71	0.45	445	6415	2.3E-5	58	0.04	45.7	0.116	2.7	5.101	1.7	0.3236	1.6	0.942	0.1143	0.6	1807	26	1869	11	+4
12084-105.1	47	27	0.60	138	9382	2.9E-5	71	0.05	21.8	0.174	5.2	15.350	1.9	0.5454	1.8	0.945	0.2041	0.6	2806	42	2859	10	+2
12084-109.1	211	82	0.40	153	11593	1.4E-4	19	0.24	92.7	0.095	3.7	13.479	1.6	0.5121	1.6	0.973	0.1909	0.4	2665	35	2750	6	+4
12084-110.1	126	99	0.82	196	9921	-5.8E-5	41	-0.10	37.0	0.242	2.1	5.492	1.8	0.3430	1.7	0.926	0.1161	0.7	1901	27	1897	12	0
12084-111.1	70	14	0.20	207	9255	4.7E-5	50	0.08	30.8	0.056	5.0	13.175	1.9	0.5149	1.8	0.945	0.1856	0.6	2677	38	2703	10	+1
12084-114.1	49	8	0.16	131	9938	4.7E-5	58	0.08	22.1	0.044	6.7	13.756	5.0	0.5220	4.9	0.990	0.1911	0.7	2708	108	2752	11	+2
12084-118.1	227	86	0.39	101	12103	3.5E-6	100	0.01	104.5	0.108	1.9	14.088	1.6	0.5353	1.6	0.981	0.1909	0.3	2764	36	2750	5	-1
12084-121.1	57	46	0.83	170	10496	1.4E-5	100	0.02	26.0	0.246	2.5	13.947	1.9	0.5329	1.8	0.942	0.1898	0.6	2754	40	2741	11	-1
12084-125.1	127	50	0.41	281	13116	3.6E-5	41	0.06	57.1	0.087	2.9	14.017	3.7	0.5236	3.6	0.974	0.1942	0.8	2714	80	2778	14	+3
12084-128.1	66	78	1.22	89	11145	1.4E-13	9999	0.00	30.8	0.344	2.0	14.177	1.9	0.5412	1.8	0.950	0.1900	0.6	2788	40	2742	10	-2
12084-130.1	92	56	0.63	223	9050	7.6E-5	33	0.13	42.7	0.180	2.3	14.692	1.8	0.5422	1.7	0.958	0.1965	0.5	2793	39	2798	8	+0

Appendix B: Sample LL-06 U-Pb SHRIMP data

U, Th, Yb, Hf, $^{206}Pb^*$, are in parts per million (ppm)

										Atomic Ratios							Model Age (Ma)					
Spot name	**U**	**Th**	**Th/U**	**Yb**	**Hf**	**$^{204}Pb/^{206}Pb$**	% err	**f(206) 204**	**$^{206}Pb^*$**	**$^{208}*Pb/^{206}*Pb$**	% err	**$^{207}*Pb/^{235}U$**	% err	**$^{206}*Pb/^{238}U$**	% err	**Corr Coeff**	**$^{207}*Pb/^{206}*Pb$**	% err	**$^{206}Pb/^{238}U$**	**$\pm^{206}Pb/^{238}U$**	**$^{207}Pb/^{206}Pb$**	**$\pm^{207}Pb/^{206}Pb$**	**Disc. %**
LL-06, Meall Dearg Fm. (Upper Stoer)																							
12085-004.1	166	133	0.83	221	13100	2.8E-5	41	0.05	78.6	0.234	1.5	15.151	1.7	0.5519	1.6	0.975	0.1991	0.4	2833	37	2819	6	-1
12085-005.1	161	86	0.55	159	10343	8.3E-6	100	0.01	43.0	0.166	2.3	4.574	1.7	0.3113	1.6	0.939	0.1066	0.6	1747	25	1741	11	-0
12085-005.2	147	82	0.58	187	10278	9.8E-5	30	0.17	39.3	0.171	2.5	4.480	3.2	0.3109	3.1	0.972	0.1045	0.7	1745	47	1706	14	-3
12085-008.1	30	26	0.92	84	10808	1.6E-4	41	0.27	13.5	0.262	3.5	13.348	2.3	0.5318	2.0	0.898	0.1820	1.0	2749	45	2671	16	-4
12085-009.1	77	62	0.84	337	9607	8.4E-5	35	0.15	33.8	0.187	2.5	14.887	1.8	0.5130	1.7	0.952	0.2105	0.6	2669	38	2909	9	+10
12085-010.1	70	22	0.33	99	9767	1.2E-4	33	0.20	29.5	0.090	4.3	10.899	2.1	0.4884	1.8	0.836	0.1618	1.2	2564	37	2475	20	-4
12085-011.1	53	33	0.65	200	11394	1.0E-4	38	0.18	24.8	0.178	3.1	14.728	2.0	0.5456	1.8	0.936	0.1958	0.7	2807	42	2791	11	-1
12085-012.1	165	19	0.12	110	13135	2.5E-5	41	0.04	82.5	0.032	4.0	18.701	1.7	0.5808	1.6	0.950	0.2335	0.5	2952	38	3076	9	+5
12085-013.1	78	105	1.39	128	10939	-4.6E-14	9999	0.00	32.6	0.364	1.9	12.504	1.8	0.4844	1.7	0.949	0.1872	0.6	2546	36	2718	10	+8
12085-014.1	281	55	0.20	94	12260	1.2E-5	50	0.02	119.6	0.041	4.9	12.235	1.7	0.4950	1.6	0.954	0.1793	0.5	2592	34	2646	8	+2
12085-016.1	174	23	0.14	70	11752	-8.3E-6	71	-0.01	85.0	0.040	3.4	16.024	2.5	0.5699	1.6	0.658	0.2039	1.9	2907	38	2858	30	-2
12085-017.1	158	37	0.24	107	12869	1.9E-5	50	0.03	74.1	0.057	3.2	14.732	1.7	0.5463	1.6	0.975	0.1956	0.4	2810	37	2790	6	-1
12085-019.1	49	42	0.88	79	10077	-1.6E-5	100	-0.03	23.5	0.252	2.7	15.154	2.0	0.5581	1.9	0.939	0.1969	0.7	2859	43	2801	11	-3
12085-020.1	91	69	0.79	127	10024	5.2E-5	41	0.09	43.9	0.220	2.1	15.515	1.8	0.5616	1.7	0.959	0.2004	0.5	2873	40	2829	8	-2
12085-021.1	38	165	4.51	250	11122	4.3E-5	71	0.07	17.1	1.277	1.4	13.711	2.1	0.5269	1.9	0.923	0.1887	0.8	2728	43	2731	13	+0
12085-022.1	24	14	0.61	95	9338	3.0E-4	35	0.52	9.7	0.172	5.5	10.580	2.6	0.4751	2.2	0.838	0.1615	1.4	2506	45	2471	24	-2
12085-024.1	79	55	0.72	334	8843	-1.2E-13	9999	0.00	38.2	0.204	2.3	16.280	1.8	0.5655	1.7	0.958	0.2088	0.5	2889	41	2896	8	+0
12085-025.1	100	102	1.06	175	10544	3.1E-5	50	0.05	45.7	0.305	3.5	13.803	1.9	0.5330	1.7	0.905	0.1878	0.8	2754	38	2723	13	-1
12085-029.1	87	107	1.26	73	11132	3.5E-14	9999	0.00	38.9	0.365	1.6	12.984	1.8	0.5189	1.7	0.958	0.1815	0.5	2695	38	2666	8	-1

12085-029.2	112	152	1.40	89	11505	2.6E-5	58	0.04	48.0	0.385	1.6	12.483	1.8	0.4972	1.7	0.957	0.1821	0.5	2602	36	2672	8	+3
12085-029.3	72	89	1.28	126	12084	1.4E-5	100	0.02	29.4	0.358	2.0	12.286	1.9	0.4772	1.8	0.942	0.1867	0.6	2515	37	2713	10	+9
12085-031.1	27	78	3.01	140	11633	1.2E-4	50	0.21	12.0	0.820	2.1	12.830	2.3	0.5205	2.1	0.893	0.1788	1.1	2701	46	2642	18	-3
12085-032.1	131	25	0.20	206	10200	-6.1E-6	100	-0.01	61.6	0.057	3.4	15.224	3.2	0.5490	3.1	0.992	0.2011	0.4	2821	72	2835	7	+1
12085-033.1	77	73	0.97	168	10424	-2.0E-5	71	-0.03	33.9	0.285	2.0	12.560	1.8	0.5125	1.7	0.952	0.1778	0.6	2667	38	2632	9	-2
12085-034.1	391	167	0.44	187	12207	8.3E-6	50	0.01	177.0	0.123	1.4	13.425	1.6	0.5268	1.6	0.988	0.1848	0.2	2728	35	2697	4	-1
12085-035.1	65	31	0.49	268	7750	2.4E-5	71	0.04	31.8	0.141	3.1	16.741	2.1	0.5736	1.8	0.848	0.2117	1.1	2922	42	2918	18	-0
12085-036.1	64	50	0.81	104	10133	4.9E-14	9999	0.00	30.4	0.228	2.4	15.275	1.9	0.5535	1.8	0.950	0.2002	0.6	2840	41	2828	10	-1
12085-037.1	90	64	0.74	202	10705	1.3E-5	100	0.02	27.4	0.215	2.8	5.925	1.9	0.3547	1.7	0.921	0.1212	0.7	1957	29	1973	13	+1
12085-038.1	103	23	0.02	224	13115	1.8E-4	8	0.31	298.1	0.005	15.2	7.374	2.1	0.3362	2.0	0.982	0.1591	0.4	1868	33	2446	7	+27
12085-039.1	79	37	0.49	320	11178	9.7E-5	38	0.17	24.5	0.140	3.5	5.929	1.9	0.3629	1.7	0.897	0.1185	0.9	1996	30	1934	15	-4
12085-040.1	60	42	0.72	97	10898	3.5E-5	58	0.06	27.8	0.198	2.6	14.290	1.9	0.5373	1.8	0.947	0.1929	0.6	2772	40	2767	10	-0
12085-044.1	574	52	0.09	284	12993	8.1E-4	5	1.40	147.4	0.025	7.0	7.160	1.9	0.2989	1.6	0.828	0.1737	1.1	1686	23	2594	18	+40
12085-045.1	33	31	0.96	118	10634	7.5E-5	58	0.13	15.3	0.266	3.3	14.494	2.2	0.5375	2.0	0.915	0.1956	0.9	2773	45	2790	14	+1
12085-046.1	24	0	0.02	65	10004	2.0E-4	41	0.35	11.3	0.000	1377.6	14.742	2.4	0.5451	2.2	0.888	0.1962	1.1	2805	49	2794	18	-0
12085-047.1	9	182	21.81	100	10897	2.8E-4	58	0.49	4.0	6.759	1.6	14.170	3.6	0.5386	3.0	0.834	0.1908	2.0	2778	67	2749	32	-1
12085-048.1	43	14	0.34	147	8815	-6.6E-5	50	-0.11	20.2	0.093	4.5	15.295	2.0	0.5441	1.9	0.937	0.2039	0.7	2800	42	2858	11	+2
12085-049.1	41	16	0.40	131	10600	3.7E-5	71	0.06	20.3	0.115	4.4	16.350	2.0	0.5767	1.9	0.934	0.2056	0.7	2935	45	2871	12	-3
12085-051.1	137	49	0.37	142	9662	-5.5E-6	100	-0.01	62.2	0.107	2.4	14.175	1.7	0.5299	1.6	0.972	0.1940	0.4	2741	37	2776	7	+2
12085-052.1	70	33	0.49	173	13038	6.0E-5	45	0.10	26.1	0.101	4.1	11.376	2.1	0.4374	1.7	0.813	0.1886	1.3	2339	34	2730	21	+17
12085-053.1	24	9	0.38	95	10158	1.5E-4	50	0.25	10.2	0.104	6.9	11.728	2.5	0.4960	2.1	0.873	0.1715	1.2	2596	46	2572	20	-1
12085-054.1	118	33	0.29	199	12349	-1.3E-5	71	-0.02	52.6	0.086	5.1	13.774	1.7	0.5205	1.7	0.967	0.1919	0.4	2701	37	2759	7	+3
12085-057.1	194	60	0.32	42	10579	4.1E-6	100	0.01	85.0	0.093	2.2	12.438	1.6	0.5102	1.6	0.977	0.1768	0.4	2658	35	2623	6	-2
12085-059.1	22	9	0.40	72	10136	2.3E-4	38	0.39	10.5	0.090	7.4	15.561	2.4	0.5496	2.1	0.894	0.2053	1.1	2824	49	2869	17	+2
12085-060.1	47	78	1.72	90	9963	1.7E-5	100	0.03	21.5	0.508	2.0	13.652	2.0	0.5326	1.9	0.933	0.1859	0.7	2752	42	2706	12	-2
12085-061.1	194	209	1.11	326	10260	2.9E-5	35	0.05	94.6	0.310	1.1	15.678	1.6	0.5666	1.6	0.980	0.2007	0.3	2894	37	2832	5	-3
12085-062.1	85	76	0.93	204	10491	3.5E-5	50	0.06	40.1	0.252	2.0	15.046	1.8	0.5521	1.7	0.959	0.1976	0.5	2834	39	2807	8	-1

12085-063.1	38	46	1.25	152	9621	-6.3E-5	71	-0.11	11.0	0.364	3.1	4.889	2.3	0.3337	2.0	0.836	0.1062	1.3	1857	32	1736	24	-8
12085-063.2	56	64	1.18	189	9898	-1.5E-4	41	-0.27	14.0	0.336	3.0	4.400	2.6	0.2930	1.8	0.711	0.1089	1.8	1657	27	1781	33	+8
12085-064.1	204	101	0.51	70	9528	-3.5E-6	100	-0.01	100.4	0.142	1.6	16.003	3.4	0.5741	3.4	0.995	0.2022	0.3	2924	80	2844	5	-4
12085-065.1	154	32	0.21	143	11975	4.1E-5	35	0.07	68.0	0.056	3.3	13.473	3.3	0.5128	3.3	0.993	0.1906	0.4	2668	72	2747	7	+3
12085-066.1	251	23	0.09	125	12545	2.4E-5	35	0.04	118.4	0.024	6.4	14.807	1.7	0.5485	1.6	0.960	0.1958	0.5	2819	36	2791	8	-1
12085-070.1	142	58	0.42	251	11866	4.6E-5	41	0.08	44.6	0.117	2.8	6.069	1.7	0.3644	1.6	0.941	0.1208	0.6	2003	28	1968	10	-2
12085-071.1	186	41	0.23	139	11787	8.2E-6	71	0.01	86.4	0.066	2.6	14.544	1.7	0.5401	1.6	0.951	0.1953	0.5	2784	36	2787	9	+0
12085-072.1	223	91	0.42	184	9974	4.7E-5	27	0.08	103.4	0.110	1.9	14.569	1.6	0.5391	1.6	0.981	0.1960	0.3	2780	36	2793	5	+1
12085-073.1	27	2	0.06	40	10586	5.5E-5	71	0.10	12.6	0.017	16.9	14.846	2.3	0.5487	2.1	0.914	0.1962	0.9	2820	47	2795	15	-1
12085-074.1	70	106	1.55	112	11258	1.1E-4	32	0.19	32.5	0.438	1.7	13.756	1.9	0.5391	1.8	0.944	0.1850	0.6	2780	40	2699	10	-4
12085-075.1	41	22	0.54	81	10088	5.7E-21	9999	0.00	20.4	0.151	6.8	16.363	2.0	0.5740	1.9	0.937	0.2067	0.7	2924	45	2880	12	-2
12085-077.1	49	24	0.50	203	8736	1.5E-5	100	0.03	23.5	0.143	3.4	15.898	1.9	0.5593	1.8	0.942	0.2062	0.7	2864	42	2876	11	+1
12085-078.1	56	30	0.56	124	10058	8.0E-5	45	0.14	23.0	0.148	3.6	10.928	2.0	0.4814	1.8	0.922	0.1647	0.8	2533	38	2504	13	-1
12085-079.1	266	52	0.20	93	10012	1.4E-5	45	0.02	123.1	0.056	2.4	14.231	1.6	0.5379	1.6	0.984	0.1919	0.3	2775	36	2758	5	-1
12085-080.1	84	20	0.25	46	10433	7.1E-5	35	0.12	39.1	0.071	4.0	14.555	1.8	0.5434	1.7	0.955	0.1943	0.5	2798	39	2779	9	-1
12085-081.1	235	41	0.18	96	12117	2.3E-5	35	0.04	111.3	0.053	2.5	14.733	1.6	0.5523	1.6	0.984	0.1935	0.3	2835	36	2772	5	-3
12085-082.1	72	35	0.50	292	9509	2.9E-5	58	0.05	34.7	0.134	4.8	15.662	1.8	0.5622	1.7	0.957	0.2020	0.5	2876	40	2843	9	-1
12085-083.1	32	33	1.06	116	10645	1.2E-4	45	0.21	14.1	0.287	3.1	13.558	2.7	0.5197	2.0	0.741	0.1892	1.8	2698	44	2735	30	+2
12085-084.1	112	46	0.43	284	10131	1.0E-4	30	0.18	34.6	0.105	3.4	5.879	1.8	0.3603	1.7	0.921	0.1184	0.7	1983	29	1931	13	-3
12085-086.1	53	11	0.20	99	11990	1.3E-5	100	0.02	23.8	0.060	5.1	13.827	2.2	0.5183	1.8	0.814	0.1935	1.3	2692	40	2772	21	+4
12085-088.1	79	45	0.59	236	9747	1.7E-4	25	0.30	43.4	0.142	3.1	18.248	1.9	0.6425	1.8	0.947	0.2060	0.6	3199	44	2874	10	-14
12085-089.1	156	26	0.17	211	17315	4.2E-5	28	0.07	99.8	0.035	3.5	34.197	3.3	0.7464	3.3	0.982	0.3323	0.6	3594	91	3628	10	+1
12085-090.1	90	17	0.19	193	10413	9.3E-5	32	0.16	43.0	0.052	5.0	15.269	1.8	0.5543	1.7	0.954	0.1998	0.5	2843	40	2824	9	-1
12085-091.1	142	55	0.40	121	11805	-1.2E-5	71	-0.02	64.7	0.109	4.1	14.346	5.8	0.5298	5.8	0.997	0.1964	0.4	2741	129	2796	7	+2
12085-093.1	15	7	0.46	73	8378	1.5E-4	58	0.26	7.1	0.135	7.0	13.989	3.2	0.5370	2.4	0.746	0.1889	2.2	2771	54	2733	35	-2
12085-094.1	93	65	0.72	97	10245	-2.5E-5	58	-0.04	44.5	0.207	2.1	15.316	1.8	0.5575	1.7	0.962	0.1993	0.5	2856	39	2820	8	-2
12085-095.1	98	40	0.42	227	8623	3.6E-5	45	0.06	47.2	0.118	2.6	15.885	1.7	0.5634	1.7	0.966	0.2045	0.5	2881	39	2862	7	-1
12085-096.1	34	16	0.49	126	10657	1.3E-4	50	0.23	11.5	0.157	5.1	7.269	2.4	0.3992	2.0	0.840	0.1321	1.3	2165	37	2126	23	-2

12085-096.2	65	46	0.72	233	10579	3.1E-5	71	0.05	22.1	0.211	2.9	7.190	1.9	0.3939	1.8	0.914	0.1324	0.8	2141	32	2130	14	-1
12085-097.1	79	64	0.83	105	10435	1.0E-4	30	0.17	38.6	0.231	2.1	15.203	1.8	0.5672	1.7	0.954	0.1944	0.5	2896	40	2780	9	-5
12085-098.1	69	36	0.53	118	9767	3.3E-5	58	0.06	30.7	0.148	2.9	13.260	1.8	0.5156	1.7	0.949	0.1865	0.6	2680	38	2712	10	+1
12085-099.1	55	19	0.35	120	11225	-1.3E-5	100	-0.02	27.3	0.096	4.0	16.668	1.9	0.5793	1.8	0.948	0.2087	0.6	2946	43	2895	10	-2
12085-100.1	41	22	0.56	80	10959	-2.0E-5	100	-0.03	19.8	0.154	3.8	15.517	2.1	0.5609	1.9	0.932	0.2006	0.7	2870	44	2831	12	-2
12085-101.1	106	30	0.30	106	8608	7.5E-6	100	0.01	48.9	0.084	3.1	14.669	1.7	0.5373	1.7	0.965	0.1980	0.5	2772	38	2810	7	+2
12085-103.1	42	46	1.14	78	9372	8.9E-5	45	0.15	19.2	0.324	4.7	14.881	2.2	0.5399	1.9	0.846	0.1999	1.2	2783	43	2825	19	+2
12085-108.1	33	34	1.05	72	10810	7.4E-5	58	0.13	14.9	0.285	3.1	13.243	2.2	0.5195	2.0	0.910	0.1849	0.9	2697	44	2697	15	-0
12085-113.1	48	12	0.25	93	12605	5.9E-5	50	0.10	23.3	0.066	5.3	16.196	2.0	0.5659	1.8	0.941	0.2076	0.7	2891	43	2887	11	-0
12085-117.1	32	59	1.93	244	8434	4.7E-5	71	0.08	14.4	0.538	2.2	13.775	2.1	0.5309	2.0	0.919	0.1882	0.8	2745	44	2726	14	-1
12085-123.1	31	12	0.41	148	9637	7.6E-5	58	0.13	14.8	0.103	5.5	15.767	2.4	0.5557	2.0	0.829	0.2058	1.4	2849	46	2873	22	+1

Appendix C: Sample LL-09 U-Pb SHRIMP data

U, Th, Yb, Hf, $^{206}Pb^*$, are in parts per million (ppm)

										Atomic Ratios							Model Age (Ma)					
Spot name	**U**	**Th**	**Th/U**	**Yb**	**Hf**	**$^{204}Pb/^{206}Pb$**	**% err**	**f(206) 204**	**$^{206}Pb^*$**	**$^{208}*Pb/^{206}*Pb$**	**% err**	**$^{207}*Pb/^{235}U$**	**% err**	**$^{206}*Pb/^{238}U$**	**% err**	**Corr Coeff**	**$^{207}*Pb/^{206}*Pb$**	**% err**	**$^{206}Pb/^{238}U$**	**$\pm^{206}Pb/^{238}U$**	**$^{207}Pb/^{206}Pb$**	**$\pm^{207}Pb/^{206}Pb$**	**Disc. %**
LL-09, Meall Dearg Fm. (Lower Enard Bay)																							
12086-001.1	75	36	0.50	281	9686	1.1E-5	100	0.02	31.4	0.153	4.9	13.037	1.8	0.4878	1.7	0.953	0.1939	0.6	2561	37	2775	9	+9
12086-002.1	65	61	0.97	142	10527	3.3E-4	57	0.58	30.4	0.266	3.2	14.058	6.8	0.5432	6.4	0.951	0.1877	2.1	2797	146	2722	34	-3
12086-003.1	28	28	1.04	75	8968	1.0E-4	50	0.18	12.9	0.285	3.2	14.326	2.2	0.5337	2.0	0.911	0.1947	0.9	2757	45	2782	15	+1
12086-005.1	17	16	0.95	30	8914	2.4E-4	45	0.41	6.8	0.223	5.2	9.873	2.8	0.4539	2.3	0.833	0.1578	1.5	2412	46	2432	26	+1
12086-006.1	50	33	0.69	118	10824	1.8E-5	100	0.03	20.8	0.188	3.2	10.934	2.0	0.4847	1.8	0.925	0.1636	0.8	2548	39	2493	13	-3
12086-007.1	59	92	1.61	121	9426	3.8E-5	58	0.07	27.3	0.461	1.8	14.588	1.9	0.5420	1.8	0.946	0.1952	0.6	2792	40	2787	10	-0
12086-008.1	141	37	0.27	185	11189	2.5E-4	18	0.44	51.2	0.051	7.4	10.644	1.7	0.4225	1.6	0.951	0.1827	0.5	2272	31	2677	9	+18
12086-010.1	81	102	1.30	60	11058	5.6E-5	45	0.10	32.2	0.350	1.9	10.465	1.8	0.4646	1.7	0.940	0.1633	0.6	2460	35	2491	11	+1
12086-010.1	81	102	1.30	60	11058	5.6E-5	45	0.10	32.2	0.350	1.9	10.465	1.8	0.4646	1.7	0.940	0.1633	0.6	2460	35	2491	11	+1
12086-011.1	166	98	0.61	39	11284	2.6E-5	45	0.05	69.3	0.173	1.8	11.127	1.8	0.4852	1.6	0.888	0.1663	0.8	2550	34	2521	14	-1
12086-011.1	166	98	0.61	39	11284	2.6E-5	45	0.05	69.3	0.173	1.8	11.127	1.8	0.4852	1.6	0.888	0.1663	0.8	2550	34	2521	14	-1
12086-012.1	58	31	0.56	168	10993	3.8E-5	50	0.07	34.6	0.150	2.7	27.015	1.9	0.6975	1.8	0.908	0.2809	0.8	3411	47	3368	13	-2
12086-015.1	146	19	0.13	67	11459	1.6E-5	58	0.03	68.7	0.041	3.9	14.012	1.7	0.5479	1.6	0.972	0.1855	0.4	2816	37	2702	7	-5
12086-016.1	24	13	0.55	107	10920	-7.8E-5	71	-0.14	9.5	0.151	5.4	10.175	2.4	0.4548	2.1	0.872	0.1623	1.2	2417	43	2479	20	+3
12086-016.1	24	13	0.55	107	10920	-7.8E-5	71	-0.14	9.5	0.151	5.4	10.175	2.4	0.4548	2.1	0.872	0.1623	1.2	2417	43	2479	20	+3
12086-017.1	123	83	0.70	149	10200	6.3E-6	100	0.01	58.7	0.199	9.4	15.314	5.8	0.5557	5.6	0.973	0.1999	1.3	2849	130	2825	22	-1
12086-018.1	65	102	1.62	187	12636	6.0E-5	45	0.10	30.8	0.477	1.7	14.970	2.0	0.5518	1.8	0.887	0.1968	0.9	2833	41	2799	15	-1
12086-020.1	30	19	0.66	87	10860	1.7E-4	38	0.30	13.5	0.181	7.2	13.471	2.2	0.5313	2.0	0.900	0.1839	1.0	2747	45	2688	16	-3
12086-021.1	35	22	0.64	81	11042	3.8E-5	71	0.07	18.3	0.183	5.6	18.580	2.2	0.6087	2.0	0.869	0.2214	1.1	3065	48	2991	18	-3

12086-021.1	35	22	0.64	81	11042	3.8E-5	71	0.07	18.3	0.183	5.6	18.580	2.2	0.6087	2.0	0.869	0.2214	1.1	3065	48	2991	18	-3
12086-022.1	97	83	0.89	105	10722	7.9E-5	32	0.14	44.2	0.250	1.9	13.755	1.8	0.5318	1.7	0.958	0.1876	0.5	2749	38	2721	8	-1
12086-023.1	59	116	2.04	110	10289	5.8E-5	45	0.10	28.5	0.589	1.5	16.052	2.1	0.5640	1.8	0.844	0.2064	1.1	2883	41	2878	18	-0
12086-025.1	44	41	0.96	112	10042	1.8E-4	32	0.32	18.5	0.268	2.9	12.964	2.0	0.4932	1.9	0.916	0.1906	0.8	2585	40	2748	13	+7
12086-026.1	42	33	0.80	86	9983	3.8E-5	71	0.07	17.9	0.223	3.1	11.779	2.5	0.4954	1.9	0.762	0.1724	1.6	2594	40	2581	27	-1
12086-026.1	42	33	0.80	86	9983	3.8E-5	71	0.07	17.9	0.223	3.1	11.779	2.5	0.4954	1.9	0.762	0.1724	1.6	2594	40	2581	27	-1
12086-027.1	133	52	0.40	129	10168	2.9E-5	45	0.05	63.8	0.111	2.4	15.142	1.7	0.5575	1.6	0.971	0.1970	0.4	2856	38	2801	7	-2
12086-028.1	39	57	1.51	181	9283	1.2E-4	41	0.21	17.6	0.430	2.3	13.138	2.3	0.5248	1.9	0.815	0.1816	1.4	2720	42	2667	22	-2
12086-028.1	39	57	1.51	181	9283	1.2E-4	41	0.21	17.6	0.430	2.3	13.138	2.3	0.5248	1.9	0.815	0.1816	1.4	2720	42	2667	22	-2
12086-029.1	57	103	1.87	111	9858	-1.8E-13	9999	0.00	25.2	0.511	1.8	13.432	1.9	0.5137	1.8	0.941	0.1897	0.7	2672	40	2739	11	+3
12086-030.1	86	49	0.59	149	11030	1.7E-5	71	0.03	39.3	0.165	2.4	14.480	1.8	0.5317	1.7	0.961	0.1975	0.5	2749	38	2806	8	+2
12086-031.1	46	27	0.60	56	9878	1.1E-4	41	0.20	19.5	0.167	7.1	11.569	2.3	0.4893	1.9	0.809	0.1715	1.4	2568	40	2572	23	+0
12086-031.1	46	27	0.60	56	9878	1.1E-4	41	0.20	19.5	0.167	7.1	11.569	2.3	0.4893	1.9	0.809	0.1715	1.4	2568	40	2572	23	+0
12086-032.1	63	55	0.91	160	9577	5.0E-5	50	0.09	29.3	0.264	2.3	14.685	2.0	0.5427	1.8	0.869	0.1962	1.0	2795	40	2795	17	+0
12086-032.1	63	55	0.91	160	9577	5.0E-5	50	0.09	29.3	0.264	2.3	14.685	2.0	0.5427	1.8	0.869	0.1962	1.0	2795	40	2795	17	+0
12086-034.1	118	92	0.81	194	11704	4.5E-5	38	0.08	56.2	0.230	1.8	15.034	1.7	0.5552	1.7	0.967	0.1964	0.4	2847	38	2797	7	-2
12086-034.1	118	92	0.81	194	11704	4.5E-5	38	0.08	56.2	0.230	1.8	15.034	1.7	0.5552	1.7	0.967	0.1964	0.4	2847	38	2797	7	-2
12086-035.1	39	31	0.84	112	10117	3.7E-5	71	0.06	18.5	0.219	3.1	15.623	2.1	0.5582	1.9	0.934	0.2030	0.7	2859	44	2850	12	-0
12086-037.1	321	76	0.25	109	11605	3.9E-5	24	0.07	142.2	0.049	3.8	13.360	2.4	0.5156	2.4	0.994	0.1879	0.3	2680	52	2724	4	+2
12086-038.1	35	31	0.91	57	9471	2.1E-4	35	0.37	13.9	0.248	3.6	10.192	2.3	0.4595	2.0	0.874	0.1609	1.1	2437	40	2465	19	+1
12086-040.1	113	36	0.33	124	12899	6.7E-6	100	0.01	53.8	0.086	2.9	15.805	1.7	0.5566	1.7	0.969	0.2059	0.4	2853	38	2874	7	+1
12086-041.1	132	35	0.28	150	8687	2.7E-5	45	0.05	62.3	0.073	5.4	14.914	1.7	0.5487	1.6	0.972	0.1971	0.4	2820	37	2803	6	-1
12086-042.1	51	29	0.58	81	9147	1.0E-32	100	0.00	23.9	0.166	3.0	14.608	1.9	0.5445	1.8	0.945	0.1946	0.6	2802	41	2781	10	-1
12086-043.1	253	32	0.13	135	11929	6.1E-6	71	0.01	112.8	0.038	3.0	13.197	1.6	0.5182	1.6	0.983	0.1847	0.3	2692	35	2695	5	+0
12086-044.1	36	19	0.55	174	9928	9.6E-5	58	0.17	10.5	0.155	5.0	5.287	2.4	0.3363	2.0	0.828	0.1140	1.3	1869	32	1864	24	-0
12086-047.1	85	50	0.62	110	11532	-9.2E-6	100	-0.02	37.5	0.178	2.4	13.909	1.8	0.5162	1.7	0.958	0.1954	0.5	2683	38	2789	8	+5
12086-049.1	35	17	0.50	42	11042	2.3E-4	33	0.40	13.9	0.138	5.1	9.976	2.3	0.4592	2.0	0.869	0.1576	1.1	2436	40	2430	19	-0
12086-049.1	35	17	0.50	42	11042	2.3E-4	33	0.40	13.9	0.138	5.1	9.976	2.3	0.4592	2.0	0.869	0.1576	1.1	2436	40	2430	19	-0

12086-050.1	77	34	0.45	266	10515	3.6E-5	50	0.06	37.6	0.129	2.8	16.267	1.8	0.5670	1.7	0.959	0.2081	0.5	2896	40	2890	8	-0
12086-051.1	24	26	1.12	94	9352	1.8E-4	45	0.32	9.7	0.324	3.7	10.611	2.5	0.4775	2.1	0.859	0.1612	1.3	2517	45	2468	22	-2
12086-054.1	42	38	0.93	67	9847	1.2E-4	41	0.21	16.9	0.271	2.9	10.349	2.1	0.4683	1.9	0.903	0.1603	0.9	2476	39	2459	15	-1
12086-056.1	24	20	0.84	79	9727	2.1E-4	41	0.36	9.9	0.238	4.2	10.835	2.5	0.4793	2.1	0.860	0.1640	1.3	2524	44	2497	21	-1
12086-056.1	24	20	0.84	79	9727	2.1E-4	41	0.36	9.9	0.238	4.2	10.835	2.5	0.4793	2.1	0.860	0.1640	1.3	2524	44	2497	21	-1
12086-057.1	53	36	0.71	90	10330	7.5E-5	45	0.13	23.6	0.209	2.9	13.112	1.9	0.5213	1.8	0.933	0.1824	0.7	2705	40	2675	12	-1
12086-058.1	48	44	0.94	115	8577	-5.0E-5	58	-0.09	21.6	0.280	2.6	14.207	2.4	0.5235	1.9	0.781	0.1968	1.5	2714	41	2800	24	+4
12086-059.1	78	121	1.60	129	9736	8.7E-5	35	0.15	31.7	0.464	1.6	10.518	1.8	0.4737	1.7	0.938	0.1611	0.6	2500	36	2467	11	-2
12086-060.1	249	144	0.60	181	10691	2.5E-5	35	0.04	111.7	0.167	1.4	13.440	1.6	0.5220	1.6	0.982	0.1867	0.3	2708	35	2713	5	+0
12086-061.1	18	17	0.95	98	8584	-1.6E-4	50	-0.28	8.0	0.250	4.3	14.625	3.9	0.5201	2.2	0.577	0.2039	3.2	2700	49	2858	52	+7
12086-067.1	52	122	2.44	135	10182	2.9E-5	71	0.05	24.6	0.695	3.5	15.045	2.5	0.5542	1.8	0.731	0.1969	1.7	2842	42	2801	28	-2
12086-069.1	80	32	0.41	126	9937	3.6E-5	50	0.06	37.0	0.116	3.3	14.530	1.8	0.5392	1.7	0.958	0.1955	0.5	2780	39	2789	8	+0
12086-070.1	218	143	0.68	45	11077	3.6E-6	100	0.01	93.5	0.198	1.4	12.054	1.8	0.4999	1.6	0.890	0.1749	0.8	2613	34	2605	14	-0
12086-074.1	108	97	0.93	73	8254	1.8E-4	20	0.31	49.7	0.229	2.9	14.721	1.7	0.5381	1.7	0.961	0.1984	0.5	2776	38	2813	8	+2
12086-074.1	108	97	0.93	73	8254	1.8E-4	20	0.31	49.7	0.229	2.9	14.721	1.7	0.5381	1.7	0.961	0.1984	0.5	2776	38	2813	8	+2
12086-077.1	67	82	1.28	157	9937	5.9E-5	45	0.10	29.5	0.360	1.9	13.335	1.9	0.5154	1.8	0.945	0.1877	0.6	2680	39	2722	10	+2
12086-078.1	80	23	0.30	180	9750	2.6E-5	58	0.05	39.3	0.091	3.3	16.688	1.8	0.5720	1.7	0.953	0.2116	0.5	2916	40	2918	9	+0
12086-080.1	126	27	0.22	99	12098	3.7E-5	38	0.06	57.8	0.056	6.2	14.132	1.7	0.5328	1.6	0.971	0.1924	0.4	2753	37	2763	7	+0
12086-081.1	39	184	4.82	191	10614	2.0E-5	100	0.03	17.5	1.388	2.1	13.493	2.1	0.5171	1.9	0.928	0.1892	0.8	2687	42	2736	13	+2
12086-082.1	100	70	0.72	378	9444	8.1E-5	30	0.14	47.5	0.193	2.1	15.456	1.7	0.5521	1.7	0.963	0.2030	0.5	2834	39	2851	8	+1
12086-083.1	22	10	0.46	96	11969	-3.6E-5	100	-0.06	9.9	0.154	5.3	15.039	2.4	0.5285	2.2	0.909	0.2064	1.0	2735	49	2877	16	+6
12086-084.1	200	71	0.37	100	12036	1.2E-5	58	0.02	92.8	0.111	2.0	14.878	1.7	0.5410	1.6	0.935	0.1995	0.6	2788	36	2822	10	+1
12086-085.1	31	25	0.83	58	9376	1.4E-4	41	0.24	14.6	0.236	3.4	14.674	2.2	0.5389	2.0	0.913	0.1975	0.9	2779	45	2805	14	+1
12086-088.1	95	38	0.41	111	12630	7.4E-5	33	0.13	42.9	0.115	2.9	14.127	1.8	0.5270	1.7	0.958	0.1944	0.5	2729	38	2780	8	+2
12086-088.1	95	38	0.41	111	12630	7.4E-5	33	0.13	42.9	0.115	2.9	14.127	1.8	0.5270	1.7	0.958	0.1944	0.5	2729	38	2780	8	+2
12086-089.1	49	46	0.99	112	10061	6.1E-5	50	0.11	21.6	0.208	2.9	13.524	2.0	0.5183	1.8	0.936	0.1892	0.7	2692	40	2736	11	+2
12086-093.1	43	36	0.86	87	10583	1.3E-4	38	0.23	18.5	0.245	3.1	11.913	2.3	0.4974	1.9	0.803	0.1737	1.4	2603	40	2593	23	-0
12086-094.1	59	40	0.71	72	11103	2.8E-5	71	0.05	27.0	0.208	2.7	13.817	1.9	0.5313	1.8	0.940	0.1886	0.7	2747	40	2730	11	-1

12086-094.1	59	40	0.71	72	11103	2.8E-5	71	0.05	27.0	0.208	2.7	13.817	1.9	0.5313	1.8	0.940	0.1886	0.7	2747	40	2730	11	-1
12086-095.1	27	28	1.07	90	11046	2.9E-5	100	0.05	12.9	0.297	3.3	15.887	2.3	0.5641	2.1	0.917	0.2043	0.9	2883	48	2861	15	-1
12086-096.1	22	6	0.28	143	10179	1.3E-4	50	0.22	10.9	0.072	7.8	17.006	2.4	0.5792	2.2	0.910	0.2129	1.0	2946	51	2928	16	-1
12086-096.1	22	6	0.28	143	10179	1.3E-4	50	0.22	10.9	0.072	7.8	17.006	2.4	0.5792	2.2	0.910	0.2129	1.0	2946	51	2928	16	-1
12086-097.1	29	22	0.80	83	9975	1.8E-4	41	0.31	12.0	0.212	4.2	10.767	2.3	0.4825	2.0	0.873	0.1619	1.1	2538	43	2475	19	-3
12086-097.1	29	22	0.80	83	9975	1.8E-4	41	0.31	12.0	0.212	4.2	10.767	2.3	0.4825	2.0	0.873	0.1619	1.1	2538	43	2475	19	-3
12086-098.1	332	203	0.63	150	12345	4.8E-6	71	0.01	149.7	0.180	1.2	13.838	1.6	0.5254	1.6	0.986	0.1910	0.3	2722	35	2751	4	+1
12086-100.1	65	65	1.04	222	10749	4.5E-5	50	0.08	30.4	0.295	2.1	14.679	1.9	0.5481	1.8	0.949	0.1942	0.6	2817	40	2778	10	-2
12086-118.1	45	41	0.93	116	11281	8.8E-5	45	0.15	19.5	0.265	2.8	12.843	2.0	0.5033	1.9	0.924	0.1851	0.8	2628	40	2699	13	+3
12086-119.1	192	150	0.81	132	11447	4.3E-4	23	0.74	83.4	0.129	7.3	13.350	1.9	0.5062	1.6	0.877	0.1913	0.9	2640	35	2753	15	+5

Appendix D: Sample LL-10, U-Pb SHRIMP data

U, Th, Yb, Hf, $^{206}Pb^*$, are in parts per million (ppm)

										Atomic Ratios							Model Age (Ma)					
Spot name	**U**	**Th**	**Th/U**	**Yb**	**Hf**	**$^{204}Pb/^{206}Pb$**	**% err**	**f(206) 204**	**$^{206}Pb^*$**	**$^{208}*Pb/^{206}*Pb$**	**% err**	**$^{207}*Pb/^{235}U$**	**% err**	**$^{206}*Pb/^{238}U$**	**% err**	**Corr Coeff**	**$^{207}*Pb/^{206}*Pb$**	**% err**	**$^{206}Pb/^{238}U$**	**$\pm^{206}Pb/^{238}U$**	**$^{207}Pb/^{206}Pb$**	**$\pm^{207}Pb/^{206}Pb$**	**Disc. %**
LL-10, Meall Dearg Fm. (Upper Enard Bay)																							
12087-001.1	34	53	1.63	192	9791	-4.6E-5	71	-0.08	13.6	0.461	2.4	10.549	2.1	0.4692	2.0	0.910	0.1631	0.9	2480	40	2488	15	+0
12087-002.1	75	44	0.61	110	9688	4.5E-5	58	0.08	21.8	0.179	3.1	5.359	1.9	0.3400	1.7	0.902	0.1143	0.8	1887	29	1869	15	-1
12087-004.1	44	44	1.02	125	9551	-1.7E-5	100	-0.03	20.3	0.294	2.5	14.218	2.0	0.5350	1.9	0.937	0.1927	0.7	2763	42	2766	11	+0
12087-006.1	29	26	0.93	127	8593	5.4E-5	71	0.09	12.5	0.269	3.4	12.591	2.2	0.5096	2.0	0.908	0.1792	0.9	2655	44	2645	16	-0
12087-008.1	53	123	2.37	160	9997	1.6E-13	9999	0.00	23.7	0.679	1.5	13.398	1.9	0.5166	1.8	0.945	0.1881	0.6	2685	40	2725	10	+2
12087-009.1	27	28	1.07	71	9550	7.3E-4	20	1.26	10.7	0.282	3.9	9.919	2.6	0.4547	2.0	0.797	0.1582	1.5	2416	41	2437	26	+1
12087-010.1	47	71	1.56	466	10172	-2.9E-5	71	-0.05	21.9	0.420	1.9	14.586	1.9	0.5416	1.8	0.943	0.1953	0.6	2790	41	2788	11	-0
12087-014.1	20	14	0.73	119	9055	2.6E-4	38	0.45	9.2	0.189	5.1	14.508	2.5	0.5455	2.2	0.879	0.1929	1.2	2806	51	2767	20	-2
12087-016.1	112	111	1.02	62	6531	1.3E-5	71	0.02	50.6	0.280	2.8	13.948	3.6	0.5241	3.6	0.993	0.1930	0.4	2717	79	2768	7	+2
12087-017.1	30	30	1.03	170	11055	1.0E-4	50	0.17	13.9	0.281	3.3	13.406	8.6	0.5351	2.1	0.247	0.1817	8.3	2763	47	2668	137	-4
12087-018.1	69	101	1.52	169	10353	1.1E-5	100	0.02	31.6	0.422	1.7	14.176	1.8	0.5358	1.7	0.954	0.1919	0.6	2766	39	2758	9	-0
12087-019.1	93	30	0.34	34	8915	-1.2E-5	100	-0.02	27.5	0.099	3.6	5.566	1.8	0.3459	1.7	0.925	0.1167	0.7	1915	28	1906	13	-1
12087-019.1	93	30	0.34	34	8915	-1.2E-5	100	-0.02	27.5	0.099	3.6	5.566	1.8	0.3459	1.7	0.925	0.1167	0.7	1915	28	1906	13	-1
12087-021.1	43	22	0.53	94	9580	5.0E-5	58	0.09	19.8	0.144	3.7	14.586	2.0	0.5366	1.9	0.935	0.1971	0.7	2769	42	2803	12	+1
12087-022.1	33	1	0.04	60	20040	-3.5E-13	9999	0.00	15.4	0.012	14.0	14.747	2.1	0.5368	2.0	0.928	0.1992	0.8	2770	44	2820	13	+2
12087-023.1	100	89	0.92	171	8241	5.1E-21	9999	0.00	48.2	0.252	1.8	15.828	5.7	0.5585	5.3	0.923	0.2055	2.2	2861	122	2871	36	+0
12087-024.1	69	46	0.69	85	9826	8.4E-5	35	0.15	32.5	0.187	2.6	15.050	2.4	0.5514	1.8	0.721	0.1979	1.7	2831	40	2809	28	-1
12087-025.1	69	44	0.65	92	9806	2.5E-5	71	0.04	28.7	0.188	2.7	11.423	8.5	0.4816	8.5	0.997	0.1720	0.6	2534	177	2578	11	+2
12087-026.1	210	101	0.50	314	13412	2.3E-5	41	0.04	95.9	0.127	1.8	14.214	1.6	0.5329	1.6	0.979	0.1935	0.3	2753	36	2772	6	+1

12087-028.1	44	33	0.78	134	9190	7.5E-5	45	0.13	24.2	0.219	4.8	21.162	2.0	0.6331	1.9	0.948	0.2424	0.6	3162	47	3136	10	-1
12087-029.1	110	108	1.01	194	9528	6.9E-5	30	0.12	49.1	0.258	1.7	13.807	1.7	0.5199	1.7	0.966	0.1926	0.4	2699	37	2765	7	+3
12087-031.1	64	54	0.88	49	9752	6.9E-5	45	0.12	25.8	0.252	2.5	10.802	1.9	0.4698	1.8	0.931	0.1668	0.7	2483	37	2525	12	+2
12087-034.1	47	57	1.24	145	8901	8.6E-5	50	0.15	16.9	0.299	4.9	8.966	2.1	0.4145	1.9	0.900	0.1569	0.9	2235	36	2422	15	+9
12087-036.1	30	15	0.50	35	10094	1.1E-4	50	0.18	12.1	0.135	4.9	10.718	2.8	0.4696	2.1	0.754	0.1655	1.9	2482	44	2513	31	+2
12087-037.1	34	49	1.49	50	9735	2.5E-5	100	0.04	13.5	0.418	2.6	10.694	2.2	0.4619	2.0	0.910	0.1679	0.9	2448	40	2537	15	+4
12087-038.1	216	34	0.16	57	11441	1.1E-5	58	0.02	91.3	0.045	3.1	12.267	1.6	0.4916	1.6	0.979	0.1810	0.3	2578	34	2662	6	+4
12087-038.2	182	23	0.13	76	11671	8.2E-6	71	0.01	82.8	0.035	3.7	13.516	1.7	0.5293	1.6	0.975	0.1852	0.4	2739	36	2700	6	-2
12087-038.3	237	36	0.16	81	12007	1.4E-5	50	0.03	102.8	0.045	3.0	12.373	1.6	0.5046	1.6	0.979	0.1778	0.3	2634	35	2633	6	-0
12087-040.1	31	28	0.93	68	10264	1.9E-4	38	0.33	13.2	0.246	3.7	12.033	2.3	0.5018	2.0	0.887	0.1739	1.1	2622	44	2596	18	-1
12087-041.1	196	41	0.22	85	11568	-3.2E-14	9999	0.00	86.8	0.059	2.7	13.519	1.6	0.5168	1.6	0.979	0.1897	0.3	2686	35	2740	6	+2
12087-042.1	122	70	0.59	122	11030	-2.0E-5	58	-0.04	54.5	0.176	2.1	13.343	1.7	0.5212	1.7	0.965	0.1857	0.5	2704	37	2704	7	+0
12087-045.1	63	61	1.00	125	9288	2.4E-5	71	0.04	30.0	0.274	5.1	14.946	6.0	0.5548	5.9	0.988	0.1954	0.9	2845	136	2788	15	-3
12087-046.1	78	148	1.97	120	10254	6.9E-5	41	0.12	30.4	0.546	1.6	10.260	1.9	0.4568	1.7	0.938	0.1629	0.6	2425	35	2486	11	+3
12087-047.1	62	62	1.03	219	9628	4.9E-5	50	0.09	28.7	0.290	2.2	14.532	1.9	0.5380	1.8	0.946	0.1959	0.6	2775	40	2792	10	+1
12087-048.1	33	25	0.80	129	9342	1.5E-4	41	0.26	13.9	0.236	3.6	12.093	2.7	0.4980	2.0	0.722	0.1761	1.9	2605	42	2617	32	+1
12087-049.1	40	15	0.39	123	9107	4.9E-5	58	0.08	20.4	0.107	6.5	18.268	2.0	0.5864	1.9	0.942	0.2259	0.7	2975	45	3024	11	+2
12087-050.1	163	29	0.18	162	9174	3.0E-5	38	0.05	81.5	0.052	3.1	17.404	1.7	0.5821	1.6	0.974	0.2168	0.4	2957	39	2957	6	+0
12087-051.1	25	22	0.89	43	10083	-7.0E-5	71	-0.12	10.1	0.253	3.9	9.898	2.8	0.4639	2.2	0.786	0.1547	1.7	2457	45	2399	29	-3
12087-052.1	28	20	0.74	76	9276	-5.3E-5	71	-0.09	13.0	0.196	6.3	14.352	2.2	0.5330	2.1	0.915	0.1953	0.9	2754	46	2787	15	+1
12087-053.1	52	82	1.63	152	9853	6.0E-5	50	0.10	24.1	0.446	1.9	13.927	2.0	0.5398	1.8	0.937	0.1871	0.7	2783	41	2717	11	-3
12087-055.1	36	15	0.42	69	8773	2.1E-5	100	0.04	16.7	0.111	4.6	13.779	2.1	0.5347	1.9	0.927	0.1869	0.8	2761	43	2715	13	-2
12087-055.1	36	15	0.42	69	8773	2.1E-5	100	0.04	16.7	0.111	4.6	13.779	2.1	0.5347	1.9	0.927	0.1869	0.8	2761	43	2715	13	-2
12087-056.1	45	39	0.89	119	10214	5.8E-14	9999	0.00	24.1	0.252	2.5	19.383	2.0	0.6162	1.9	0.951	0.2281	0.6	3095	46	3039	10	-2
12087-057.1	47	39	0.85	107	8318	1.9E-5	100	0.03	22.8	0.237	3.1	14.699	2.1	0.5686	1.9	0.914	0.1875	0.9	2902	45	2720	14	-8
12087-059.1	103	70	0.70	184	10776	5.0E-5	38	0.09	49.3	0.194	2.0	15.221	1.7	0.5576	1.7	0.964	0.1980	0.5	2857	39	2810	8	-2
12087-059.1	103	70	0.70	184	10776	5.0E-5	38	0.09	49.3	0.194	2.0	15.221	1.7	0.5576	1.7	0.964	0.1980	0.5	2857	39	2810	8	-2
12087-060.1	28	20	0.73	68	9795	3.6E-5	100	0.06	11.4	0.210	4.4	10.963	2.4	0.4743	2.1	0.891	0.1676	1.1	2503	44	2534	18	+2

12087-060.1	28	20	0.73	68	9795	3.6E-5	100	0.06	11.4	0.210	4.4	10.963	2.4	0.4743	2.1	0.891	0.1676	1.1	2503	44	2534	18	+2
12087-061.1	36	32	0.93	110	9876	6.8E-21	9999	0.00	16.5	0.260	3.2	13.536	2.8	0.5407	2.0	0.720	0.1815	1.9	2787	45	2667	32	-6
12087-062.1	41	25	0.62	180	7884	6.0E-5	58	0.10	20.2	0.180	3.5	15.779	2.1	0.5732	1.9	0.929	0.1996	0.8	2921	45	2823	13	-4
12087-063.1	176	24	0.14	78	10079	9.3E-6	71	0.02	84.9	0.036	3.9	15.286	1.7	0.5600	1.6	0.976	0.1980	0.4	2867	38	2810	6	-3
12087-064.1	210	21	0.10	154	13424	2.3E-21	9999	0.00	96.5	0.029	3.9	13.836	1.6	0.5355	1.6	0.978	0.1874	0.3	2765	36	2719	6	-2
12087-065.1	239	218	0.94	178	9167	1.0E-5	71	0.02	70.0	0.277	1.4	5.420	1.7	0.3412	1.6	0.961	0.1152	0.5	1892	26	1884	8	-1
12087-066.1	157	128	0.84	109	10921	-6.0E-6	100	-0.01	60.0	0.244	1.6	9.235	1.7	0.4436	1.6	0.964	0.1510	0.4	2367	32	2357	8	-0
12087-067.1	90	117	1.35	141	9162	1.7E-5	71	0.03	43.2	0.370	1.6	15.264	1.8	0.5588	1.7	0.960	0.1981	0.5	2862	40	2811	8	-2
12087-068.1	47	33	0.73	117	10101	-6.5E-5	50	-0.11	21.2	0.209	3.1	13.063	6.3	0.5222	6.2	0.993	0.1814	0.7	2709	137	2666	12	-2
12087-069.1	156	225	1.49	201	11464	1.6E-5	58	0.03	70.9	0.422	1.2	13.827	1.7	0.5284	1.6	0.973	0.1898	0.4	2735	36	2740	6	+0
12087-070.1	57	54	0.98	156	11917	6.0E-5	50	0.10	23.7	0.270	2.5	11.772	1.9	0.4795	1.8	0.932	0.1781	0.7	2525	38	2635	12	+5
12087-072.1	244	66	0.28	56	11242	2.3E-5	38	0.04	104.4	0.078	2.2	12.656	1.6	0.4985	1.6	0.980	0.1841	0.3	2607	34	2690	5	+4
12087-075.1	46	9	0.21	31	9613	1.7E-4	33	0.29	19.1	0.047	8.2	11.097	2.1	0.4838	1.9	0.905	0.1664	0.9	2544	40	2521	15	-1
12087-076.1	99	20	0.21	74	12890	3.6E-5	50	0.06	46.0	0.061	4.2	15.115	1.9	0.5430	1.7	0.904	0.2019	0.8	2796	39	2842	13	+2
12087-078.1	42	59	1.46	221	8320	5.6E-5	58	0.10	19.5	0.407	2.3	14.636	2.1	0.5446	1.9	0.928	0.1949	0.8	2803	43	2784	13	-1
12087-079.1	22	9	0.39	39	12296	2.7E-13	9999	0.00	10.6	0.107	5.8	14.988	2.4	0.5523	2.2	0.913	0.1968	1.0	2835	50	2800	16	-2
12087-080.1	123	95	0.80	109	12859	1.2E-5	71	0.02	57.0	0.230	2.8	13.829	1.7	0.5390	1.7	0.970	0.1861	0.4	2779	37	2708	7	-3
12087-083.1	73	38	0.55	97	10390	3.3E-5	71	0.06	21.1	0.168	3.3	5.408	2.0	0.3378	1.8	0.898	0.1161	0.9	1876	29	1898	15	+1
12087-084.1	68	97	1.46	90	10894	2.4E-5	71	0.04	29.8	0.416	1.8	12.398	1.9	0.5065	1.8	0.944	0.1775	0.6	2642	38	2630	10	-1
12087-085.1	84	51	0.62	148	7827	3.5E-5	50	0.06	42.0	0.187	2.3	16.458	3.3	0.5787	1.7	0.517	0.2063	2.9	2943	41	2877	46	-3
12087-087.1	135	77	0.59	327	10457	4.7E-6	100	0.01	75.1	0.165	2.9	22.780	1.7	0.6488	1.6	0.980	0.2547	0.3	3223	42	3214	5	-0
12087-089.1	85	88	1.07	144	9666	-2.7E-5	58	-0.05	40.6	0.302	1.8	15.289	4.2	0.5566	4.2	0.993	0.1992	0.5	2853	96	2820	8	-1
12087-092.1	35	22	0.66	73	10455	2.5E-5	100	0.04	14.3	0.199	3.7	11.015	2.6	0.4740	2.0	0.755	0.1685	1.7	2501	41	2543	29	+2
12087-094.1	64	34	0.54	128	10440	1.4E-13	9999	0.00	28.5	0.150	3.0	13.067	1.9	0.5172	1.8	0.948	0.1832	0.6	2687	39	2682	10	-0
12087-095.1	249	90	0.37	96	10644	-1.2E-5	50	-0.02	114.9	0.108	1.8	14.221	1.8	0.5381	1.6	0.897	0.1917	0.8	2775	36	2757	13	-1
12087-096.1	23	22	1.00	112	11245	1.7E-4	45	0.29	10.6	0.259	3.9	14.810	2.4	0.5486	2.2	0.887	0.1958	1.1	2819	49	2791	18	-1
12087-097.1	56	24	0.45	97	11784	4.2E-5	58	0.07	26.8	0.129	3.5	15.703	3.0	0.5593	1.8	0.614	0.2036	2.3	2864	42	2856	38	-0
12087-099.1	54	58	1.11	165	9434	1.1E-4	38	0.18	25.0	0.312	2.4	14.172	2.0	0.5385	1.8	0.932	0.1909	0.7	2777	41	2750	12	-1

12087-100.1	49	35	0.73	107	9679	4.5E-5	58	0.08	23.3	0.198	2.9	14.648	2.0	0.5495	1.8	0.938	0.1933	0.7	2823	42	2771	11	-2
12087-101.1	61	24	0.41	75	10168	-2.5E-5	71	-0.04	28.7	0.113	3.6	14.750	2.1	0.5473	1.8	0.856	0.1954	1.1	2814	41	2789	18	-1
12087-109.1	52	73	1.45	126	10653	6.3E-5	50	0.11	24.4	0.409	2.1	14.147	2.0	0.5470	1.8	0.934	0.1876	0.7	2813	42	2721	12	-4
12087-113.1	52	58	1.14	104	10596	9.6E-5	41	0.17	22.5	0.340	2.3	12.203	2.0	0.5027	1.8	0.925	0.1761	0.7	2625	39	2616	12	-0
12087-119.1	59	39	0.68	52	10144	5.5E-5	50	0.09	25.8	0.191	5.3	13.545	8.4	0.5109	7.7	0.908	0.1923	3.5	2661	167	2762	58	+4
12087-122.1	192	110	0.59	185	9951	-1.6E-14	9999	0.00	92.1	0.163	2.6	15.313	3.4	0.5593	3.4	0.995	0.1986	0.3	2864	79	2814	5	-2
12087-125.1	81	35	0.44	86	8208	4.6E-5	45	0.08	39.7	0.124	4.4	16.661	6.4	0.5706	6.3	0.976	0.2118	1.4	2910	147	2919	22	+0
12087-126.1	64	61	0.98	231	9494	-2.6E-5	71	-0.04	29.8	0.271	2.3	14.340	2.9	0.5428	1.8	0.623	0.1916	2.2	2795	40	2756	37	-2
12087-126.1	64	61	0.98	231	9494	-2.6E-5	71	-0.04	29.8	0.271	2.3	14.340	2.9	0.5428	1.8	0.623	0.1916	2.2	2795	40	2756	37	-2
12087-130.1	79	77	1.00	113	9365	5.1E-5	45	0.09	37.6	0.286	2.0	14.700	1.8	0.5512	1.7	0.953	0.1934	0.6	2830	40	2771	9	-3